MEASUREMENT OF THE EFFICIENCY OF EVACUATED TUBE SOLAR COLLECTORS UNDER VARIOUS OPERATING CONDITIONS

BY

STEPHANIE ERIN ZUBRISKI

A THESIS SUBMITTED TO THE FACULTY OF GRADUATE STUDIES

IN PARTIAL FULFILLMENT OF THE REQUIREMENTS FOR THE DEGREE OF

MASTER OF SCIENCE

DEPARTMENT OF BIOSYSTEMS ENGINEERING

UNIVERSITY OF MANITOBA

WINNIPEG, MANITOBA

Abstract

The operating efficiency of evacuated tubes themselves under varying environmental conditions and installation scenarios, independent of water and space heating auxiliary equipment, are not readily available values. Further, Manitoba specific data has not been established. The purpose of this research program was to measure the efficiency of evacuated tube solar collectors under various operating conditions including: the angle of inclination towards the incident solar radiation, heat transfer fluid flow rate, glazing installation, and number of evacuated tubes. The operating conditions and configurations were chosen to represent realistic or probable installation scenarios and environmental conditions. Furthermore, the research aimed to identify the suitability of evacuated tube solar collectors to each of the scenarios. These design values are of use for appropriate sizing of water or space heating systems, system configuration and optimization, and calculation of return on investment. The scope of the research project was limited to the efficiency of a single tube, and various configurations of a 32-tube panel, not the entire solar domestic hot water or space heating system. Thus, factors such as heat loss in the tubing, solar storage tank, and heat exchanger efficiency were not investigated. The findings indicated that efficiency varied by approximately 5% in general between the different collector configurations, as observed from the overlay graph of results.

Keywords: solar collector**,** evacuated tube

Acknowledgements:

I would like to thank my thesis advisor Dr. Kris Dick, of the Department of Biosystems Engineering, for his support and guidance throughout the course of this research project.

Thanks also to my graduate thesis committee, Dr. Ron Britton and Dr. James Blatz for providing valuable feedback.

To the Department of Biosystems Engineering technicians, Dale Bourns, Robert Lavallee, and Matt McDonald, many thanks for your technical and manufacturing support.

Also, thanks to Matt Froese who helped me work through a number of mechanical design and simulation issues.

The author would like to acknowledge MB Hydro for the generous financial support that made much of this project possible.

And to John Verway of Copperhill for supplying the evacuated tube collectors.

Finally, thank you to my partner Bryan Ward and to my family for your support and encouragement throughout this endeavor.

Table of Contents:

List of Figures:

1 Introduction

1.1 Field of Interest

In Canada, approximately 80% of residential energy consumption is apportioned to domestic hot water and space heating applications (Sibbitt et al. 2007). According to Kemp (2005), on average, Manitoba residents can expect to obtain approximately 56% of the energy required for water heating purposes from solar thermal sources, while those as far north as Inuvik in the Northwest Territories can expect approximately 33%. These statistics indicate that even the most northerly locations with extremely cold climates and minimal solar radiation during the winter months are able to benefit from solar water heating technologies, which will consequently reduce the demand on other energy sources such as electricity and gas. Sibbitt et al. (2007) note that a common, unsubstantiated barrier to large-scale adoption of solar heating technologies for domestic hot water and space heating is the relative lack of sunshine during the fall and winter months when heating demand is high.

If the use of alternative energy sources for hot water systems, either domestic hot water or space heating, is demonstrated to be a viable option for both commercial and residential consumers then a portion of their current energy demand could be redistributed. This is of particular interest in the residential market, where current trends point toward the acquisition of greater numbers of electric water heaters, creating an electrical energy demand on Manitoba Hydro's resources. A viable alternative energy strategy, such as evacuated tube technology, could offset this demand. The potential to

create consumer incentives to purchase such units for water heating purposes could also be investigated.

Similarly, as the use of ground source heat pumps to control the climate of built environments increases, evacuated tube technology could be implemented to restore thermal energy in the reservoirs, potentially prolonging the lifespan of the entire system. Such system integration has proven to be successful in the Drake Landing Solar Community Project in Okotoks, Alberta. This community connects 52 detached houses to a district heating and seasonal storage system that has been designed to use solar energy to supply greater than 90% of the space heating energy requirements. Seven hundred and ninety-eight flat-plate collectors have been mounted to the roofs of detached garages, which have been connected by covered breezeways to create a large, uninterrupted roof surface for mounting. The flat-plate collectors supply thermal energy to charge a long-term borehole thermal energy storage field which later supplies heat through a district system to each home in the subdivision (Sibbitt et al. 2007).

Other commercial and residential applications in which evacuated tube technology could be implemented to offset the electrical energy demand for water heating within Manitoba include, but are not limited to, car washes, laundry facilities, hospitals, recreation centers, pools, spas, hot tubs, and restaurants.

Evacuated tube efficiency design values would be of use for appropriate sizing of water or space heating systems, system configuration and optimization, and calculation of return on investment.

1.2 Purpose of the Research

The purpose of this research program was to measure the efficiency of evacuated tube solar collectors under various operating conditions. These efficiencies were of interest to the author, as they will serve to inform the overall system design, sizing, and optimization of evacuated tube collectors in any number of configurations and installation scenarios, such as water, space, or pool heating applications. Operating conditions including the angle of inclination towards the incident solar radiation, heat transfer fluid flow rate, glazing installation, and number of evacuated tubes were of particular interest due to design and installation consequences encountered in practice.

1.3 Nature and Scope of the Problem

A number of evacuated tube solar water heating and space heating systems are available for purchase for both residential and commercial use. The overall efficiencies of these systems may or may not be available from the manufacturer and may or may not reflect efficiencies obtainable in real operating conditions. Often, efficiencies are measured in laboratories under artificial illumination, not taking into account environmental conditions such as cloud cover, visibility, shading, wind speed and direction, and ambient outdoor temperature. In addition, the operating efficiency of the evacuated tubes

themselves under varying environmental conditions and installation scenarios, independent of water and space heating auxiliary equipment, are not readily available values. Further, Manitoba specific data has not been established. These design values would be of use for appropriate sizing of water or space heating systems, system configuration and optimization, and calculation of return on investment.

From a practical and architectural point of view, there are a number of possible installation scenarios for evacuated tube collectors that may be more or less appropriate under different environmental, structural, and aesthetic restrictions. For instance, collectors could be mounted vertically to the south facing side of a building. If space is tight, a full panel may not be appropriate and perhaps a smaller collector could perform suitably in less space. If vandalism or hail is a potential problem, perhaps a covered collector would alleviate the concern for damage. The author was interested in the effect that installation situations such as these would have on the efficiency of the collector.

The scope of the research project was limited to the efficiency of a single tube, and various configurations of a 32-tube panel, not the entire solar domestic hot water or space heating system. Thus, factors such as heat loss in the tubing, solar storage tank, and heat exchanger efficiency were not investigated. Figure 1 in Appendix D outlines the energy flow through the system and indicates the research boundaries.

1.4 Research Objectives

The objective of this research program was to determine the efficiency of evacuated tube solar collectors under various operating conditions and configurations. The operating conditions and configurations were chosen to represent realistic or probable installation scenarios and environmental conditions. Furthermore, the research aimed to identify the suitability of evacuated tube solar collectors to each of the scenarios.

1.5 General Description of Research Method / Research Approach

As previously mentioned, due to various considerations, there are a number of possible installation scenarios for evacuated tube collectors. The author was specifically interested in the effect that the following configurations would have on the efficiency of the collector:

- Single Evacuated Tube
- Collector at 50º to Horizontal, Intermediate Flow Rate (Astro pump) (Control)
- Collector at 50º to Horizontal, Intermediate Flow Rate (Astro pump), Covered with Glazing
- Collector at 50º to Horizontal, Increased Flow Rate (Astro pump)
- Collector at 90º to Horizontal, Low Flow Rate (Grundfos pump)
- Collector at 50º to Horizontal, Intermediate Flow Rate (Astro pump), 16 Tubes Removed

Apart from the single evacuated tube efficiency measurements, these scenarios represent actual or probable installation configurations. The single evacuated tube measurements were a continuation of an undergrad research project and provide insight into the capabilities of a single evacuated tube. Four collectors were erected along the south side of the straw bale building at the Alternative Village on the University of Manitoba Fort Garry Campus. Data were collected over the course of approximately two years and the collectors were modified as necessary to accommodate the above configurations. The collector angled at 50º to the horizontal with intermediate flow rate was the control for the experiment and represents the base line or the standard operation and installation configuration. The efficiencies of the remaining collector configurations were compared to that of the control, and to each other in terms of overall performance.

Measured experimental variables include the incident solar radiation, ambient outdoor temperature, indoor temperature, inlet and outlet temperatures of the manifold, and inlet and outlet temperatures of the fin-tube heat exchanger. Experimental variables that were not measured and recorded directly, but were observed less formally include ambient outdoor weather conditions, pump flow rates, and circuit operating pressures.

1.6 Organization of Thesis

The thesis is organized as follows: Chapter 2 is a literature review covering background information on solar energy measurement, evacuated tube collectors, and efficiency measurement test procedures. The materials and methods employed to conduct this research are described in detail in Chapter 3. Results and discussion are covered in Chapter 4. Finally, Chapter 5 presents research conclusions and recommendations.

2 Literature Review

2.1 Introduction: Scope of Literature Review

Through review of literature on the subject of efficiency of evacuated tube water or space heating systems, it was expected that insight into appropriate methodology for efficiency measurement would be obtained. The scope of the literature review was limited to that pertaining to the efficiency measurements of solar water or space heating applications, regardless of the technology investigated, be it evacuated tube, flat plate, or any other technology. In addition, literature pertaining to solar energy measurement, determination of absorber surface area for evacuated tubes, and the effects of shading from adjacent tubes was also considered. Literature that examined factors affecting efficiency including dust accumulation, reflection from adjacent buildings or the absorber's surroundings, and the effects of the addition of reflectors or concentrators behind the tubes was reviewed to a lesser extent, and mainly for thermal analysis content.

2.2 Review of Relevant Literature

2.2.1 Solar Energy Measurement

The sun provides energy to our planet at a rate of 1367 W/m^2, as measured outside of the earth's atmosphere (Duffie and Beckman 2006). This value is referred to as the solar constant, G_{sc}, and is defined as "the energy from the sun per unit time received on a unit area of surface perpendicular to the direction of propagation of the radiation at mean earth-sun distance outside of the atmosphere" (Duffie and Beckman 2006). Scattering of the radiation as it passes through the Earth's atmosphere is a result of interaction with

dust particles, water molecules in both liquid and vapour form, and air molecules. In addition, radiation is absorbed within the atmosphere by molecules of ozone, water, and carbon dioxide. These two phenomena are responsible for variations in irradiance at the Earth's surface (Duffie and Beckman 2006). Beam radiation is the solar radiation received from the sun without having been scattered by the atmosphere, whereas diffuse radiation is that received from the sun after its direction has been altered as a result of scattering. The sum of these two solar radiation components is referred to as total solar radiation, or global radiation. The proposed research will require measurements of total solar radiation.

Two main types of equipment are available to measure solar radiation, namely pyrheliometers and pyranometers. Detailed descriptions of both these technologies, including the limitations of their use, are provided by Duffie and Beckman (2006). Pyrheliometers measure beam radiation only, while pyranometers measure both beam and diffuse radiation. It is from the latter that most of the available data on solar radiation are obtained (Duffie and Beckman 2006).

The accuracy of the data obtained by a pyranometer is specific to the model in use, and should be noted prior to its implementation. Sharma et al. (2004) utilized two pyranometers to measure the solar irradiance on an evacuated tube solar collector; they report an accuracy of 1.5% for a pyranometer inclined at 20° to the horizontal, and an accuracy of 2.5% for another measuring the irradiance on a horizontal surface.

2.2.2 Evacuated Tubes

Although solar energy is free for the taking, particular challenges are encountered in the effective collection and storage of this energy. Radiation from the sun is available only during the day, so the energy must be collected in an efficient manner to make the most of daylight hours. This collected energy must then be stored for use during the non-daylight hours. A variety of technologies exist to capture this radiation. Of particular interest is evacuated tube technology for use in water and space heating applications. Numerous authors (Duffie and Beckman 2006; Kalogirou 2004; Morrison et al. 2004) have noted that evacuated tube collectors have much greater efficiencies than the common flat plate collector, especially at times of cold temperature and low isolation.

Evacuated tube collectors vary widely in their construction and operation (Morrison et al. 2004). For instance, the evacuated space may be created between a single tube of glass and a metal absorber pipe. In one version of this metal-in-glass type of evacuated tube, referred to as a flow through absorber, the metal absorber pipe only touches the glass tube at the base, and a glass-to metal seal at the top maintains the vacuum space between them. A central metal tube delivers the heat transfer fluid to the base of the absorber pipe. The fluid then flows up the annular space between the central tube and the absorber pipe, collecting energy from the absorber as it flows. In another version of this model, a U-shaped tube containing flowing heat transfer fluid is attached to the absorber pipe. Configurations that incorporate this glass-to-metal seal are costly and susceptible to damage due to shock when the cold heat transfer fluids enter the hot evacuated tube (Morrison et al. 2004).

Alternatively, an evacuated space may be created between two concentric glass tubes as in the all- glass types. Although the heat transfer mechanism may be different, the double walled glass tubes themselves are generally consistent in design. The annealed glass tubes are manufactured with an evacuated space between them. A low emissivity selective coating is applied to the inside face (vacuum side) of the inner tube and acts as the absorber surface, minimizing radiation heat loss. The evacuated space between the two tubes of glass creates excellent insulation and minimizes convective heat loss, which therefore allows for greater temperatures to be attained at the absorber surface (Morrison et al. 2004). Essentially, the solar radiation strikes the surface of the evacuated tube and the beam of radiation passes through the outer glass tube and then strikes the selective coating on the inner glass tube surface. This selective coating increases the absorptive properties of the glass while reducing the reflective properties, to achieve better use of the radiation. The all-glass type of evacuated tube is simpler in design and less expensive to manufacture compared to the metal-in-glass type, but it is more difficult to reliably extract energy from the glass absorber surface (Morrison et al. 2004).

The mechanism of heat transfer to the working fluid may vary from direct contact with the absorber tube to intermediate transfer to a metal rod or hollow heat-pipe (Ramlow 2006). For example, one of the most common types of evacuated tube is hollow, and is referred to as a water-in glass type. Budihardjo and Morrison (2009) evaluated the performance of water-in-glass evacuated tube solar collectors. The authors used experimental measurements of optical and heat loss characteristics together with a computer simulation model of the thermosyphon circulation in single-ended tubes to

evaluate the performance of water-in-glass type evacuated tube solar water heaters. The performance of this system was compared to flat plate collectors and was found to be lower than a typical two-panel flat plate collector. In an earlier study, Morrison et al. (2004) note that the water-in-glass concept has been found to be the most successful due to its simplicity; however, the operating pressure of the heat transfer fluid is limited to a few metres of water head.

The water-in-glass type of evacuated tube is most commonly used for solar water heating due to its high thermal efficiency compared to heat-pipe (metal-in-glass) types, simpler construction requirements and lower manufacturing costs. The system typically consists of 15-40 flooded single-ended tubes directly connected to a horizontal solar hot water storage tank. The absorber portion of the water-in-glass evacuated tube consists of two concentric glass tubes sealed at one end with an annular vacuum space and a selective surface absorber on the outer surface of the inner tube. Water fills the hollow of the tube and the heat transfer is driven by the natural convection of water between the open end of the tube and the solar hot water storage tank. As the water in the tube is heated by solar radiation, it rises to the top of the tube and into the storage tank where it is replaced by cooler water from within the tank. The natural circulation flow rate of the water between the evacuated tube and solar hot water storage tank depends on the following factors: heat input per unit absorber area, solar hot water storage tank temperature, collector inclination, tube length to diameter ratio, circumferential heat flux distribution (Budihardjo and Morrison 2009).

Other evacuated tube collectors use a solid metal rod attached to the absorber to fulfill the heat transfer role. The rod extends out the end of the glass tube and is plugged into a manifold, much like the heat-pipe design. As the sun shines on the absorber, heat is transferred to the metal rod, which conducts the energy to its tip, and then to a heat-transfer fluid flowing through the manifold (Ramlow 2006).

Other evacuated tube collectors have a hollow pipe, usually copper, fastened to or in contact with the absorber surface via a conductive metal such as aluminum fins. The hollow copper pipe is closed at the end within the glass tubes and the other end terminates with a slightly larger diameter condenser tip, outside the glass tube and sealed by a rubber gasket to prevent moisture from entering the space between the glass and the copper. A small quantity of liquid within the copper pipe, usually a couple of drops of distilled water, is heated by heat transfer between the absorber glass and the copper, vaporizes, and rises to the condenser end. Here it condenses, and in the process, releases its energy to the heat transfer fluid flowing past the condenser ends of the evacuated tubes within the manifold. The condensed water drops back down the hollow copper pipe to be heated again. This design is referred to as a heat-pipe type of evacuated tube, and is the type used for the research presented in this thesis. Figure 2.1 indicates the elements of a single, heat-pipe type of evacuated tube.

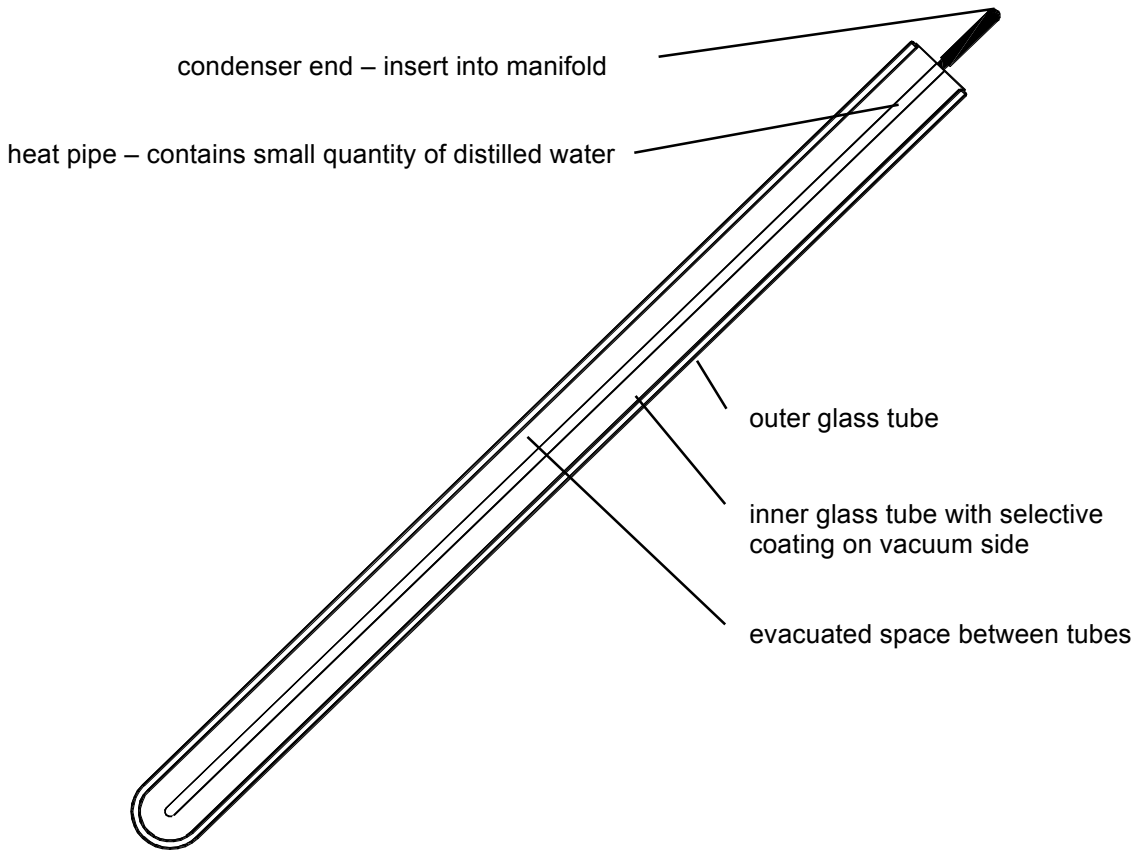

Figure 2.1. Main elements of an evacuated tube.

In turn, the heat transfer fluid passes its heat energy on to either water, by flowing through a heat exchanger within a hot water storage tank in the case of water heating, or simply radiates out into a space or a massive floor, in the case of space heating. A photograph of the solar panel, including the manifold and inlet and outlet lines, is provided in Figure 2.2.

Figure 2.2. A photograph of a panel of evacuated tubes installed into the manifold. The panel is mounted at an angle of approximately 45 degrees.

2.2.3 Test Procedures from Existing Standards

A number of standard test procedures exist for the determination of system efficiency as it pertains to solar domestic hot water systems. Although the issue in question relates to the efficiency of the evacuated tubes themselves, these standards provide basic guidelines and many useful considerations.

The Canadian Standards Association's (CSA) standard number CAN/CSA-F379.1-88 (1988a) is concerned with the performance, durability, and safety of packaged solar domestic hot water systems, as proposed by a manufacturer, designed for use in small buildings. The standard exists to evaluate solar domestic hot water systems meant for year-round operation that are based on liquid heat transfer to a liquid storage medium. Section 8.7 of this standard describes a thermal performance test, with reference to American National Standards Institute/American Society of Heating, Refrigerating and Air-Conditioning Engineers (ANSI/ASHRAE) Standard 95. The purpose of this thermal test is "to determine the net solar energy delivered by a system when tested under

simulated standard weather and load conditions representative of year-round operation of the system" (CAN/CSA 1988a).

CAN/CSA-F378-87 (1988b) is more specific in its intentions than CAN/CSA-F379.1-88, noting that it is applicable to solar collectors capable of converting solar energy into thermal energy, including such technologies as glazed and unglazed flat plate collectors, vacuum envelope collectors, concentrating collectors, and boiling/condensing collectors. The standard is restricted to collectors having an aperture area of less than 0.5 m^2, those designed for fluid temperatures greater than 300°C, and to boiling collectors requiring a separate condensing heat exchanger (CAN/CSA 1988b). In addition, the collector must be capable of being tested independently with forced circulation of the heat transfer fluid (CAN/CSA 1988b). Unlike CAN/CSA-F379.1-88, this standard allows for outdoor testing of the apparatus, outlining the requirements of such a set-up, providing that indoor testing is prohibitive.

Both CAN/CSA-F378-87 and CAN/CSA-F379.1-88 make reference to ANSI/ASHRAE Standards 93 and 95. This research derives its analysis from ASHRAE Standard 93-2003: Methods of Testing to Determine the Thermal Performance of Solar Collectors. The purpose of this standard "*is to provide test methods for determining the thermal performance of solar energy collectors that use single-phase fluids and have no significant internal energy storage* (American Society of Heating, Refrigerating and Air-Conditioning Engineers, Inc. 2003)*."*

Other test methods cited in the literature by many authors (Carvalho and Naron 2001; Marshall 1999; Morrison et al. 2003) are the International Standard Organization (ISO) ISO 9459-2 and 9459-5.

2.2.4 Test Procedures Proposed in the Literature

Most of the literature indicates a similar approach to the efficiency measurement of solar collectors. In general, the incident radiation is measured and compared to the output of the system in terms of temperature rise of the working fluid or the storage fluid, in effect producing an energy balance for the system. The resulting ratio of input to output energy is the efficiency of the system.

Morrison et al. (2003) investigated the performance of water-in-glass type evacuated tubes using the International Standard Organization test method ISO 9459-2, noting that this method of heat extraction, in which absorbed heat is conducted through an inner glass wall directly in contact with the heat transfer fluid, has been the most successful method due to its simplicity of design and low manufacturing cost. Carvalho and Naron (2001) also used International Standard Organization test methods to determine the efficiencies of various collector types. In particular, the objective was to compare the Dynamic System Testing (DST) test method, ISO 9459-5, with the Collector and System Testing Group (CSTG) test method, ISO 9459-2. Marshall (1999) expanded upon the test method presented in ISO 9459-5 by proposing a generalized performance model, stating that pipe losses cannot be ignored when determining overall system performance.

Nagaraju et al. (1999) tested the performance of a single flat plate collector and that of two flat plate collectors in series in accordance with the ASHRAE Standard 93 suggested test methods. In short, the performance was calculated based on the amount of net useful heat gain by the collector to the total solar radiation incident on the solar collector absorber surface throughout the duration of the test. Single collector efficiency was found to be approximately 60%, while that of the array was around 52%. The decrease in efficiency associated with a series configuration is a result of increased inlet temperature to the second panel, resulting in a decreased temperature difference and a corresponding drop in energy acquisition (Nagaraju et al. 1999).

Although the test methods presented in the standards appear to be common practice for determination of system efficiency, some researchers have opted to create their own unique methodology. Mathioulakis and Belessiotis (2001) investigated the performance of a heat-pipe type solar hot water system both theoretically and experimentally. The experimental apparatus consisted of a typical flat plate collector of 1.8 m x 1.0 m dimensions and a 95 L water storage tank. Several physical quantities were measured, including the temperature at several locations within the evaporator, the condenser and the tank; the absolute pressure within the heat-pipe; the ambient air temperature; and the solar irradiance. After making a number of assumptions regarding heat loss throughout the system, an energy balance of the system was used to determine the useful energy gain. The authors state a number of general conclusions for the typical operating conditions, temperature distributions and energy transfer in heat-pipes as follows: high instantaneous efficiencies of approximately 60% were achieved, the system operated

under a wide range of temperatures, and finally that the system operated effectively even as the temperature difference between the collector and tank decreased.

Other researchers chose to use a theoretical, model-based approach to determine the efficiency of the solar collector systems in question. El-Nashar (2003) employed the computer simulation program SOLDES, which had been previously verified to be a reliable tool, to investigate the performance of a solar desalination plant as a function of glass transmittance as affected by dust accumulation on the evacuated tube collector field. Similarly, Tsilingiris (1996) and Yohanis et al. (2005) both chose to utilize the TRYNSYS computer simulation model. While Yohanis et al. (2005) used the program to simulate a solar water heating system to determine the number of days in each month that solar heated water would meet set temperature demands, Tsilingiris (1996) used the TRYNSYS model to validate the results of his own intermediate complexity computer simulation model. Other models mentioned in the literature are the WATSUN, Polysun, and F-Chart simulations models (Kalogirou 2004).

Budihardjo and Morrison (2009) chose to use the computer simulation program TRNSYS to predict the long term performance of the solar water heater rather than experimentation, to reduce costs and time required to conduct the study.

3 Materials and Methods / Procedures

3.1 Collector Configurations

Through extensive review of the literature, a test procedure outlining the steps required to obtain the efficiency of an evacuated tube itself, without consideration of the application, be it water or space heating, was not found. However, much has been written on the entire system efficiency of solar collectors, from that of flat plate to evacuated tube collectors in various applications, though mostly for domestic or industrial water heating purposes. Thus, a new methodology must be proposed here to fulfill the objective of this project.

As previously mentioned, most of the research to date employs an energy balance in which the incident radiation is measured and compared to the output of the system, resulting in a ratio of input to output energy, or the efficiency of the system. In the present work a similar approach was taken to investigate the performance of a heat-pipe type of evacuated tube.

To accurately determine efficiency, the incident radiation was measured simultaneously with the temperature rise of the heat transfer fluid or of the condenser end of the heat pipe itself. In addition, the ambient temperature both inside and outside of the straw bale building was measured. As with Sharma et al. (2004) the incident radiation was measured with a pyranometer. An Agilent data acquisition system with Benchlink software was used to collect both the solar radiation and temperature measurements.

The following five collector configurations were investigated to determine base line, or standard operating conditions. Except for 3.1.1, Single Tube Efficiency, each configuration required one 32-tube collector, for a total of four collectors. The time frame allotted for data collection on a whole was approximately one and a half years, beginning in July of 2008, and concluding in January of 2010. However, the actual amount of time dedicated to each collector configuration varied due to setup time and system malfunction.

Each collector was set up on top of a 10' long by 5' high scaffold. The scaffold was anchored to the ground by tension webbing tied to 3' screw piles. Four scaffold systems were set up in a line on the south side of the strawbale building at the Alternative Village, on the University of Manitoba Fort Garry Campus. The distance between the scaffold/panel set up and the south-facing wall was approximately 15 ft. There were no shading structures in front of the collectors; they received full sun exposure all day. A platform was constructed on top of the scaffold, behind the collectors to allow for ease of access for installation, measurement, and maintenance.

Figure 3.1 is a labeled photo of the collectors taken facing the bale building indicating the overall panel installations and set up. Figures 3.2 and 3.3 are labeled photos of the control panels and accompanying apparatus, taken from inside the bale building.

1 = Mini manifold and single evacuated tubes
2 = Panel 4
3 = Panel 3
4 = Panel 2
5 = Panel 1
6 = Manifold inlet
7 = Manifold outlet
8 = Pyranometer
9 = PEX tube runs from panels
10 = PEX tube run into bale building (through wall)
11 = Tension straps and screw pile
12 = Scaffold
13 = Platform
14 = South facing side of strawbale building

Figure 3.1. Photo of the collectors taken facing the bale building indicating the overall panel installations and set up.

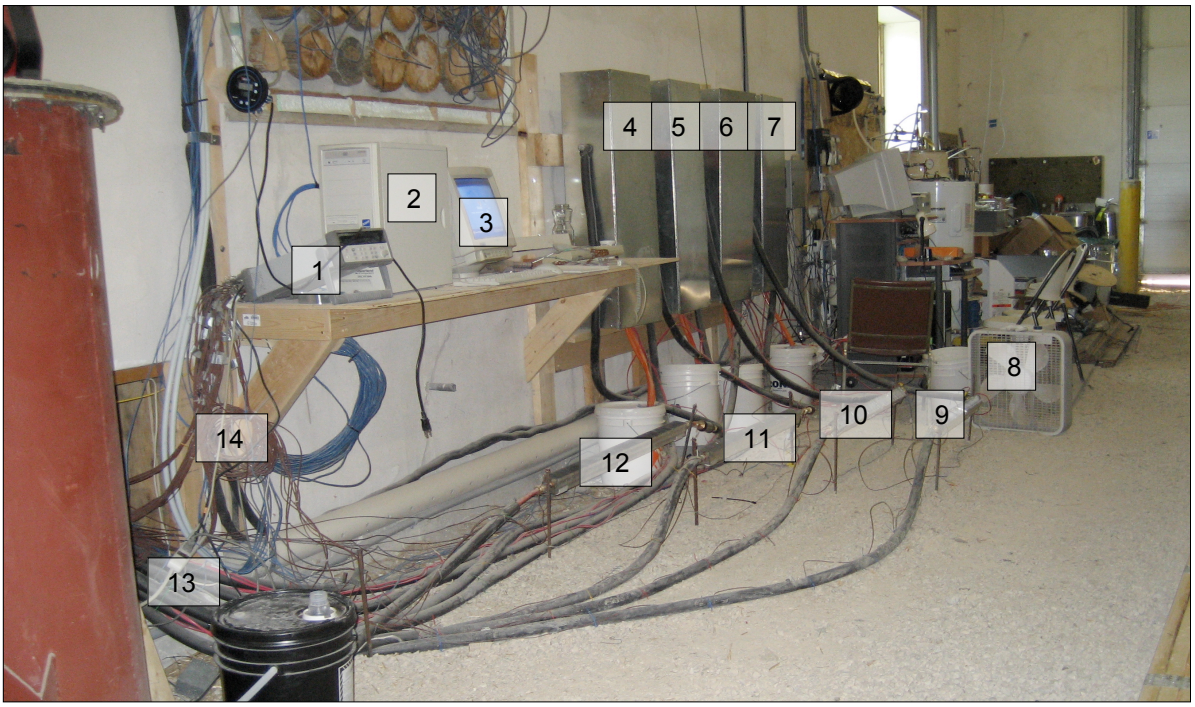

1 = Agilent data acquisition system
2 = Computer
3 = Monitor
4 = Control panel 1
5 = Control panel 2
6 = Control panel 3
7 = Control panel 4
8 = Box fan
9 = Fin tube heat exchanger 4
10 = Fin tube heat exchanger 3
11 = Fin tube heat exchanger 2
12 = Fin tube heat exchanger 1
13 = PEX tube run out of bale building (through wall)
14 = Thermocouple wire

Figure 3.2. Photo of the control panels, fin tube heat exchangers, data acquisition, and accompanying apparatus, taken from inside the bale building.

1 = Control panel
2 = Control panel inlet
3 = Control panel outlet
4 = Fin tube heat exchanger outlet
5 = Fin tube heat exchanger
6 = Fin tube heat exchanger inlet
7 = Box fan
8 = Draindown reservoir

Figure 3.3. Photo of the control panels, fin tube heat exchangers, box fan, and draindown reservoirs, taken from inside the bale building.

3.1.1 Single Evacuated Tube

The output of a single evacuated tube was quantified by measuring the temperature increase of the condenser end of the heat pipe as a function of time, with measurements taken at a maximum of 5-minute intervals, as the tube was subjected to solar radiation. The condenser end was seated into a miniature manifold. The single tube was set up in the same location as the other collectors.

3.1.2 Collector 2 at 50º to Horizontal, Intermediate Flow Rate (Control)

As noted by Duffie and Beckman (2006), solar collectors are most efficient when mounted at an angle equal to the latitude of the site. Winnipeg is located at 50º N latitude, thus the collector was mounted at a similar angle. The intermediate pump flow rate of the Armstrong Astro 3-Speed pump, 4.92 lpm (1.3 gpm), was used to simulate an actual installation.

This configuration represents the standard for comparison for every other collector efficiency test. In each of the tests described hereafter only one variable will differ from those described here, such as the angle, flow rate, or other.

The paragraphs to follow provide an explanation of the methodology for efficiency measurement for the various collector configurations under investigation.

The temperature rise of the heat transfer fluid, an equal part mixture of propylene glycol and water, was measured at the inlet and outlet ends of the collector manifold.

To obtain a continuous energy demand, the heat transfer fluid loop passed through a fin tube heat exchanger which was open to ambient conditions within the strawbale building, thus promoting the maintenance of a temperature difference by providing a heat sink into which the heat transfer fluid could unload its energy. Figure 3.4 is a schematic of the set-up for the various panel efficiency measurements, indicating the direction of flow of the transfer fluid.

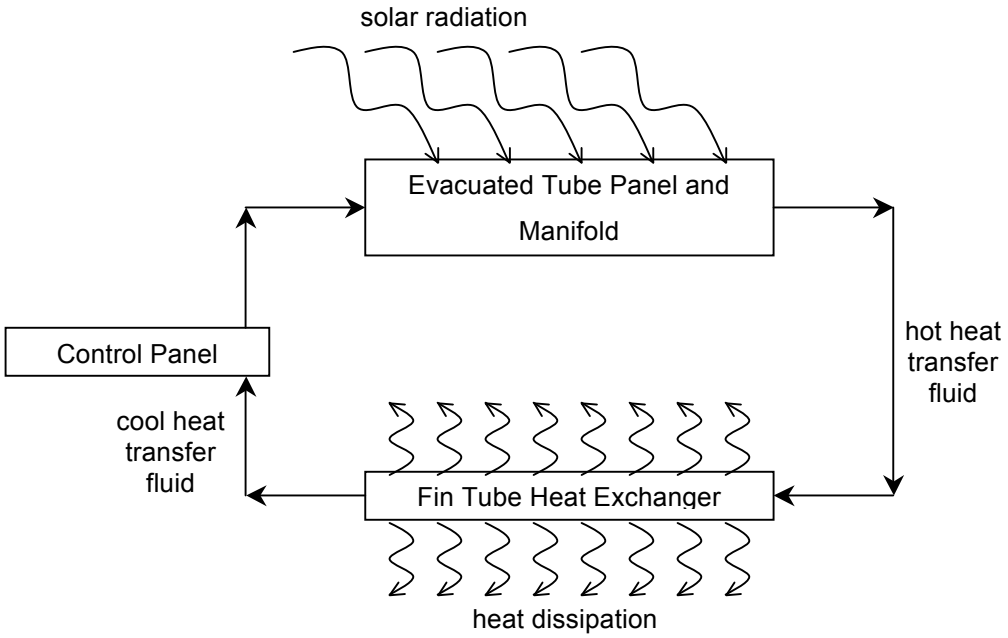

Figure 3.4. Flow diagram of the heat transfer fluid flow through the evacuated tube collector system.

A temperature rise indicated the quantity of energy that the evacuated tube was able to extract from the incoming solar radiation, or in other words, it represented the usable energy obtained. The collector configurations are more accurate representations of the service conditions since the specific heat of the heat transfer fluid, and the ability of the condenser end to transfer energy to this fluid must be considered. Thermocouples were used for temperature measurements. Of the literature reviewed, this approach is most

similar to that taken by Mathioulakis and Belessiotis (2001) in which the operation parameters of the heat-pipe itself are specifically investigated.

3.1.3 Collector 1 at 50º to Horizontal, Intermediate Flow Rate, Covered

Evidence in the literature indicates a decrease in collector efficiency as a result of dust accumulation in the summer, and snow accumulation in the winter, on the evacuated tubes. It is implied that due to the shape of the tubes and the close proximity of adjacent tubes, cleaning and snow removal may prove to be difficult. To alleviate this loss, it is proposed that a glazing material, either glass or plastic, depending on the durability and physical properties of the material, be mounted in front of the evacuated tubes, to facilitate cleaning and snow shedding. For the purposes of this investigation, Suntuf corrugated polycarbonate panels were installed over one evacuated tube collector and the effect on collector efficiency was measured. The intermediate pump flow rate of the Armstrong Astro 3-Speed pump, 4.92 lpm (1.3 gpm), was used.

3.1.4 Collector 3 at 50º to Horizontal, Increased Flow Rate

Increasing the flow rate of the heat transfer fluid, in theory, should increase the efficiency of a panel of evacuated tubes as it maintains a larger temperature difference across the manifold by removing heat energy at a greater rate. This increase in flow rate was accomplished by running the Astro3-Spreed circulation pump on its highest setting,

corresponding to a flow rate of 5.58 lpm (1.475 gpm) in this setting. The efficiency loss or gain, if applicable, was compared to the standard efficiency obtained in 3.1.2.

3.1.5 Collector 4 at 90º to Horizontal, Low Flow Rate (Grundfos Pump)

The efficiency of a panel mounted at an angle of 90º to the horizontal is of interest to determine the feasibility of creating solar collector walls, with the collectors mounted flush with the wall to reduce the possibility of snow accumulation on and between the tubes, which could prove to be difficult to remove on large, tall walls. The rationale for this test is to evaluate the potential for vertical installation of collectors within a south-facing wall in a residential, commercial or industrial application. If the collector performs well then it is proposed that building designers could include a set of collectors within as an architectural and functional feature for new buildings or renovations. The intermediate pump flow rate of the Grundfos circulation pump, 6.34 lpm (1.675 gpm), was used. The efficiency loss or gain, if applicable, was compared to the standard efficiency obtained in 3.1.2.

It is expected that the efficiency of the vertical collector will be greater than that of the control during the winter months due to more direct incident solar radiation. This may be supported by the findings of Budihardjo and Morrison (2009), who although they did not test a vertical panel, found that as the inclination of the collector was increased to 45°, the annual savings during the winter months was 12% higher than when the collector was mounted at 22°.

3.1.6 Collector 3 at 50º to Horizontal, Intermediate Flow Rate, 16 Tubes Removed

As previously mentioned, through plotting the temperature of the condenser ends as a function of location within the manifold it should become apparent, if the plot plateaus, whether or not the efficiency of the collector is a function of the number of tubes per collector. To verify this theory, 16 adjacent tubes, half of the total number of tubes in a full collector, were removed from the manifold and once again the efficiency of the panel was measured. The intermediate pump flow rate of the Armstrong Astro 3-Speed pump, 4.92 lpm (1.3 gpm), was used. The efficiency loss or gain, if applicable, was compared to the standard efficiency obtained in 3.2.2.

3.2 Description of Copperhill Evacuated Tube Collectors

The evacuated tube collectors used in this research project were designed and manufactured by Copperhill Alternate Energy Inc., an Ontario based company. The TM-32 collectors consist of 32 all-glass tubes and a stainless steel manifold mounted on a stainless steel frame.

The condenser ends of the evacuated tubes seat into sockets in a copper manifold inside of a polyurethane foam and fiberglass insulated stainless steel header cylinder. The header is 2.215 metres in length and 0.170 metres in diameter.

The tubes themselves are manufactured out of borosilicate glass, with an outer tube diameter of 47 mm and a length of 1.43 metres. The chemical composition of the absorptive coating is unknown as it is considered proprietary information. The total gross area of the collector is 3.429 m^2.

The heat transfer fluid is a mixture of 50% propylene glycol and 50% distilled water.

3.3 Description of the Pyranometer

The device proposed for the purposes of this research project was the CMP11 Kipp & Zonen Thermopile Pyranometer distributed by Campbell Scientific. This pyranometer is capable of measuring natural sunlight, most types of artificial light, and reflected solar radiation. With a measurement waveband of 310 to 2800 nm, a maximum irradiance of 4000 W/m^2, and an expected daily accuracy of 62%, this equipment is recommended for thermal collector testing. In addition, this particular device may be used under plant canopies or lamps, cloudy conditions, or for reflected radiation measurements. The versatility of this pyranometer will allow it to be used for subsequent research on solar technologies.

3.4 Description of the Circulation Pumps

Although it was requested upon ordering the evacuated tube collectors that all four collectors be identical in design and manufacture, three of the four collectors arrived with

Armstrong Astro 30-3 circulation pumps installed, while another was assembled with a Grudnfos UPS 15-58 FC pump.

The Armstrong Astro 30-3 circulation pump is a three-speed pump with an operation range of 0-20 USgpm while the Grudnfos UPS 15-58 FC circulation pump is also a three speed pump with an operation range of 0-17 USgpm.

The difference in pump make and model had direct effects on the theoretical circulation flow rates and thus calculation of efficiencies.

3.5 Description of the Flow Rate Determination

It was not within the project budget to obtain a digital flow meter, nor did it prove possible to find a flow meter that could accurately measure the flow rate of the heat transfer fluid, given that the flow rates were very low and the temperature very high. Thus, the theoretical flow rate of the two pumps was estimated via the use of the pump curves and empirical data for PEX tubing in an iterative process. A sample calculation from this iterative process is provided in Section 5, Analysis. The pump curves are provided in Appendix A.

First, the number of sharp 90-degree turns in the pipe run was converted to an equivalent length and added to the longest pipe run. The longest pipe run, 175 ft, was used to be conservative in the estimate. Each collector has eight 90-degree pipe fittings. Each 90-degree turn in the iron pipe has an L_e/D of 30, where L_e is equal to the equivalent length of the fitting and D is the inside diameter of the tubing (1/2") (Fox and McDonald, 1998).

This equates to an equivalent length of 10 ft for all of the 90-degree fittings. Thus, the total working length for flow rate estimations was taken to be 140 ft.

Using the highest temperature available on the PEX tubing empirical data sheets of 180°F (60°C), and starting with an estimate of flow rate equal to 7.57 lpm (2 gpm), a pressure loss per foot of pipe length of 0.15177 ft head/ft of tubing was read off the empirical data chart (UPONOR WIRSBO, 2004). Multiplying this number by 140 ft resulted in a total head of 21.15 ft. Using the second speed performance curves for both pumps (refer to the previous section) it was noted that the total head was too large and did not register on the chart. The aforementioned procedure was repeated iteratively, strategically choosing the starting point lpm (gpm) until the initial estimate was equal to that read off the graph. The resulting flow rates for the Armstrong Astro 30-3 and Grundfos UPS 15-58 FC circulation pumps set to the intermediate speed was determined to be approximately 4.92 lpm and 6.34 lpm (1.3 gpm and 1.675 gpm), respectively. The procedure was repeated for the Armstrong Astro 30-3 circulation pump set to its highest speed with a resulting flow rate of 1.475 gpm.

3.6 Description of the Data Acquisition

An 64 channel, Agilent data acquisition system was used in conjunction with Benchlink software to collect temperature and irradiance data. Type-T thermocouple wire was used to take temperature readings in a number of strategically chosen locations, as listed in Table 1 of Appendix B.

One of the principal components of this research is to investigate whether a 32-tube array is more efficient then one with fewer tubes. Thus, in addition to measuring the inlet and outlet temperatures of the manifold and fin tube heat exchanger, the temperature increase of the condenser ends plugged into the manifold was measured to obtain the heat dissipation trend along the length of the manifold. The difference between the temperature of the condenser ends and that of the heat transfer fluid is directly related to the efficiency of the condenser–manifold interface. Figure 3.5 illustrates the temperature monitoring locations along the length of the manifold, as indicated by the symbol "T".

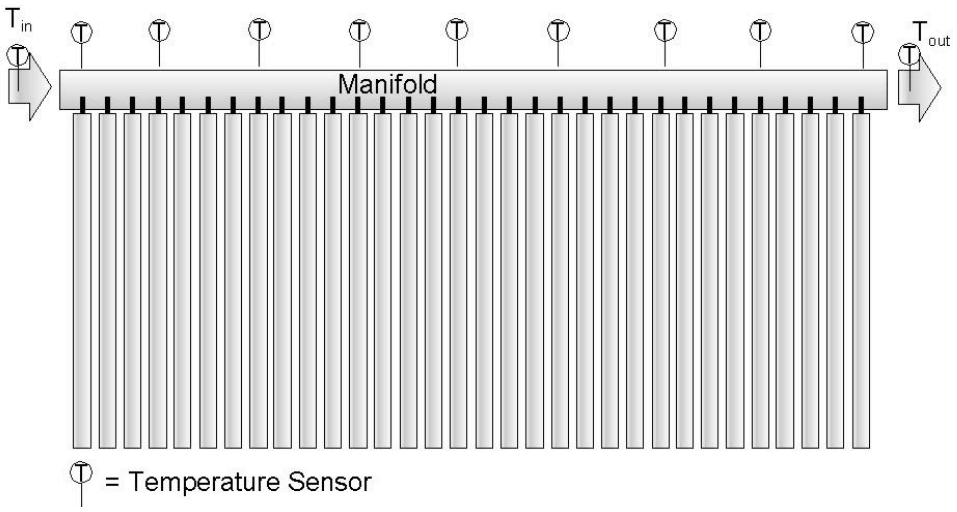

Figure 3.5. Location of temperature measurements along the length of the manifold, as indicated by "T".

Figure 3.6 is a diagram of the labeling convention used for the circuit. M1IN represents the cold side of the manifold, while M1OUT is the hot side, with reference to the temperature of the heat transfer fluid. Similarly, F1IN represents the hot side of the fin tube heat exchanger and F1OUT is the cold side. Numbers 1 through 4 designate which collector the data belongs to.

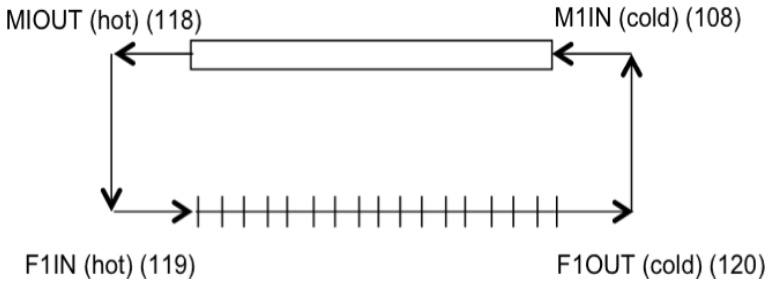

Figure 3.6. Labeling convention used for the circuit.

3.7 Description of Efficiency Measurement Procedures

As previously mentioned, this research derives its analysis from ASHRAE Standard 93-2003: Methods of Testing to Determine the Thermal Performance of Solar Collectors. The purpose of this standard "*is to provide test methods for determining the thermal performance of solar energy collectors that use single-phase fluids and have no significant internal energy storage* (American Society of Heating, Refrigerating and Air-Conditioning Engineers, Inc. 2003).

ASHRAE Standard 93-2003 defines the solar collector efficiency as:

$$\eta_g = \frac{\text{actual useful energy collected}}{\text{solar energy intercepted by the collector gross area}} \tag{3.1}$$

and further defines this mathematically as (American Society of Heating, Refrigerating and Air-Conditioning Engineers, Inc. 2003):

$$\eta_g = \left(\dot{m} c_p \left(t_{f,e} - t_{f,i}\right) \Big/ A_g G_t\right) \tag{3.2}$$

Where: η_g = collector efficiency based on gross collector area, %

$\dot{m}$ = mass flow rate of the heat transfer fluid, kg/s

c_p = specific heat of the heat transfer fluid, J/(kg·°C)

$t_{f,e}$ = temperature of the heat transfer fluid leaving the collector, °C

$t_{f,i}$ = temperature of the heat transfer fluid entering the collector, °C

A_g = gross collector area, m^2

G_t = global solar irradiance incident upon the aperture plane of collector, W/m^2

The mass flow rate of the heat transfer fluid, $\dot{m}$, was derived from the flow rate as follows;

$$\dot{m} = \rho Q \tag{3.3}$$

Where: $\dot{m}$ = mass flow rate of the heat transfer fluid, kg/s

ρ = the density of the heat transfer fluid (kg/L)

Q = the volume flow rate of the heat transfer fluid, L/s

The specific gravity of the heat transfer fluid for each collector was measured with a hydrometer and the average value of was converted to density units and used for analysis purposes. Note also that the units of density are kg/L rather than kg/m^3.

The volume flow rates used were those theoretical values calculated as described in Subsection 3.5 and converted to metric units.

Since the pyranometer was mounted horizontal to the ground, and since the collectors were mounted at either 50 or 90 degrees to the horizontal, the solar radiation as measured by the pyranometer had to be adjusted to reflect the actual global solar irradiance incident upon the aperture plane of collectors. To accomplish this, the ratio of beam radiation on the tilted surface to that on a horizontal surface, R_b, had to be determined (Duffie and Beckman, 2006) (Figure 3.7).

$$R_b = \frac{G_{b,T}}{G_b} = \frac{G_{b,n}\cos\theta}{G_{b,n}\cos\theta_z} = \frac{\cos\theta}{\cos\theta_z} \tag{3.4}$$

Where: R_b = the ratio of beam radiation on the tilted surface to that on a horizontal surface

$G_{b,T}$, $G_{b,,}$ $G_{b,n}$ = are defined in Figure X below, W/m^2

θ = the angle of incidence, degrees

θ_z = the Zenith angle, degrees

Figure 3.7. Definitions of angles in Equation 3.4.

The angle of incidence, θ, is the angle between the beam radiation on a surface and the normal to that surface. The Zenith angle, θ_z, is defined as the angle between the vertical and the line to the sun, which is to say, the angle of incidence of beam radiation on a horizontal surface. β, is the slope of the collector, the angle between the plane of the surface in question and the horizontal.

The following relationship can be used to calculate the angle of incidence of beam radiation on a surface, θ (or θ_z), when certain other angles are known (Duffie and Beckman, 2006).

$$\begin{aligned}\cos\theta = {} & \sin\delta\sin\phi\cos\beta - \sin\delta\cos\phi\sin\beta\cos\gamma \\ & + \cos\delta\cos\phi\cos\beta\cos\omega + \cos\delta\sin\phi\sin\beta\cos\gamma\cos\omega \\ & + \cos\delta\sin\beta\sin\gamma\sin\omega\end{aligned} \tag{3.5}$$

Where:

ϕ = Latitude, the angular location north or south of the equator, north positive; $-90° \leq \phi \leq 90°$.

δ = Declination, the angular position of the sun at solar noon with respect to the plane of the equator, north positive; $-23.45° \leq \delta \leq 23.45°$.

β = Slope, the angle between the plane of the surface in question and the horizontal; $0° \leq \beta \leq 180°$.

γ = Surface azimuth angle, the deviation of the projection on a horizontal plane of the normal to the surface from the local meridian, with zero due south, east negative, and west positive; $-180° \leq \gamma \leq 180°$.

ω = Hour angle, the angular displacement of the sun east or west of the local meridian due to rotation of the earth on its axis at 15° per hour; morning negative, afternoon positive.

θ = Angle of incidence, the angle between the beam radiation on a surface and the normal to that surface.

Further, the declination, δ, may be approximated by the following (Duffie and Beckman, 2006):

$$\delta = 23.45 \sin\left(360 \frac{284 + n}{365}\right) \tag{3.6}$$

Where: n = the day of the year, with day 1 equaling January 1, and using 28 days in February (Therefore, on December 31, n = 365).

All data were collected with the Agilent Data Acquisition System and Benchlink software. Data were manipulated in Microsoft Excel prior to import into Stata statistical software. A program was created in Stata to run the above calculations on data for all four panels, and to further compare the panel efficiencies statistically.

3.8 Description of the Data Reduction and Calculation Procedures

Data were collected every 5 minutes, 24 hours a day, for approximately a year and a half. Data were downloaded on approximately a biweekly basis. Files were saved by date and time of download. Manipulation of the full data set in Microsoft Excel 2004 for Mac was not practical, nor even possible for that matter, due to the shear size of the data set. Thus, more robust software was required to manipulate the data into a workable form. The program used for data analysis and reduction purposes was Intrecooled Stata 9.0 for Macintosh. The programs are provided in Appendix C.

The data sets resulting from the data reduction in Stata were copied into Microsoft Excel 2004 for Mac and used to generate the graphs presented in the Results and Discussion Section to follow. Some further manipulation in Excel was required to produce the desired graphs. In particular, mean daily solar irradiance and efficiency was further reduced to mean monthly solar irradiance and efficiencies for each collector configuration. The graphs themselves are discussed in greater detail in Section 4

4 Results and Discussion

The data lends itself well to graphical rather than tabular representation. Due to the large number of graphs produced from the data analysis, it was deemed more appropriate to combine the Results section with the Discussion section, for ease of reading. Graphs are presented and immediately followed by a discussion of the trends and implications of the findings.

4.1 Collector Configuration Results

In general, except for the single evacuated tube, graphs of collector efficiency as a function of solar irradiance, efficiency as a function of time, solar irradiance as a function of time, and mean daily and monthly efficiency and mean daily and monthly solar irradiance as a function of time were generated in Microsoft Excel 2004 for Mac for each collector and are presented in the following subsections. In the case of the control, additional graphs presenting the efficiency and irradiation as a function of time of day are presented for summer and winter solstice data. In addition, for comparison purposes, Section 4.1.7 overlays the results from each collector onto one graph for efficiency as a function of time and also compares the same data from each collector directly to the control.

Note also the scales on the graphs. For efficiency, the scale range is 0 – 100 %, the minimum and maximum efficiencies. For solar irradiation, the scale ranges from 0 – 1400 W/m^2, the minimum and just past maximum solar irradiation levels. These scale

ranges have been implemented on each graph, to provide a more appropriate depiction of the results without visually skewing the trends with adjusted scales. Therefore, each graph can be directly compared to others of its type.

The following abbreviations were used:

C1 = Collector 1 (Either uncovered or covered with Suntuf panel)

C2 = Collector 2 (Control)

C3 = Collector 3 (Either with increased flow rate or with 16 tubes removed)

C4 = Collector 4 (Vertical)

E1 = Efficiency of Collector 1

E1 (Uncovered) = Efficiency of Collector 1 prior to the installation of the Suntuf Panel

E1 (Covered) = Efficiency of Collector 1 following the installation of the Suntuf Panel

E2 = Efficiency of Collector 2

E3 = Efficiency of Collector 3

E3 (Flow Rate Increased) = Efficiency of Collector 3 with the flow rate increased

E3 (16 Tubes Removed) = Efficiency of Collector 3 following removal of 16 tubes

E4 = Efficiency of Collector 4

4.1.1 Single Evacuated Tube

As mentioned in the Materials and Methods section, the output of a single evacuated tube was quantified by measuring the temperature increase at the condenser end of the heat pipe as a function of time, as the tube was subjected to solar radiation. In this instance the mathematical expression used to calculate panel efficiency (Equation 3.2), was not

considered appropriate for analysis purposes, as there was no load, and therefore no temperature difference (numerator of Equation 3.2). In this case, the efficiency was measured in terms of input solar radiation compared to output temperature as measured at the condenser end of the single tube. Figures 4.1 through 4.3 are plots of the temperature and solar irradiance measurements as a function of time.

The mean daily temperatures were calculated in Microsoft Excel 2004 for Mac by averaging the temperature measurements, taken every 5 minutes, over the duration of each operational hour of the day. As expected, there is an obvious rise and fall in temperature over the course of a day, as can be seen on the "Mean Daily Temperature" line in Figure 9 below. More solar radiation is available for use mid-day, as opposed to morning and late afternoon, and thus, a peak in the "Mean Daily Temperature" curve occurs on each day. Even through light cloud cover, it was observed that more solar radiation was available during the mid-day hours. This was not documented through data analysis and comparison to Environment Canada climate statistics; rather, visual observations were made on a random basis while visiting the project site.

Mean monthly temperatures were calculated in Microsoft Excel 2004 for Mac by averaging the temperature measurements, over the duration of each month. These average temperatures are marked on the graph in Figure 4.1 and connected with a trend line to better observe temperature behavior over the course of the years of measurement. The year 2009 was the only complete year of measurement. It is noted, that as expected, there is a rise in temperature during the spring and summer months, with the highest

temperatures occurring in July and August. Conversely, temperatures decrease from fall to winter, with the lowest temperatures occurring in late winter.

However, there is also a notable constant decrease in temperature over the entire duration of data collection, from July 2008 to January 2010. This could partially be explained by the overly cloudy, rainy and cool spring and summer months of 2009. But the trend may also hint at a subtler, but nonetheless interesting cause; specifically, the possibility that the evacuated tubes degrade over time and lose some capacity to absorb solar radiation. This particular evacuated tube has been installed and exposed to the elements for approximately a year longer than the other four collectors since it was used for an undergraduate research project. Along these lines, it was observed, during collector set up, that prior to installation into the manifold, the seal between the copper heat pipe and the double walled glass tube would be compromised when exposed to the sun. This indicated that the air within this space was heating and expanding to such a degree that the plastic gasket would be pushed out due to the increase in pressure. This also occurred after installation into the manifold. Once this seal was broken, it was observed that dirt and moisture could enter the space between the copper heat pipe and the double walled glass tube, degrading the glass surface and impeding the penetration of solar irradiance.

It should be noted here, that the temperature measurements might not be accurate, as the method of installing the thermocouple wire was found to be unreliable. The thermocouple wire could not be consistently connected to the condenser, and would

move out of place as the tube was installed, as will be explained in greater detail in Section 4.2.

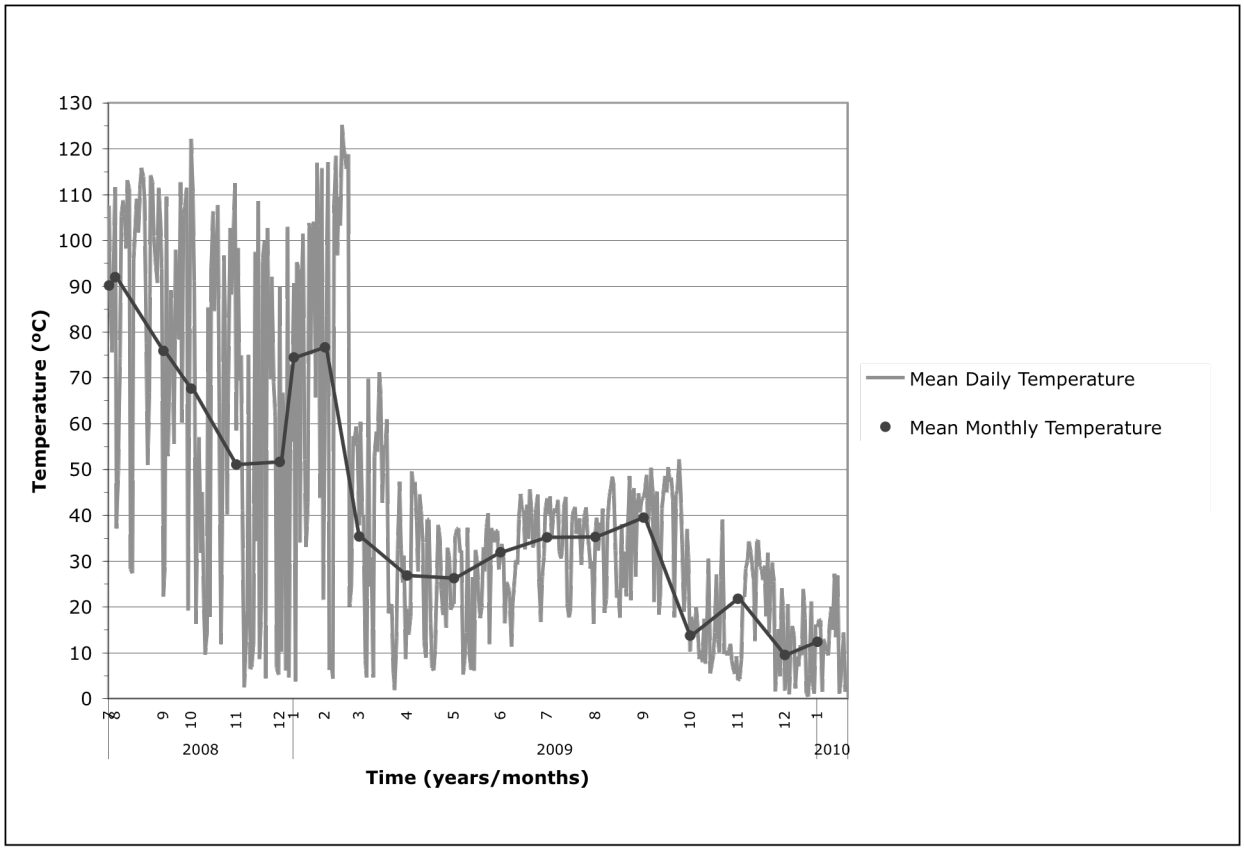

Figure 4.1. Mean daily temperature and mean monthly temperature of the condenser end of the control tube as a function of time of year.

Similarly, the mean daily and monthly irradiances for the single evacuated tube were plotted as a function of time, for the same points and duration used for the mean daily and monthly temperatures described above (Figure 4.2). Although the mean daily solar irradiances vary, for the reasons previously explained, the line of mean monthly irradiance indicates that, in general, solar irradiance tends to increase as spring progresses to summer, with summer having the highest overall irradiance, then decreasing through fall, with winter having the lowest overall irradiances.

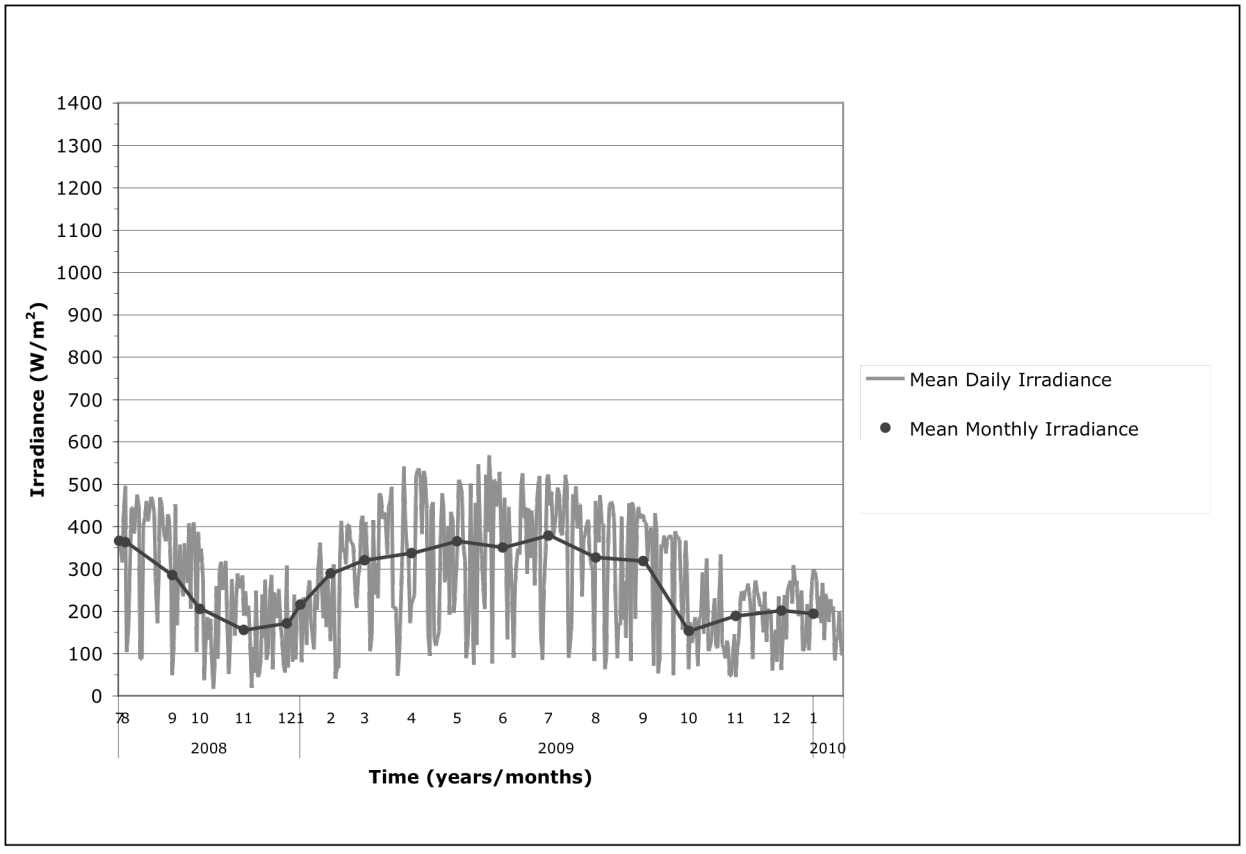

Figure 4.2. Mean daily solar irradiance and mean monthly solar irradiance for the control tube as a function of time of year.

In Figure 4.3, mean monthly temperature and mean monthly solar irradiance for the single evacuated tube were plotted as a function of time to observe the relationship, if

any, between collector temperature and solar irradiance. As previously mentioned in the above graphical analysis, the highest temperatures and highest irradiances occur in the summer months, while the lowest temperatures and lowest irradiances occur in the winter months, and thus both curves follow roughly the same paths albeit on different scales. The two curves begin to converge in the spring of 2009. Temperature measurements were at a low compared to July and August of 2008; approximately 35 degrees lower August 2008 to August 2009. Solar irradiance appears to be similar from summer 2008 to summer 2009, which may contradict the earlier suggestion that the overly cloudy, rainy and cool spring and summer months of 2009 contributed to the lower evacuated tube output.

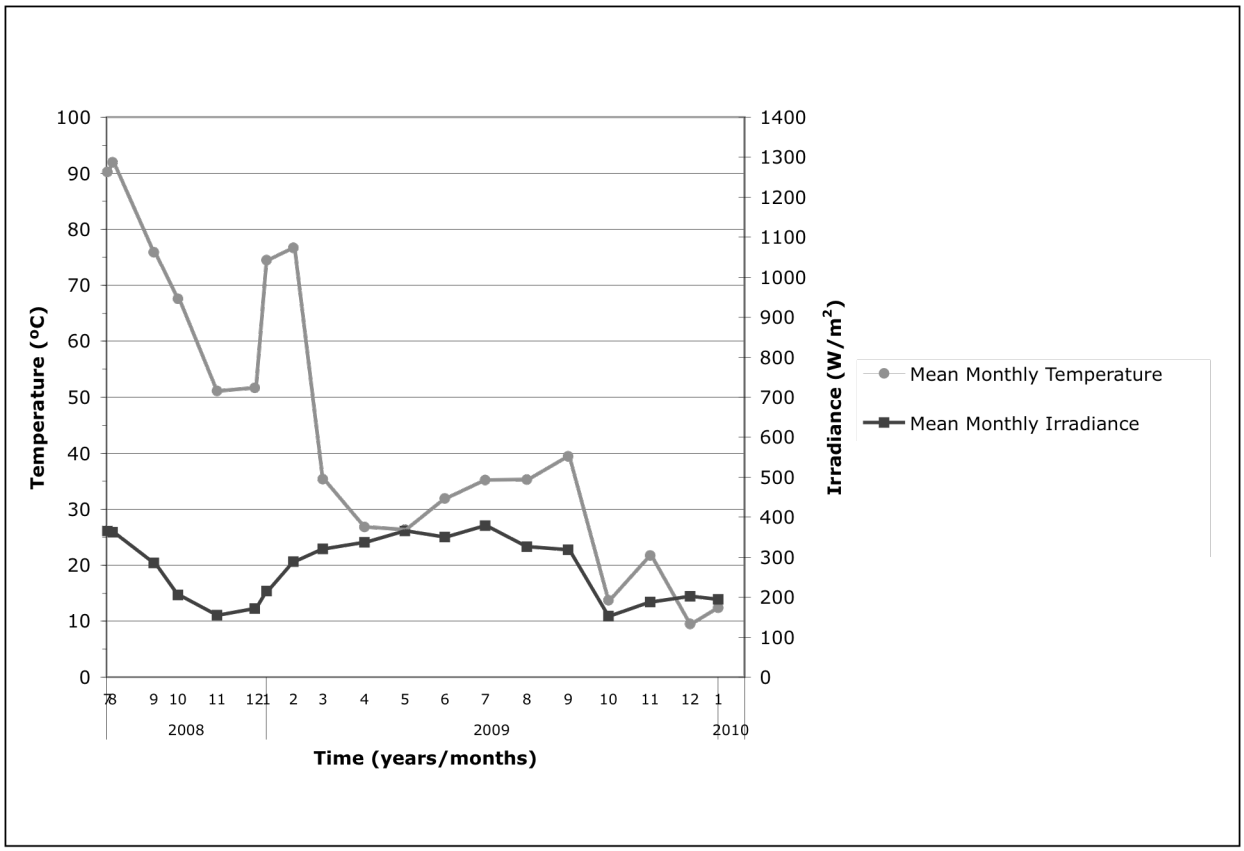

Figure 4.3. Mean monthly temperature of the condenser end and mean monthly solar irradiance of the control tube and irradiance as a function of time of year.

4.1.2 Collector 2 at 50º to Horizontal, Intermediate Flow Rate (Control)

The control collector was set up at 50º to horizontal and the intermediate flow rate on the Astro 3-Speed pump of 4.92 lpm (1.3 gpm). The control will serve as the baseline to which all other collector configurations will be compared. The control configuration was held constant throughout the duration of data collection.

To observe the relationship, if any, between efficiency and solar irradiance, a scatterplot of efficiency of the control collector (collector 2), calculated using Equation 2, as a function of solar irradiance was produced (Figure 4.4). There is no obvious simple geometric correlation, such as linear or exponential, between the two variables. The distribution indicates a density or clustering of points on the low end of the efficiency scale across a wide range of solar irradiance values. The plotted points take on a somewhat negative association with each other; high efficiency values appearing to be more prominent at low- to mid-range irradiance values, and with high irradiance values resulting in lower efficiencies. It is apparent that high efficiencies are not as prominent as those below approximately 20% and that solar irradiance dwindles past approximately1000 W/m^2.

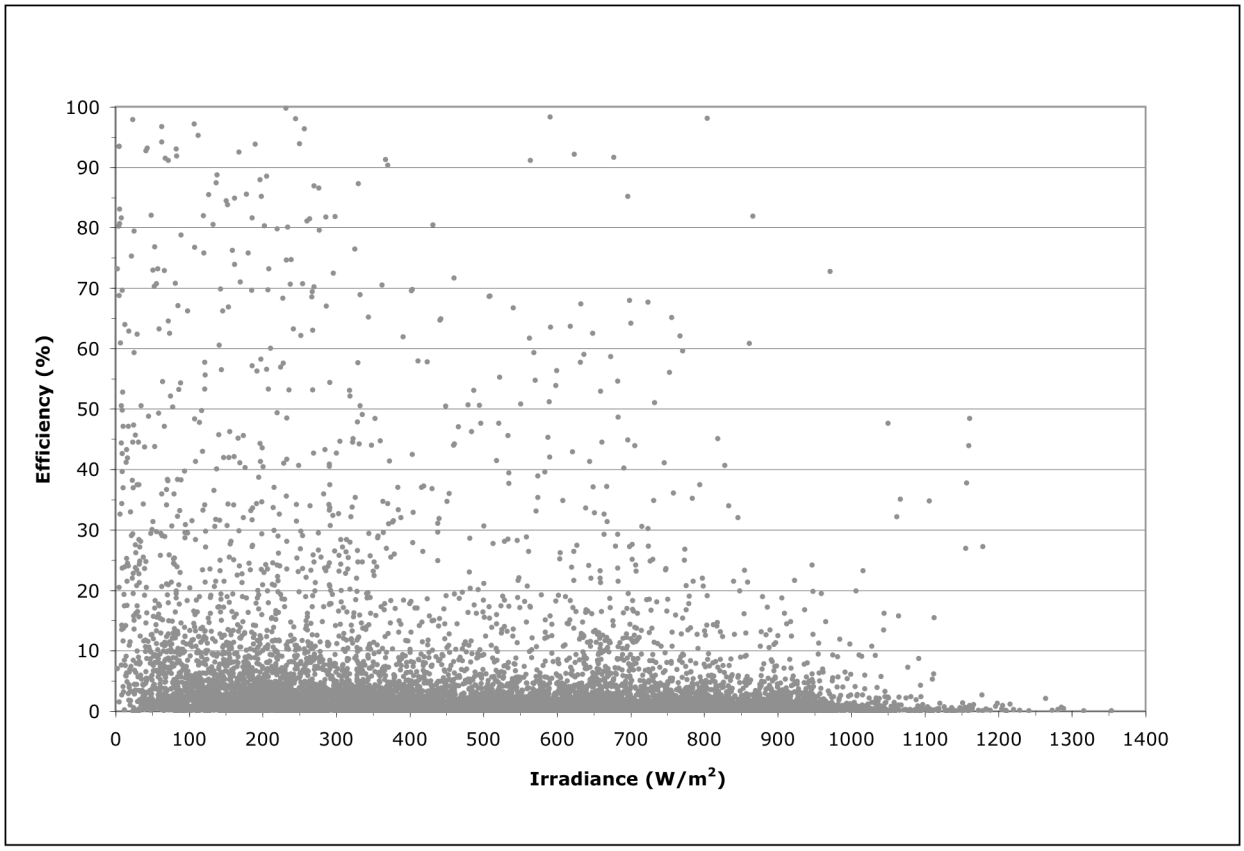

Figure 4.4. Efficiency of collector 2 (Control) as a function of solar irradiance.

The mean daily efficiencies and mean monthly efficiencies of the control collector were plotted as a function of time in Figure 4.5. Although the mean daily efficiencies sometimes vary substantially from day to day, the line of mean monthly efficiency indicates that, in general, efficiencies tend to decrease as spring progresses to summer, with summer having the lowest overall efficiencies, then increase through fall, with winter having the highest overall efficiencies. There is an obvious outlier of approximately 35% in August of 2008, and again in November and December of 2008, when the efficiency was near 2% or less. In 2009 the mean monthly efficiency was more or less level between approximately 2 – 8% over the course of the year, increasing to about 12% efficiency in January of 2010.

The drastic increase in mean daily efficiency for the control (Figure 4.5) may be related to the outliers explained in Appendix C. Through initial plotting of the efficiency data, efficiencies greater than 100% were observed. These data points were outliers and were skewing the graphical analysis. It is possible that a near 100% efficiency value was caused by the same phenomena that created the greater than 100% efficiencies. This value would not have been dropped in the data reduction. The cause of the spikes in efficiency are unknown, as there is no observable or measured reasoning behind them. However, they occurred with enough regularity, twice daily, at about dusk and dawn, to suggest an external cause; perhaps a power surge.

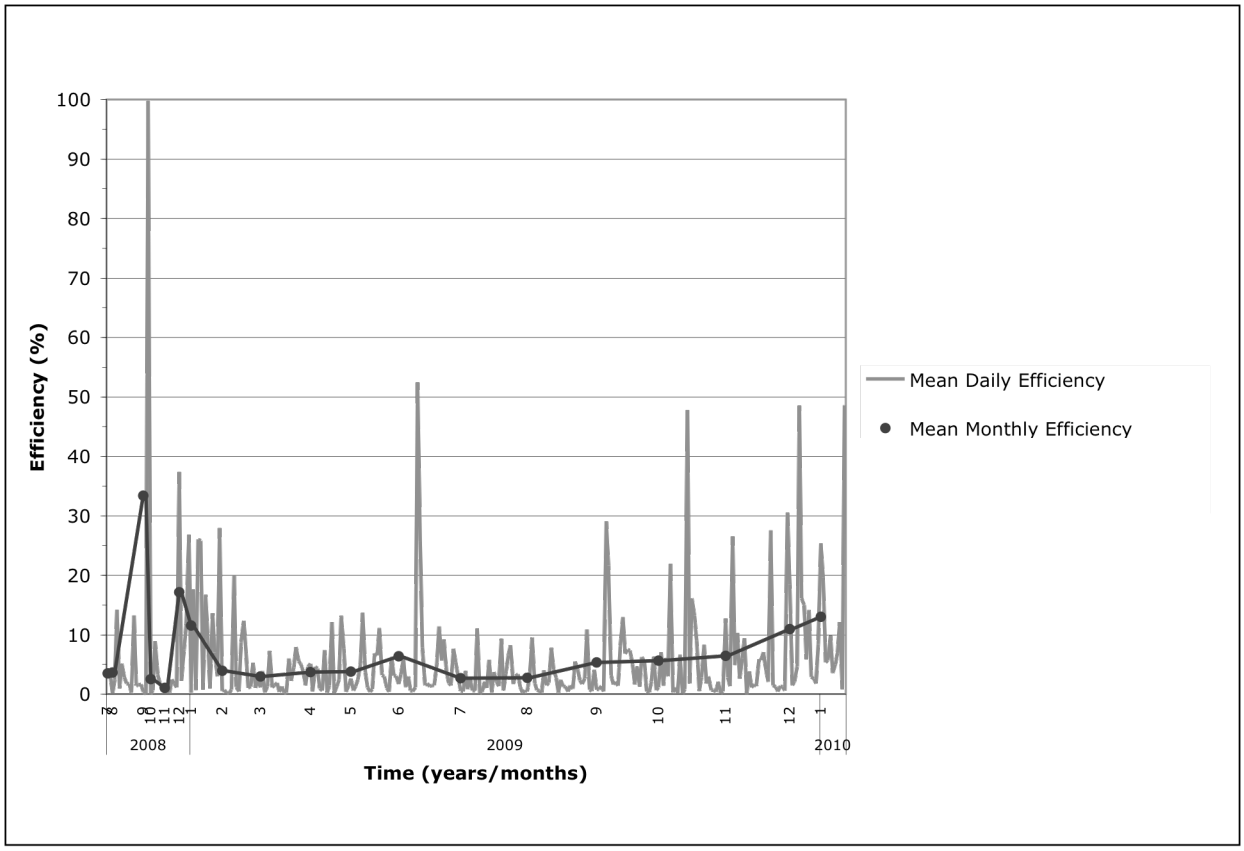

Figure 4.5. Mean daily efficiency and mean monthly efficiency for Collector 2 (Control) as a function of time of year.

The mean daily solar irradiance and mean monthly solar irradiance for the control collector were plotted as a function of time, for the same points and duration used for the mean daily and mean monthly efficiency plot described above (Figure 4.6). Although the mean daily irradiances sometimes vary substantially from day to day, the line of mean monthly irradiance indicates that, in general, solar irradiance tends to increase as spring progresses to summer, with summer having the highest overall irradiance, then decreasing through fall, with winter having the lowest overall irradiances. This is consistent with solar irradiance expectations as reported by Duffie and Beckman (2006). The greatest mean monthly solar irradiance was measured to be approximately 600 W/m^2 in July of 2009.

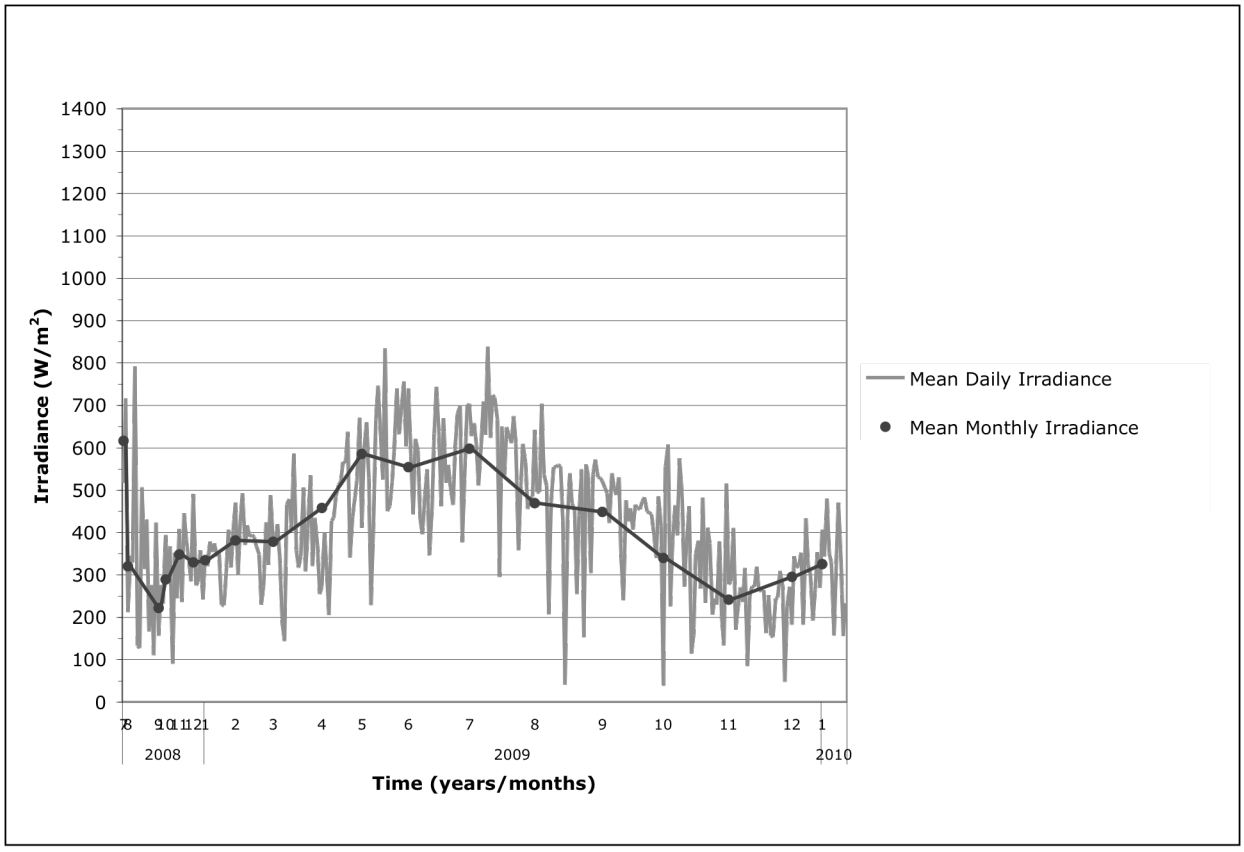

Figure 4.6. Mean daily solar irradiance and mean monthly solar irradiance for Collector 2 (Control) as a function of time of year.

In Figure 4.7, mean monthly irradiance and mean monthly efficiency for the control collector configuration were plotted as a function of time to again observe the relationship, if any, between collector efficiency and irradiance. As previously mentioned in the above graphical analysis, the highest efficiencies and lowest irradiances occur in the winter months, while the lowest efficiencies and highest irradiances occur in the summer months.

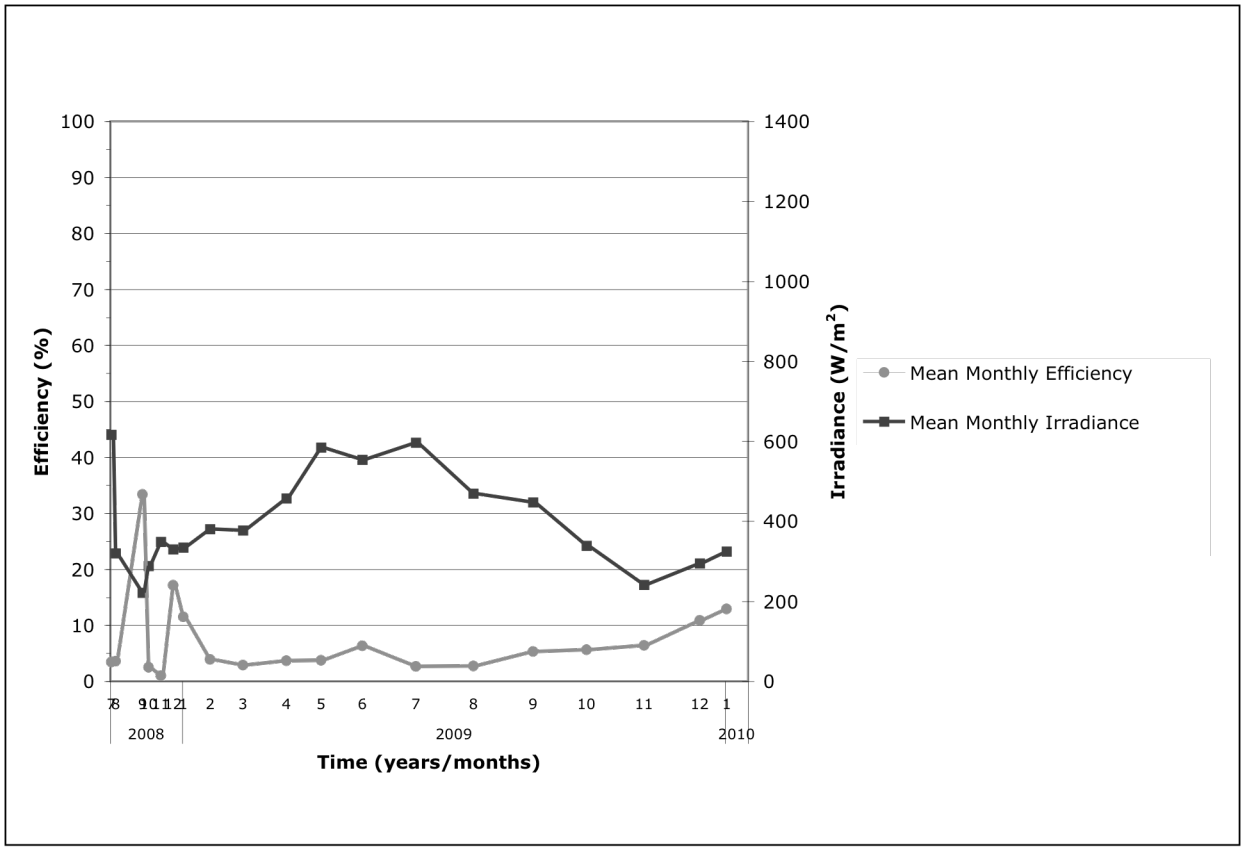

Figure 4.7. Mean monthly efficiency and mean monthly solar irradiance for collector 2 (Control) as a function of time of year.

To further study the relationship between efficiency and solar irradiance, plots of daily efficiency and irradiance were created for the summer and winter solstices. These dates were chosen since they exhibit extreme differences in solar irradiance. This analysis was only conducted on the data for the control panel and is discussed in detail below.

The summer solstice in 2009 occurred on June 21. Daily efficiency and irradiance data for this date were plotted as a function of time of day in Figure 4.8 below. The efficiency line contains a couple of noticeable bumps in an otherwise constant output. The first is an increase at 10 am, then another at 5 pm, and finally a substantial jump in efficiency at 8 pm. There is no obvious explanation for the jumps in efficiency. Otherwise, the efficiency remains quite low, in the range of 1 – 5% or so. The solar irradiance follows a much more predictable curve, increasing from approximately 500 W/m^2 through the morning, peaking at noon at about 875 W/m^2, and then decreasing through the afternoon, with a modest increase at 4 pm, before continuing to decline until 8 pm with a near 0 measurement.

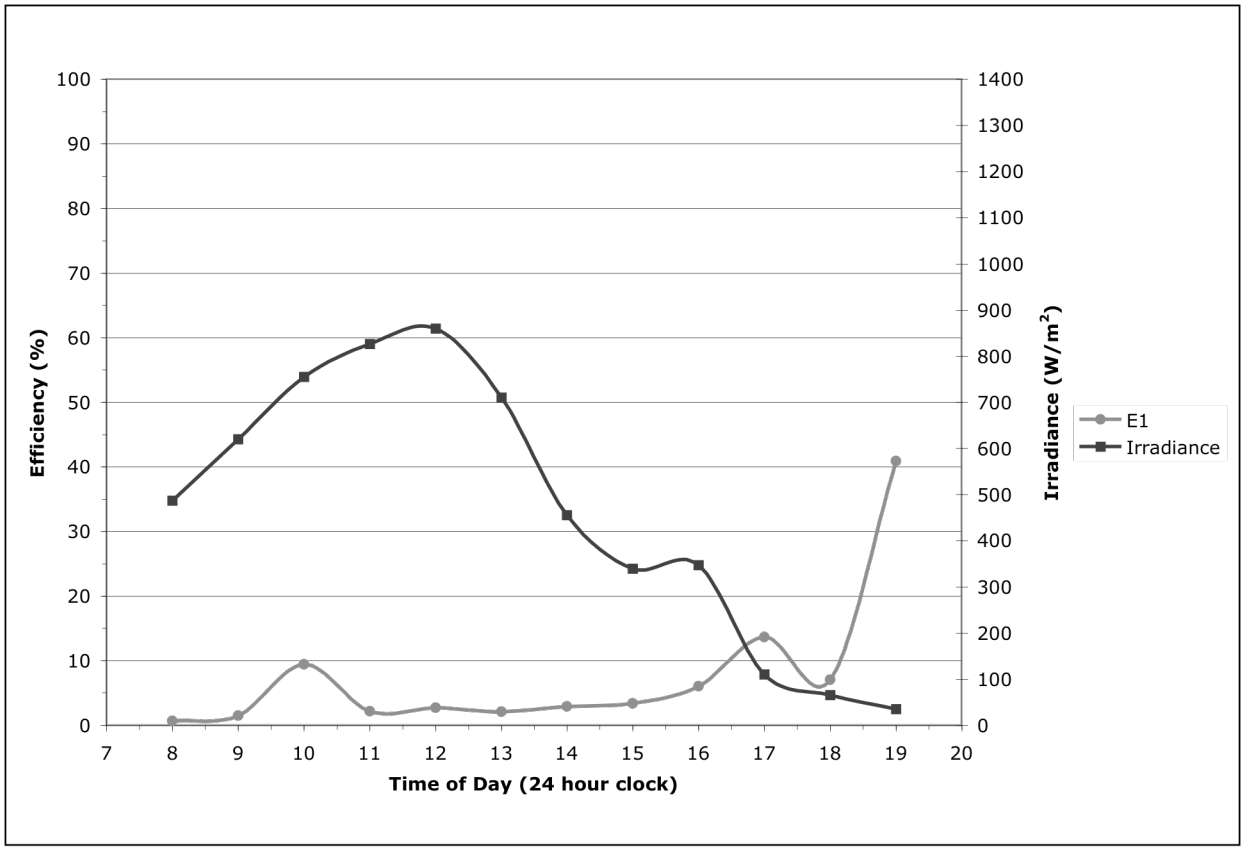

Figure 4.8. Mean daily efficiency and mean daily solar irradiance for Collector 2 (Control) on the Summer Solstice (June 21, 2009).

The winter solstice in 2009 occurred on December 21. Daily efficiency and irradiance data for this date were not available; therefore December 17, 2009 was chosen as the next closest date with data. Daily efficiency and irradiance data were plotted as a function of time of day in Figure 4.9 below. Both lines exhibit very little change over the duration of measurement, with efficiency within the range of 1 - 5 % and solar irradiance hovering around 300 W/m^2. Since the duration of measurement on this date was only four hours, it is difficult to discern any trends in the data from so few data points. Thus, an alternate winter, or cold weather and low solar irradiation, date was sought out.

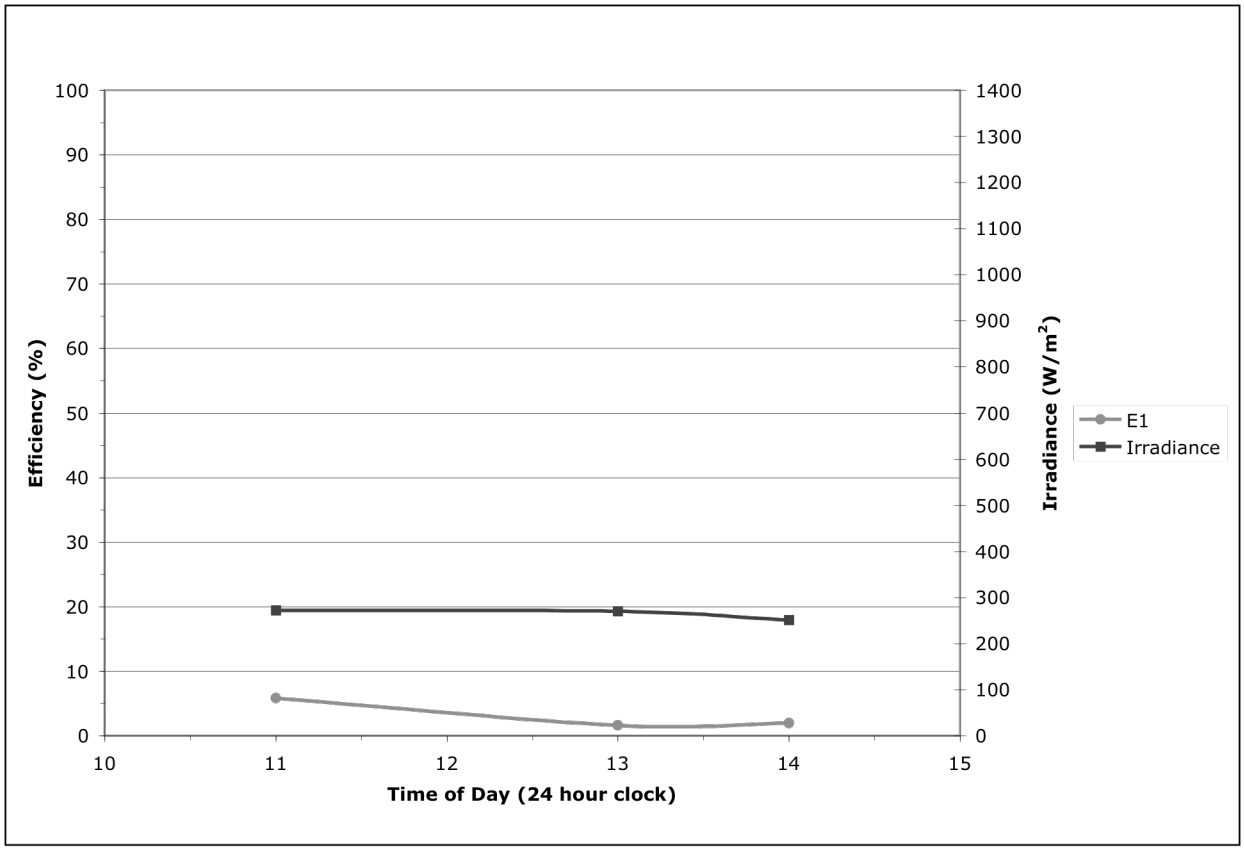

Figure 4.9. Mean daily efficiency and mean daily solar irradiance for Collector 2 (Control) on the near the Winter Solstice (December 17, 2009).

Due to technical difficulties during the winter months, namely the data acquisition system shutting down on a number of occasions, the next closest date with at least six data points was November 24, 2009. Daily efficiency and irradiance data were plotted as a function of time of day in Figure 4.10 below. Again, both lines exhibit very little change over the duration of measurement. Efficiency remains constant between the hours of 10 am and 3 pm within the range of 1 - 2 %. Solar irradiance does exhibit a slight increase from about 250 W/m^2 at 10 am to a peak of approximately 325 W/m^2 at noon, then decreasing through the afternoon, with a modest increase at 2 pm, and finally resting at about 175 W/m^2.

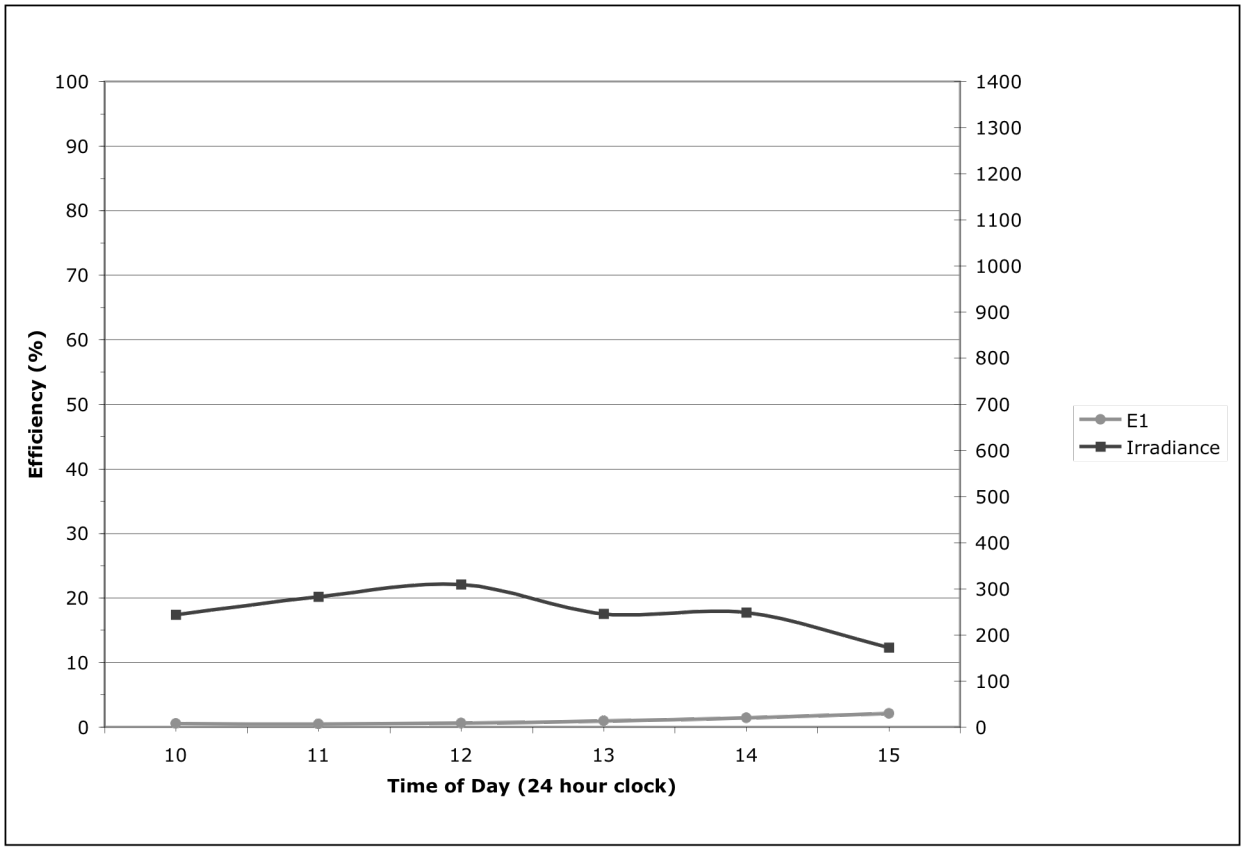

Figure 4.10. Mean daily efficiency and mean daily solar irradiance for Collector 2 (Control) on a day in late fall (November 24, 2009).

From Figures 4.8 through 4.10, there is no obvious correlation between efficiency and solar irradiance as a function of time of day.

In addition to measuring the inlet and outlet temperatures of the manifold, an attempt was also made to measure the temperature of the condenser ends plugged into the manifold to obtain the heat dissipation trend along the length of the manifold. As the difference in temperature, ΔT, decreases, each tube looses its potential to transfer heat to the fluid. It was anticipated that the temperature of the condenser ends would increase along the length of the manifold, as each subsequent tube would be transmitting less energy to the heat transfer fluid. This is due to the temperature increase of the heat transfer fluid as it flows through the manifold. By plotting the temperature of the condenser ends as a function of location along the manifold it should become apparent, if the plot plateaus, whether or not the efficiency of the panel is a function of the number of tubes per panel. A decrease in ΔT indicates minimal contribution of additional tubes connected downstream of the fluid flow, and thus minimal contribution to the overall panel efficiency. One of the principal components of this research is to investigate whether a 32-tube array is more efficient then one with fewer tubes.

After a number of months of data collection, and troubleshooting, it was determined that the temperature readings taken from the condenser ends of the tubes were not accurate. The thermocouple wire could not be consistently connected to the condenser, and would move out of place as the tube was installed. As a result, the temperature readings were

being taken from different points on each tube, resulting in erroneous data. Thus, these data points were dropped from the analysis.

4.1.3 Collector 1 at 50º to Horizontal, Intermediate Flow Rate, Covered

Collector 1 was set up at 50º to horizontal and the intermediate flow rate on the Astro 3-Speed pump of 4.92 lpm (1.3 gpm). From July 2008 to June 2009, the collector was uncovered and was therefore an identical set-up to the control. From June 2009 to January 2009, the collector was covered with a Suntuf panel. Data were collected for both scenarios and will be presented here, starting with the uncovered results.

A scatterplot of efficiency of collector 1 (uncovered), calculated via Equation 2, as a function of solar irradiance was produced (Figure 4.11). The findings are similar to those discussed for the Control in Section 4.1.2. There is no obvious simple geometric correlation, such as linear or exponential, between the two variables. The distribution indicates a density or clustering of points on the low end of the efficiency scale across a wide range of solar irradiance values. The plotted points take on a somewhat negative association with each other; high efficiency values appearing to be more prominent at low- to mid-range irradiance values, and with high irradiance values resulting in lower efficiencies. It is apparent that high efficiencies are not as prominent as those below approximately 10% and that solar irradiance dwindles past approximately 1000 W/m^2.

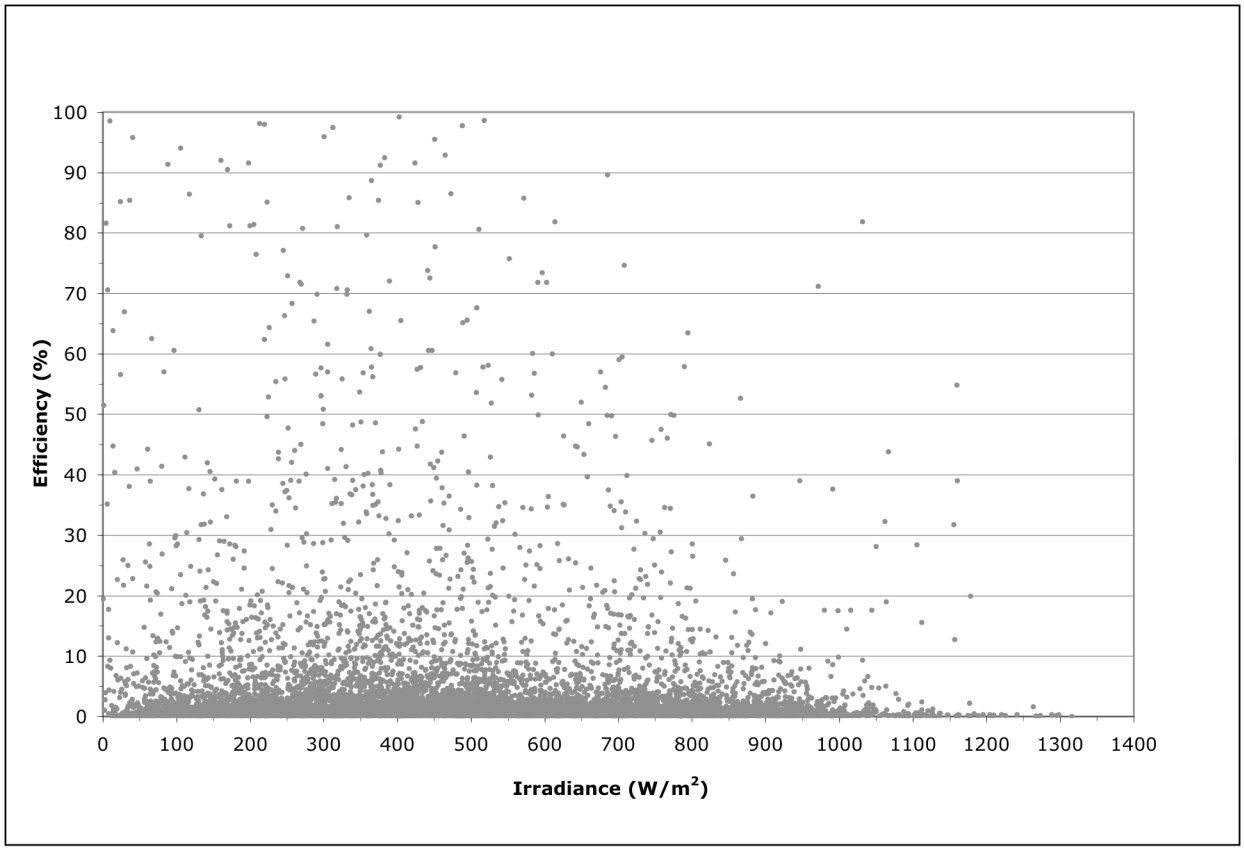

Figure 4.11. Efficiency of collector 1(uncovered) as a function of solar irradiance.

The mean daily efficiencies and mean monthly efficiencies of collector 1 (uncovered) were plotted as a function of time in Figure 4.12. As was found with the control results, although the mean daily efficiencies sometimes vary substantially from day to day, the line of mean monthly efficiency indicates that, in general, efficiencies tend to decrease as spring progresses to summer, with summer having the lowest overall efficiencies, then increase through fall, with winter having the highest overall efficiencies. In 2009 the mean monthly efficiency was more or less level between approximately 2 – 8%. The greatest efficiency, about 12%, occurred in December 2008.

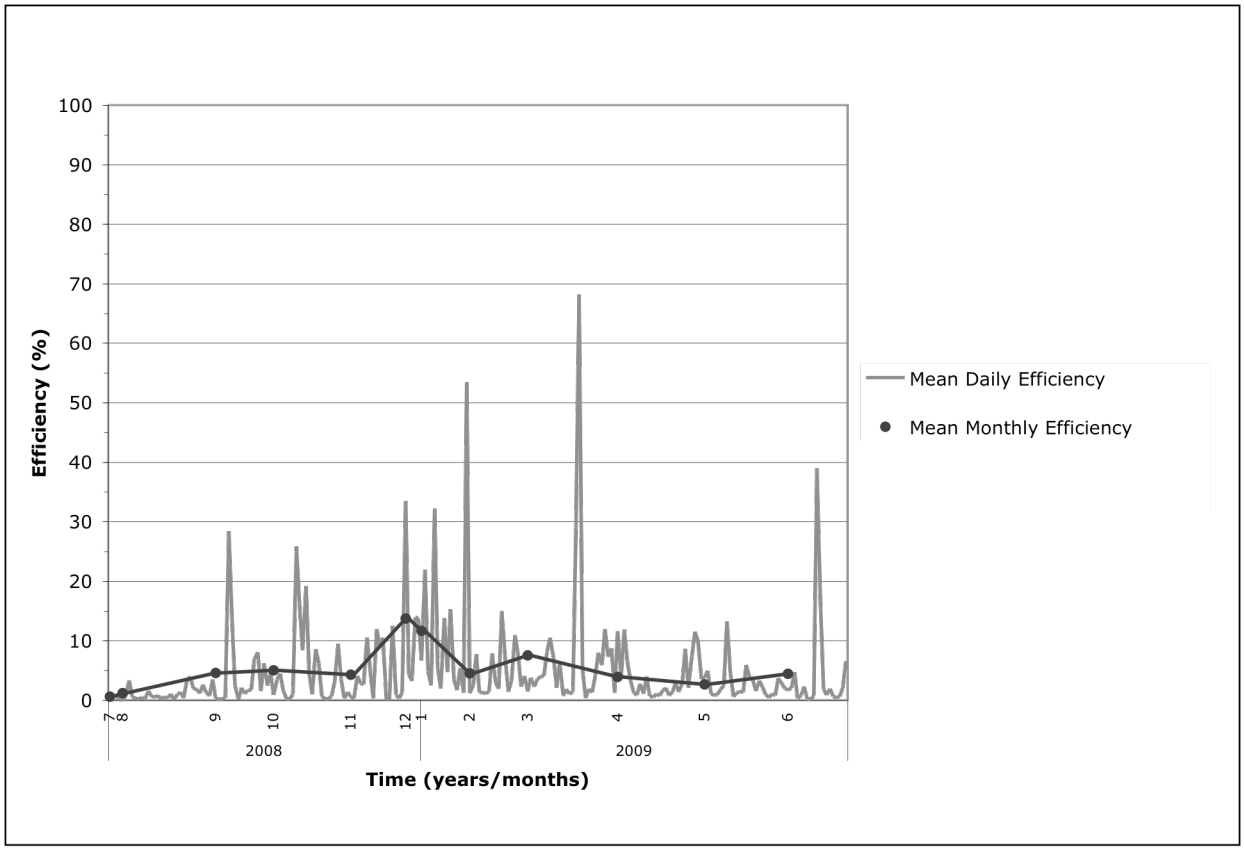

Figure 4.12. Mean daily efficiency and mean monthly efficiency for collector 1(uncovered) as a function of time of year.

The mean daily solar irradiance and mean monthly solar irradiance for collector 1 (uncovered) were plotted as a function of time, for the same points and duration used for the mean daily and mean monthly efficiency plot described above (Figure 4.13). Again, as was found with the control, although the mean daily irradiances sometimes vary substantially from day to day, the line of mean monthly irradiance indicates that, in general, solar irradiance tends to increase as spring progresses to summer, with summer having the highest overall irradiance, then decreasing through fall, with winter having the lowest overall irradiances. The greatest mean monthly solar irradiance was measured to be approximately 575 W/m^2 in July of 2009.

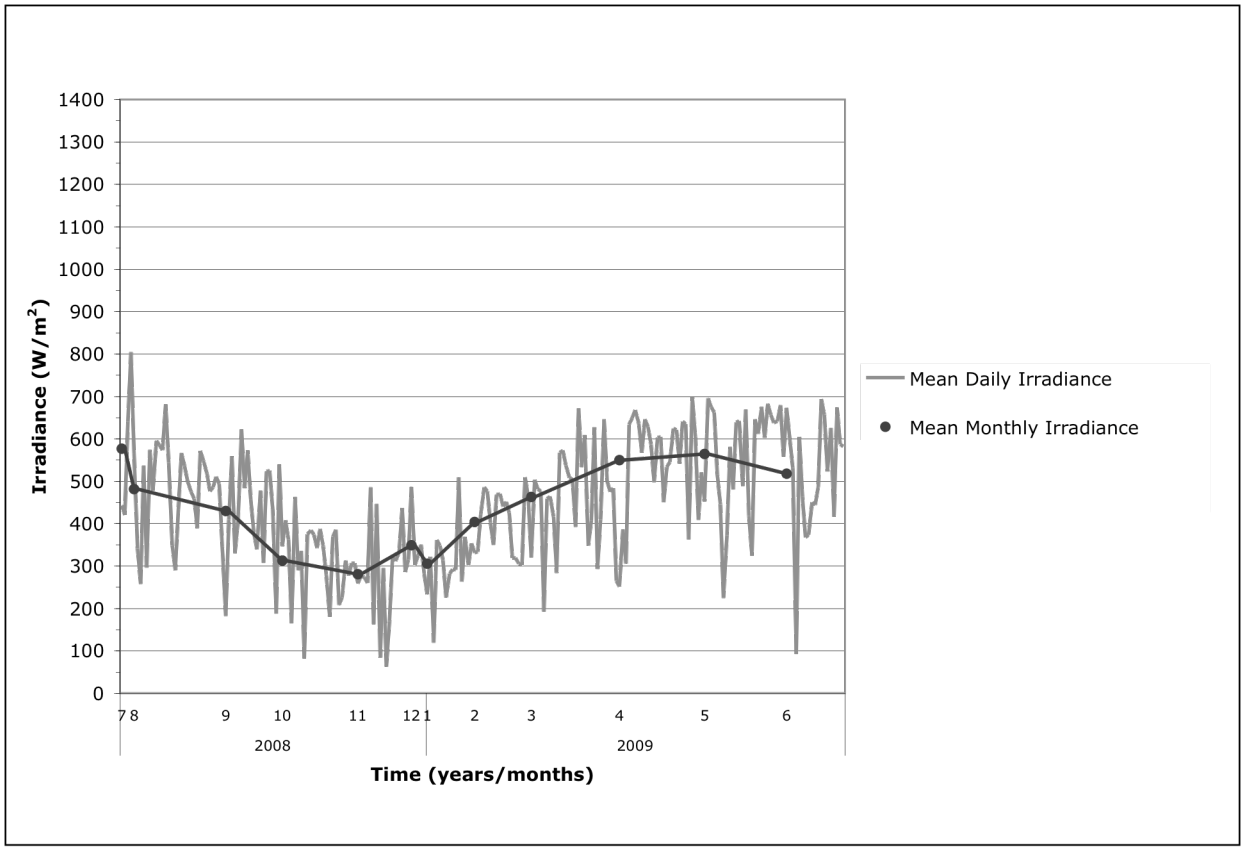

Figure 4.13. Mean daily solar irradiance and mean monthly solar irradiance for collector 1(uncovered) as a function of time of year.

Figure 4.14 presents mean monthly irradiance and mean monthly efficiency for collector 1 (uncovered) plotted as a function of time to again observe the relationship between collector efficiency and irradiance. As previously mentioned, in the above graphical analysis, the highest efficiencies and lowest irradiances occur in the winter months, while the lowest efficiencies and highest irradiances occur in the summer months. This was also found to be the case for the control results.

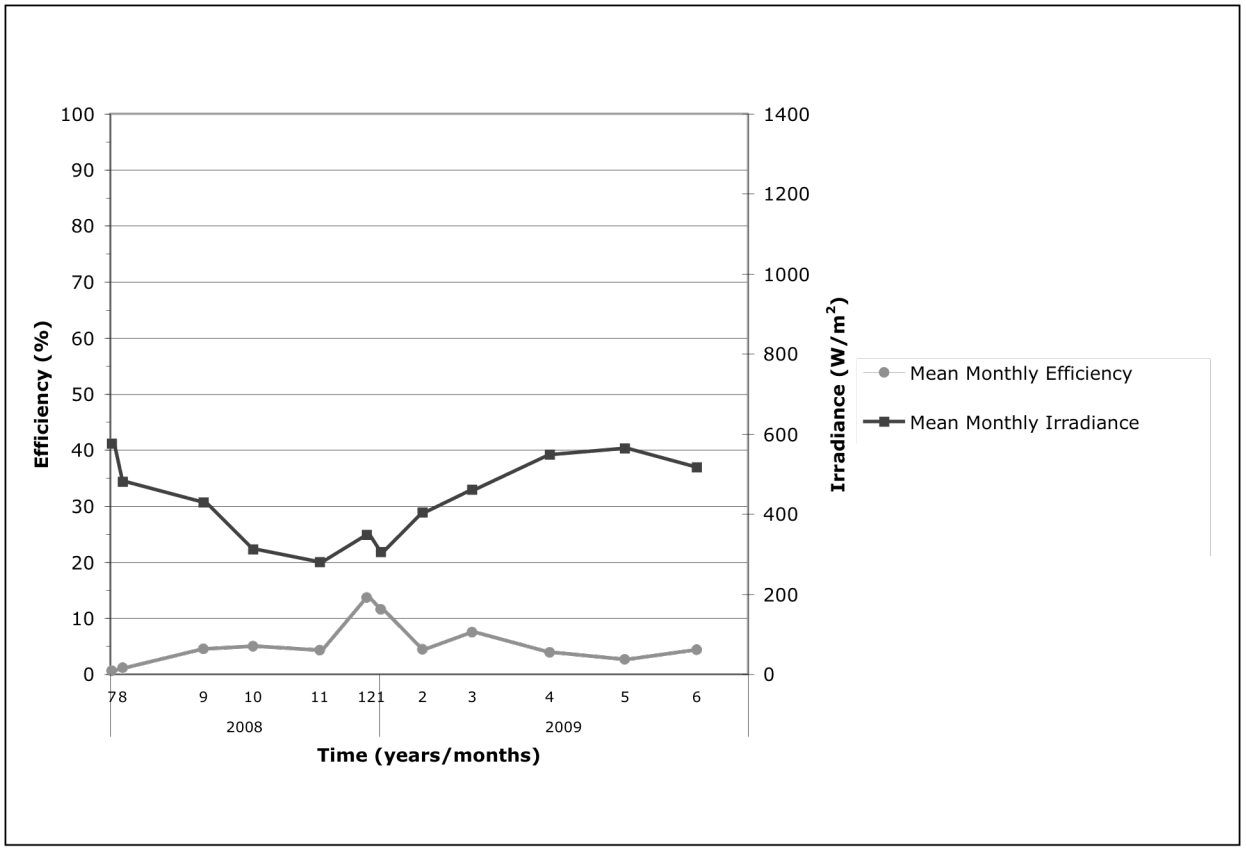

Figure 4.14. Mean monthly solar irradiance and mean monthly efficiency for collector 1 (uncovered) as a function of time of year.

A scatterplot of efficiency of collector 1 (covered), calculated via Equation 2, as a function of solar irradiance was produced (Figure 4.15). The findings are similar to those discussed for both Collector 2 and Collector 1 (uncovered). There is no obvious simple geometric correlation, such as linear or exponential, between the two variables. The distribution indicates a density or clustering of points on the low end of the efficiency scale across a wide range of solar irradiance values. The plotted points take on a somewhat negative association with each other; high efficiency values appearing to be more prominent at low- to mid-range irradiance values, and with high irradiance values resulting in lower efficiencies. It is apparent that high efficiencies are not as prominent as those below approximately 20% and that solar irradiance dwindles past approximately 1000 W/m^2.

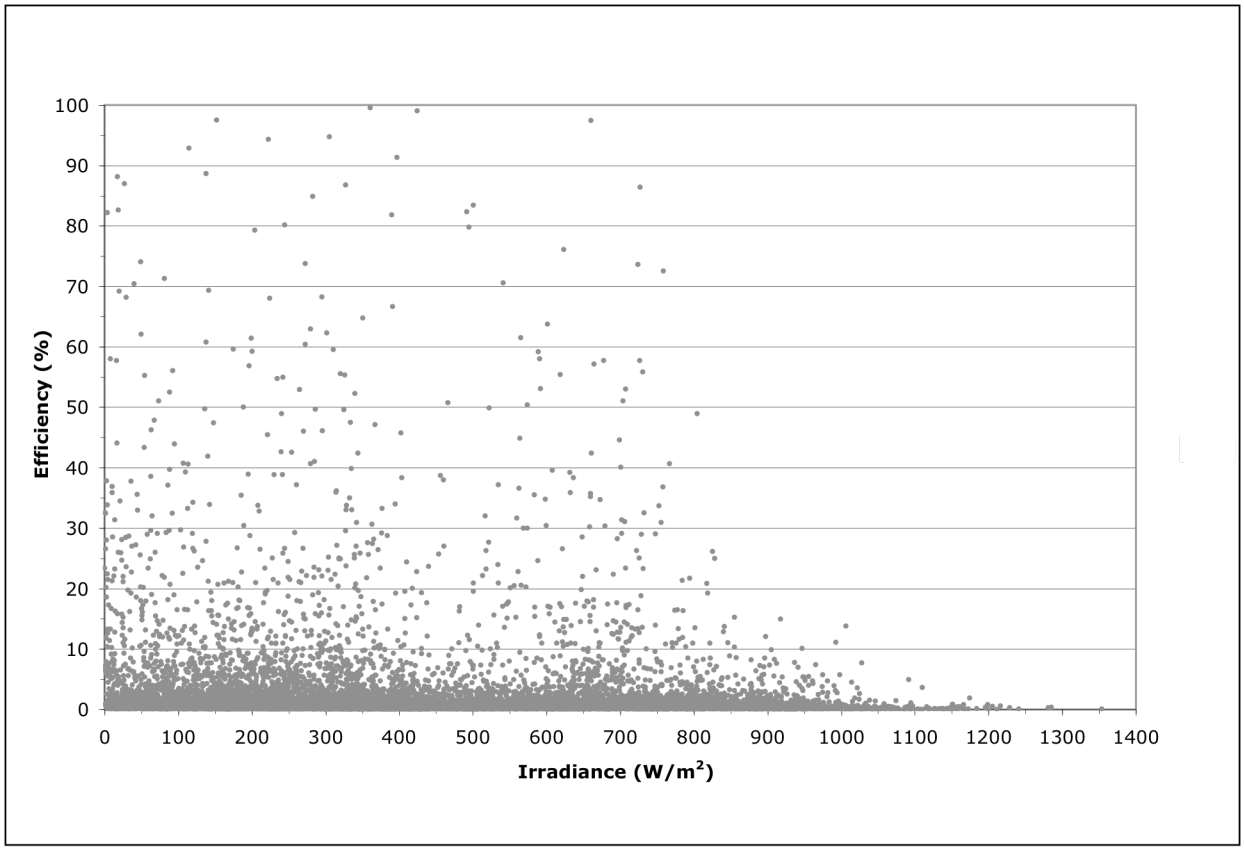

Figure 4.15. Efficiency of collector 1 (covered) as a function of solar irradiance.

The mean daily efficiencies and mean monthly efficiencies of collector 1 (covered) were plotted as a function of time in Figure 4.16. As was found with the control results, although the mean daily efficiencies sometimes vary substantially from day to day, the line of mean monthly efficiency indicates that, in general, efficiencies tend to be lowest in the summer, with summer, then increase through fall, with winter having the highest overall efficiencies. In 2009 the mean monthly efficiency was more or less level between approximately 2 – 8%. The greatest efficiency, about 12%, occurred in January 2009. Note that data were not collected for an entire year for the covered collector and spring data is not available.

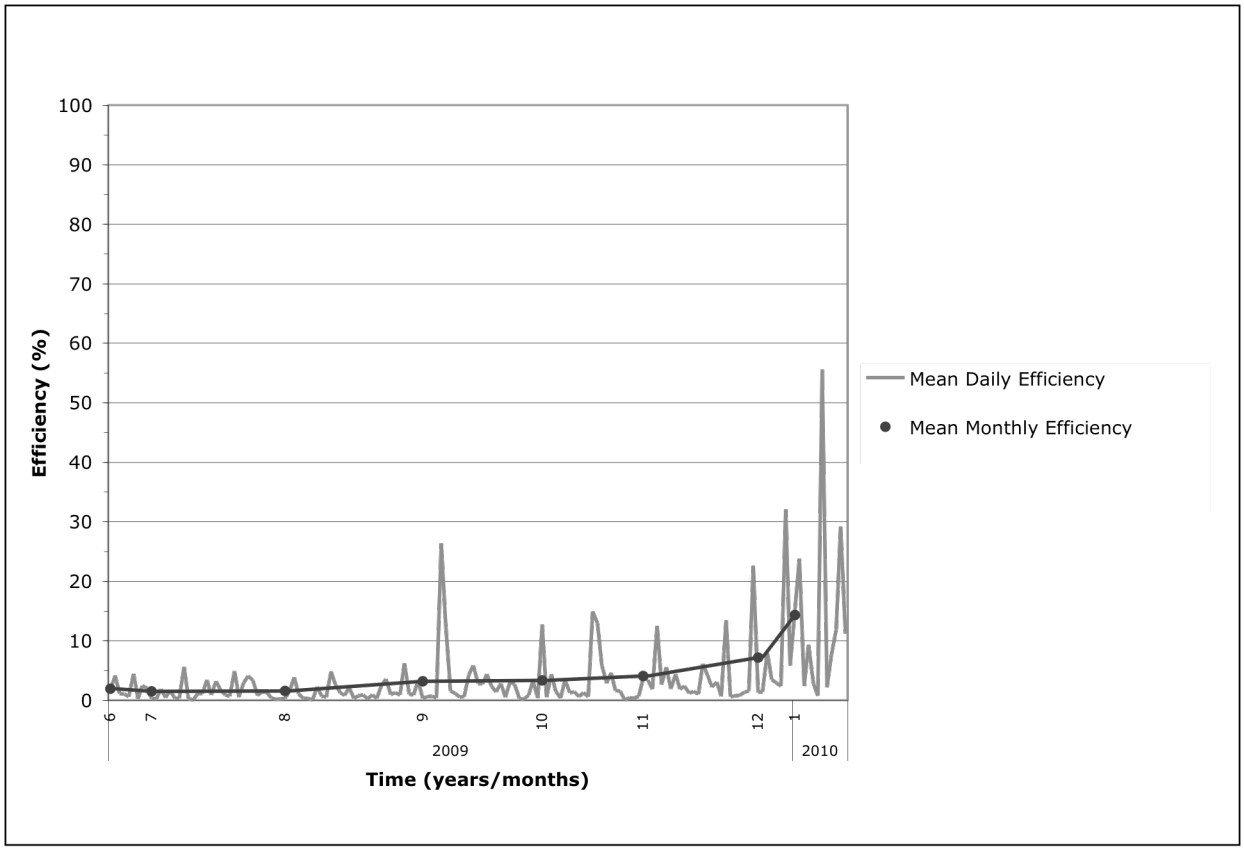

Figure 4.16. Mean daily efficiency and mean monthly efficiency for collector 1(covered) as a function of time of year.

The mean daily solar irradiance and mean monthly solar irradiance for collector 1 (covered) were plotted as a function of time, for the same points and duration used for the mean daily and mean monthly efficiency plot described above (Figure 4.17). Again, as was found with the control, although the mean daily irradiances sometimes vary substantially from day to day, the line of mean monthly irradiance indicates that, in general, solar irradiance is greatest in the summer, then decreases through fall, with winter having the lowest overall irradiances. The greatest mean monthly solar irradiance was measured to be approximately 575 W/m^2 in June and July of 2009. Note that data were not collected for an entire year for the covered collector and spring data is not available.

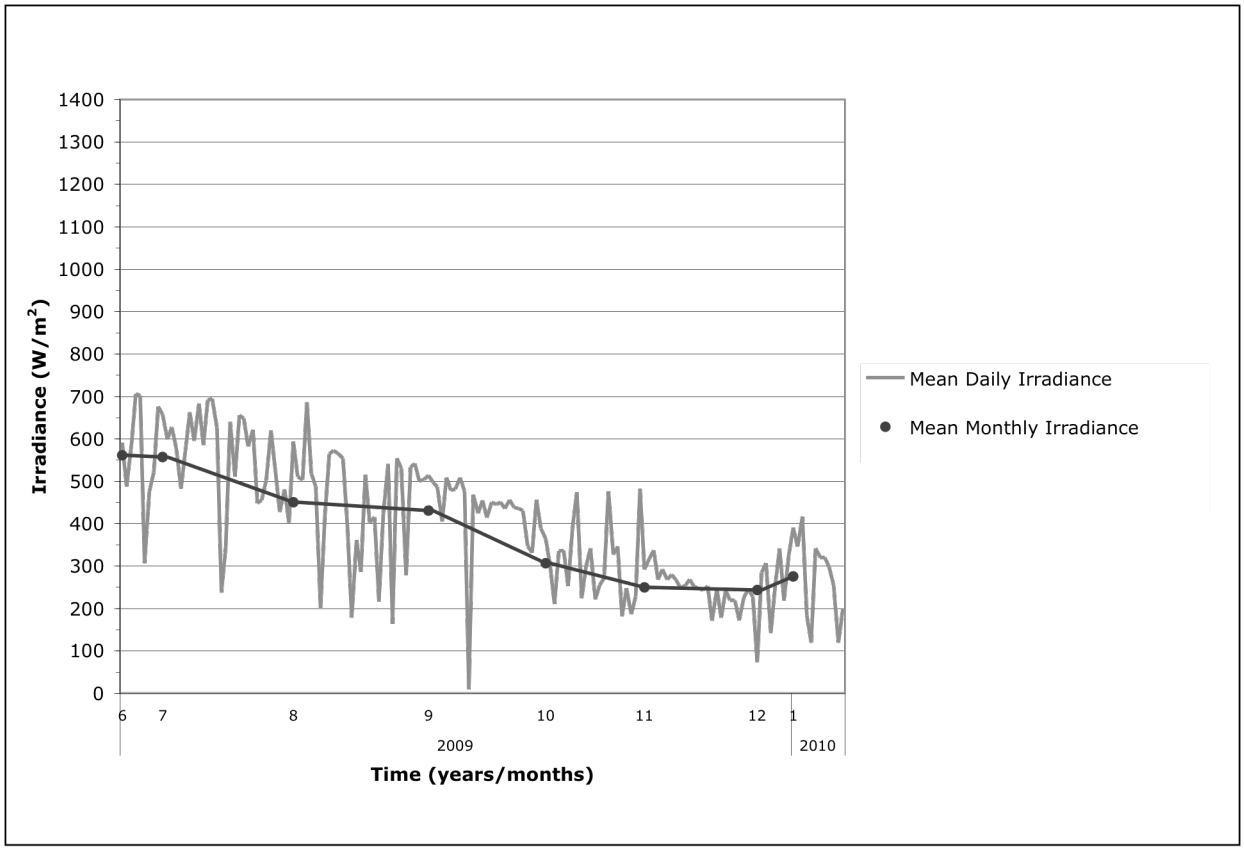

Figure 4.17. Mean daily solar irradiance and mean monthly solar irradiance for collector 1(covered) as a function of time of year.

Finally, Figure 4.18 presents mean monthly irradiance and mean monthly efficiency for collector 1 (uncovered) plotted as a function of time to again observe the relationship between collector efficiency and irradiance. As previously mentioned, in the above graphical analysis, the highest efficiencies and lowest irradiances occur in the winter months, while the lowest efficiencies and highest irradiances occur in the summer months. This was also found to be the case for the control results and the uncovered collector 1.

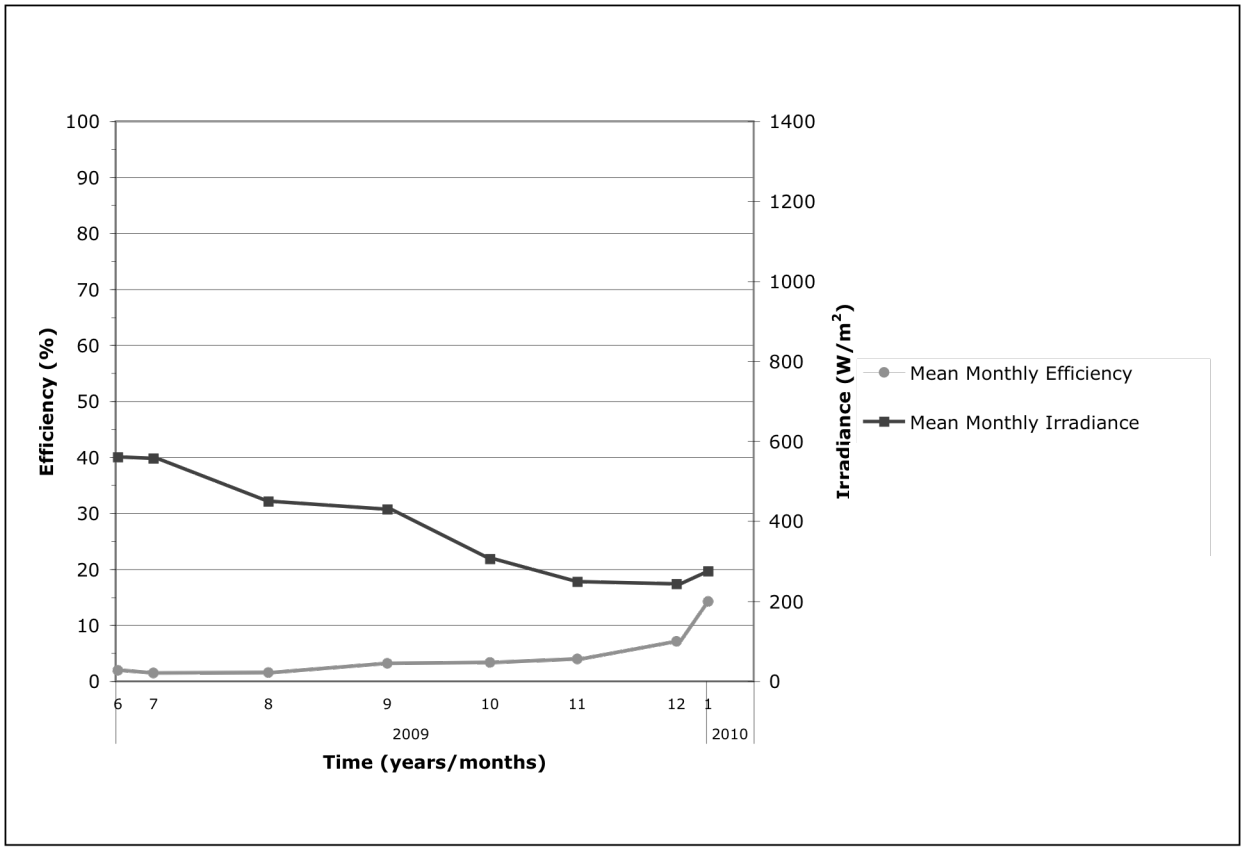

Figure 4.18. Mean monthly solar irradiance and mean monthly efficiency for collector 1 (covered) as a function of time of year.

4.1.4 Collector 3 at 50º to Horizontal, Increased Flow Rate

Collector 3 was initially set up at 50º to horizontal and the increased flow rate on the Astro 3-Speed pump of 5.58 lpm (1.475 gpm).

A scatterplot of efficiency of collector 3 (increased flow rate), calculated via Equation 2, as a function of solar irradiance was produced (Figure 4.19). Again, as has been the case for the other collector configurations, there is no obvious simple geometric correlation, such as linear or exponential, between the two variables. The distribution indicates a density or clustering of points on the low end of the efficiency scale across a wide range of solar irradiance values. The plotted points take on a somewhat negative association with each other; high efficiency values appearing to be more prominent at low- to mid-range irradiance values, and with high irradiance values resulting in lower efficiencies. It is apparent that high efficiencies are not as prominent as those below approximately 30% and that solar irradiance dwindles past approximately 1000 W/m^2. This particular graph seems to have a heavier concentration of points at the low end of the solar irradiance scale, compared to the others discussed so far. Also, the efficiencies seem to be slightly greater.

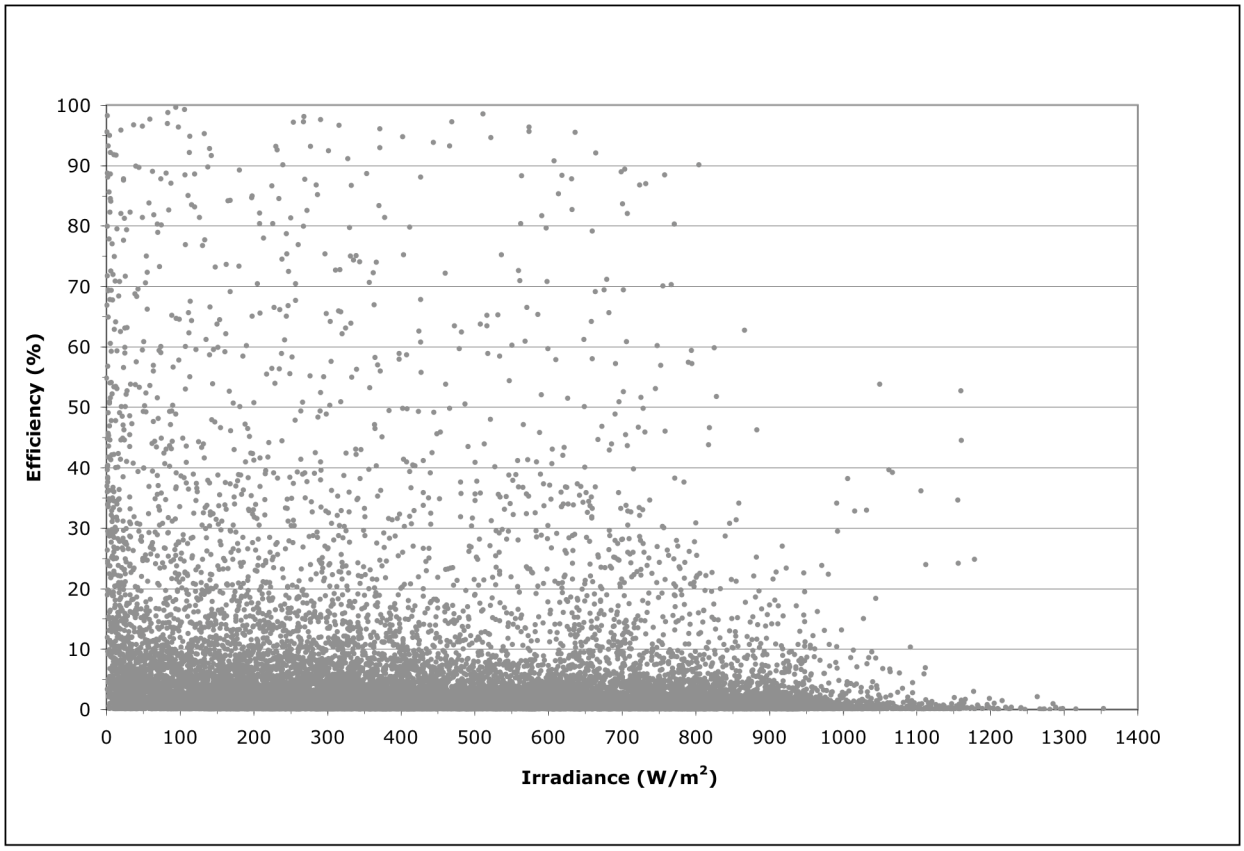

Figure 4.19. Efficiency of collector 3 (increased flow rate) as a function of solar irradiance.

The mean daily efficiencies and mean monthly efficiencies of collector 3 (increased flow rate) were plotted as a function of time in Figure 4.20. As was found with the other collector results, although the mean daily efficiencies sometimes vary substantially from day to day, the line of mean monthly efficiency indicates that, in general, efficiencies tend to decrease as spring progresses to summer, with summer having the lowest overall efficiencies, then increase through fall, with winter having the highest overall efficiencies. In 2009 the mean monthly efficiency was more or less level between approximately 3 – 8%. The greatest efficiency, about 28%, occurred in January 2010.

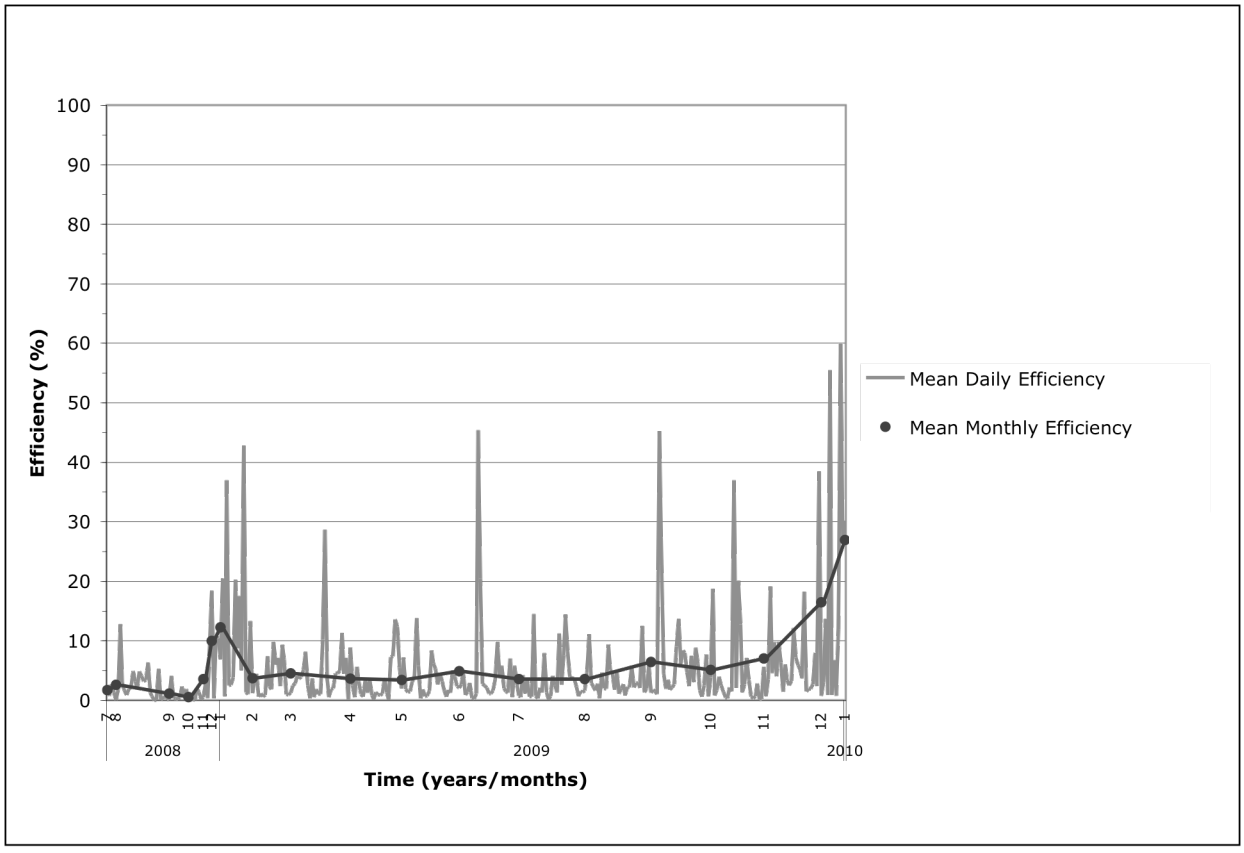

Figure 4.20. Mean daily efficiency and mean monthly efficiency for collector 3 (increased flow rate) as a function of time of year.

The mean daily solar irradiance and mean monthly solar irradiance for collector 3 (increased flow rate) were plotted as a function of time, for the same points and duration used for the mean daily and mean monthly efficiency plot described above (Figure 4.21). Again, as was found with the data for the other collectors, although the mean daily irradiances sometimes vary substantially from day to day, the line of mean monthly irradiance indicates that, in general, solar irradiance tends to increase as spring progresses to summer, with summer having the highest overall irradiance, then decreasing through fall, with winter having the lowest overall irradiances. The greatest mean monthly solar irradiance was measured to be approximately 575 W/m^2 in April of 2009.

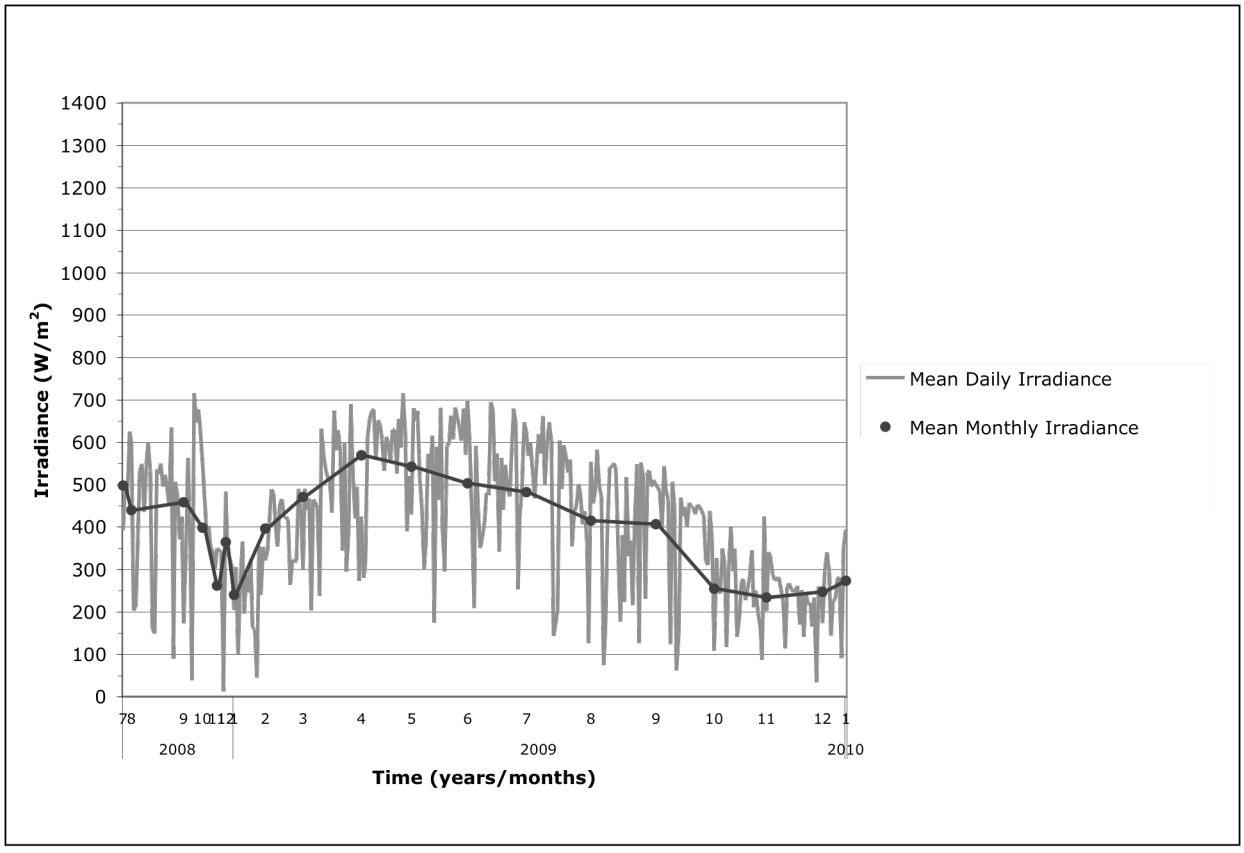

Figure 4.21. Mean daily solar irradiance and mean monthly solar irradiance for collector 3 (increased flow rate) as a function of time of year.

Again, Figure 4.22 presents mean monthly irradiance and mean monthly efficiency for collector 3 (increased flow rate) plotted as a function of time to again observe the relationship between collector efficiency and irradiance. As previously mentioned, in the above graphical analysis, the highest efficiencies and lowest irradiances occur in the winter months, while the lowest efficiencies and highest irradiances occur in the summer months.

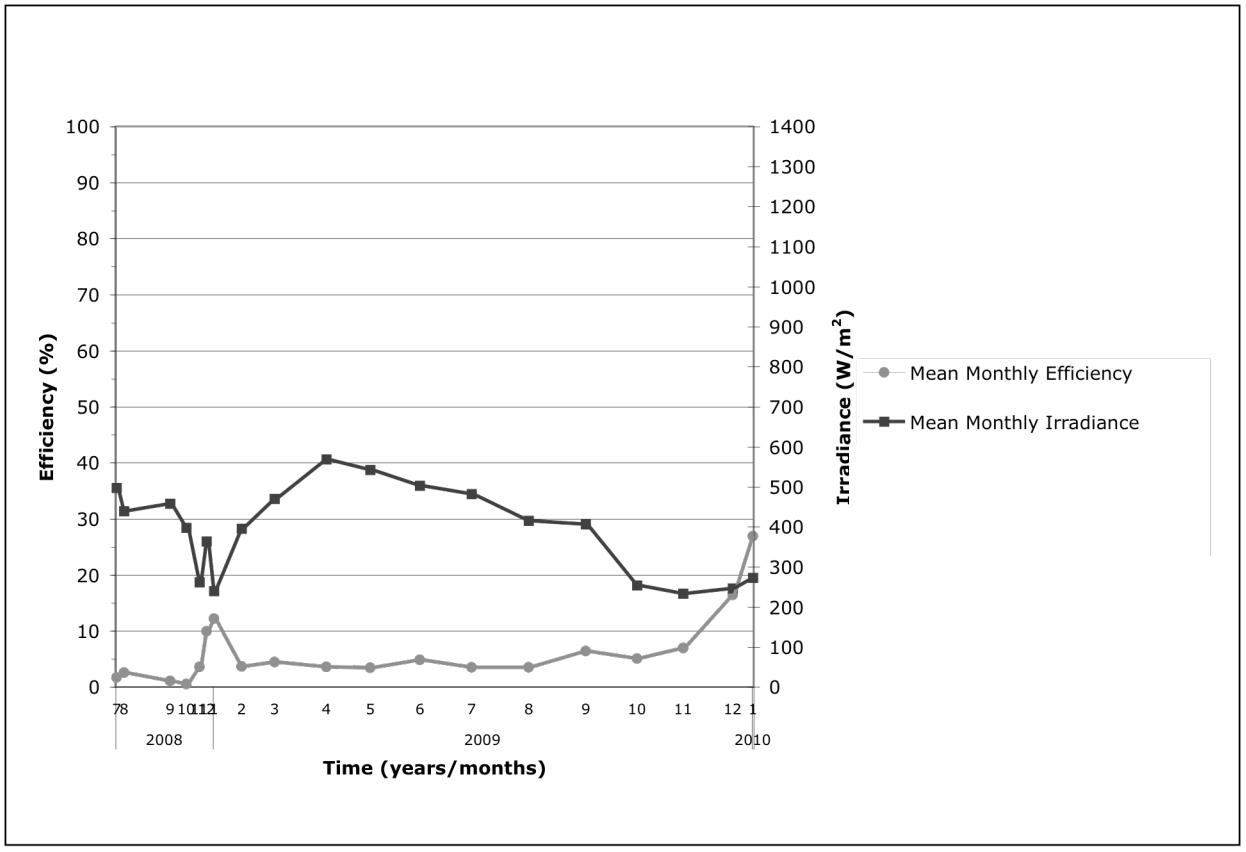

Figure 4.22. Mean monthly solar irradiance and mean monthly efficiency for collector 3 (increased flow rate) as a function of time of year.

4.1.5 Collector 4 at 90º to Horizontal, Low Flow Rate (Grundfos Pump)

Collector 4 was set up at vertically at 90º to horizontal and the low flow rate on the Grudnfos UPS 15-58 FC circulation pump of 6.34 lpm (1.675 gpm). Note collector 4 was assembled with a different pump than the others, as previously mentioned. To achieve a flow rate as close as possible to the other collectors, the lowest flow rate on the Grundfos pump was used; thus, the title "low flow rate" rather then "intermediate flow rate" as with the other collectors.

A scatterplot of efficiency of collector 4 (vertical), calculated via Equation 3.2, as a function of solar irradiance was produced (Figure 4.23). Once again, as has been the case for the other collector configurations, there is no obvious simple geometric correlation, such as linear or exponential, between the two variables. The distribution indicates a density or clustering of points on the low end of the efficiency scale across a wide range of solar irradiance values. The plotted points take on a somewhat negative association with each other; high efficiency values appearing to be more prominent at low- to mid-range irradiance values, and with high irradiance values resulting in lower efficiencies. It is apparent that high efficiencies are not as prominent as those below approximately 15% and that solar irradiance dwindles past approximately1000 W/m^2.

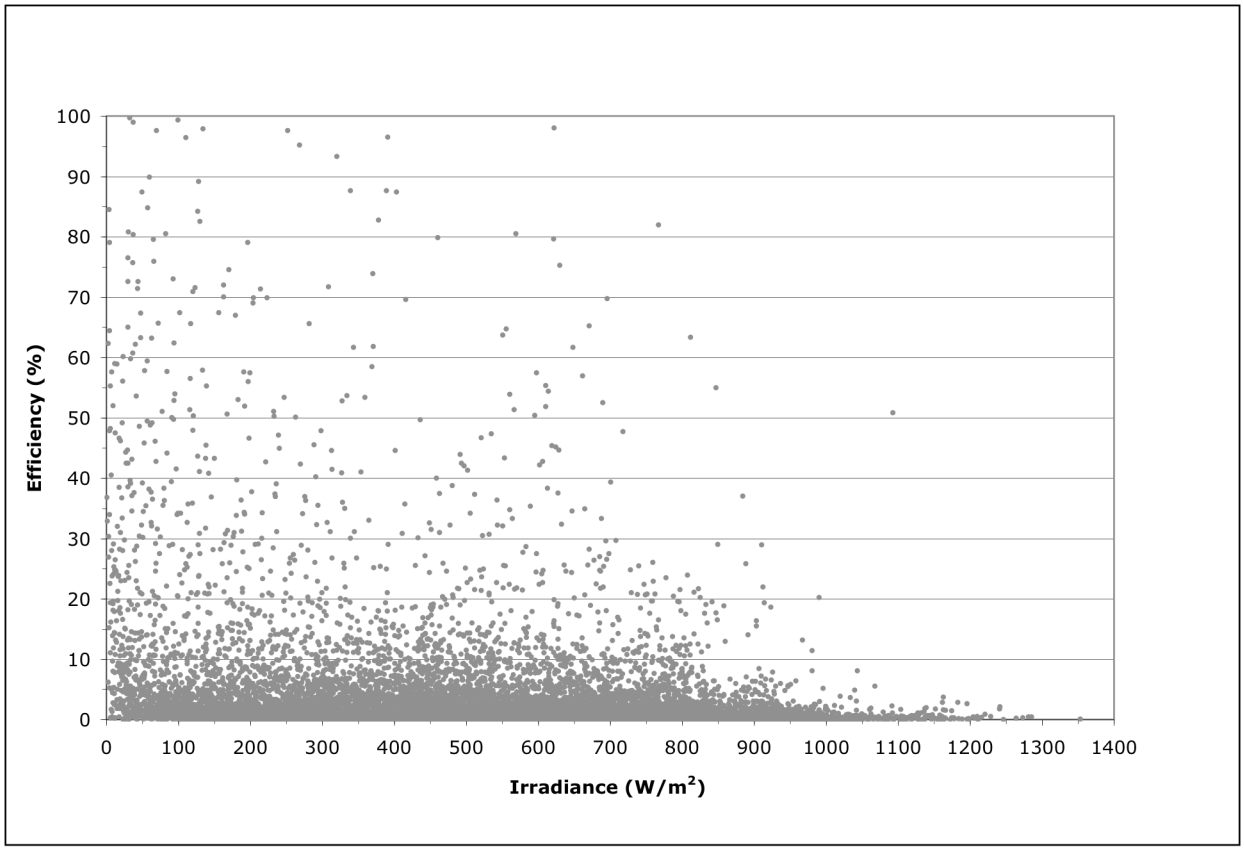

Figure 4.23. Efficiency of collector 4 (vertical) as a function of solar irradiance.

The mean daily efficiencies and mean monthly efficiencies of collector 4 (vertical) were plotted as a function of time in Figure 4.24. Again, as was found with the previous results, although the mean daily efficiencies sometimes vary substantially from day to day, the line of mean monthly efficiency indicates that, in general, efficiencies tend to decrease as spring progresses to summer, with summer having the lowest overall efficiencies, then increase through fall, with winter having the highest overall efficiencies. In 2009 the mean monthly efficiency was more or less level between approximately 2 – 8%. The greatest efficiency, about 11%, occurred in February 2009. Note that data were not collected for an entire year for the vertical collector due to malfunction of the control system for the collector.

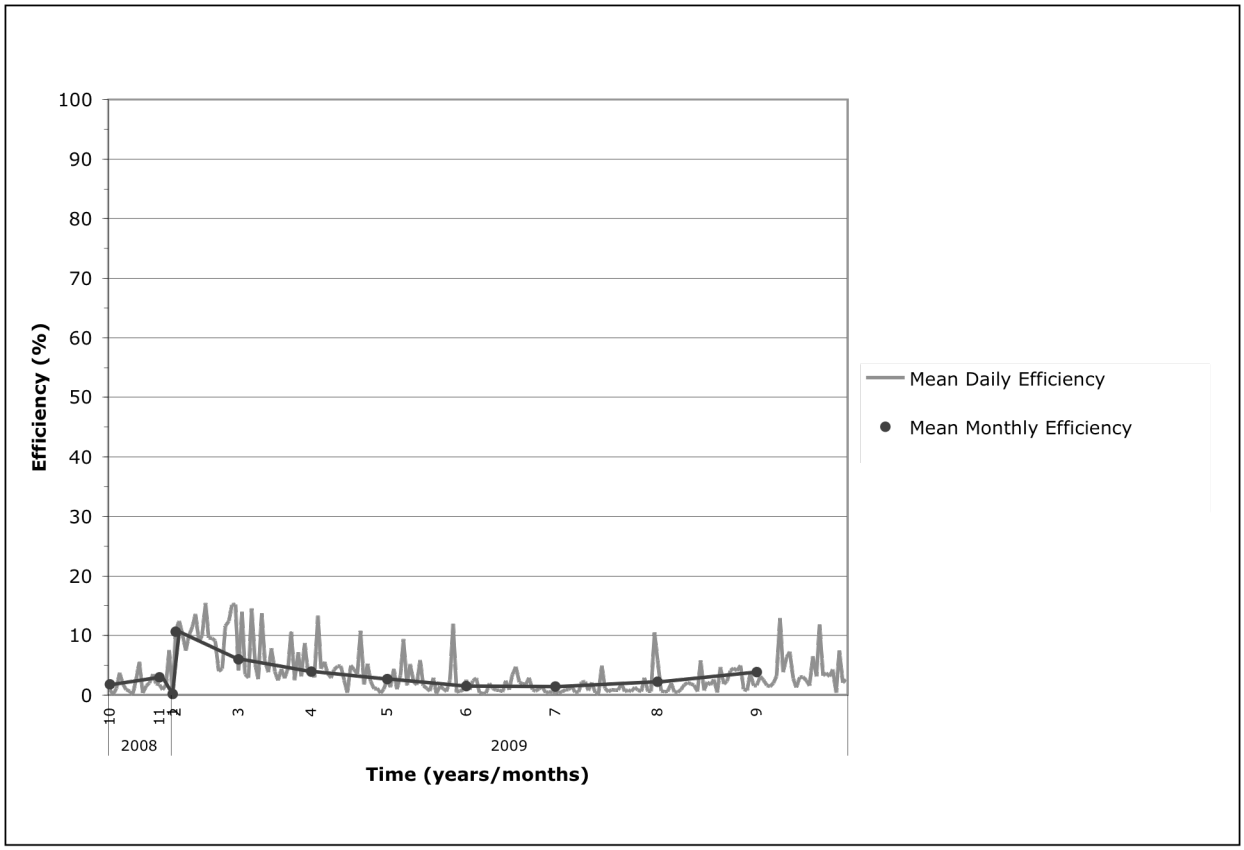

Figure 4.24. Mean daily efficiency and mean monthly efficiency for collector 4 (vertical) as a function of time of year.

The mean daily solar irradiance and mean monthly solar irradiance for collector 4 (vertical) were plotted as a function of time, for the same points and duration used for the mean daily and mean monthly efficiency plot described above (Figure 4.25). Again, as was found with the control, although the mean daily irradiances sometimes vary substantially from day to day, the line of mean monthly irradiance indicates that, in general, solar irradiance tends to increase as spring progresses to summer, with summer having the highest overall irradiance, then decreasing through fall, with winter having the lowest overall irradiances. The greatest mean monthly solar irradiance was measured to be approximately 575 W/m^2 in July of 2009. Again, note that data were not collected for an entire year for the vertical collector due to malfunction of the control system for the collector.

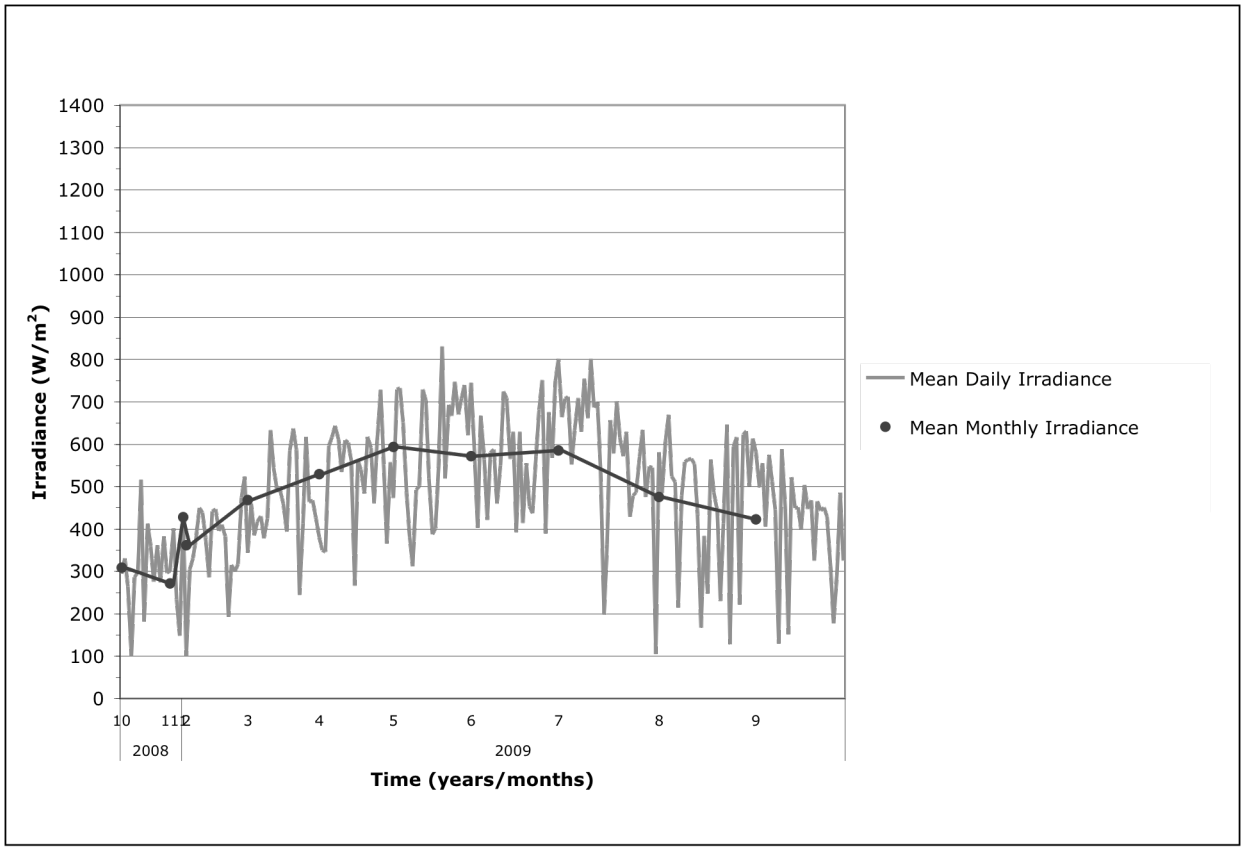

Figure 4.25. Mean daily solar irradiance and mean monthly solar irradiance for collector 4 (vertical) as a function of time of year.

Again, Figure 4.26 presents mean monthly irradiance and mean monthly efficiency for collector 4 (vertical) plotted as a function of time to again observe the relationship between collector efficiency and irradiance. As previously mentioned in the above graphical analysis, and as observed for the other collector configurations, the highest efficiencies and lowest irradiances occur in the winter months, while the lowest efficiencies and highest irradiances occur in the summer months. Again, note that data were not collected for an entire year for the vertical collector due to malfunction of the control system for the collector.

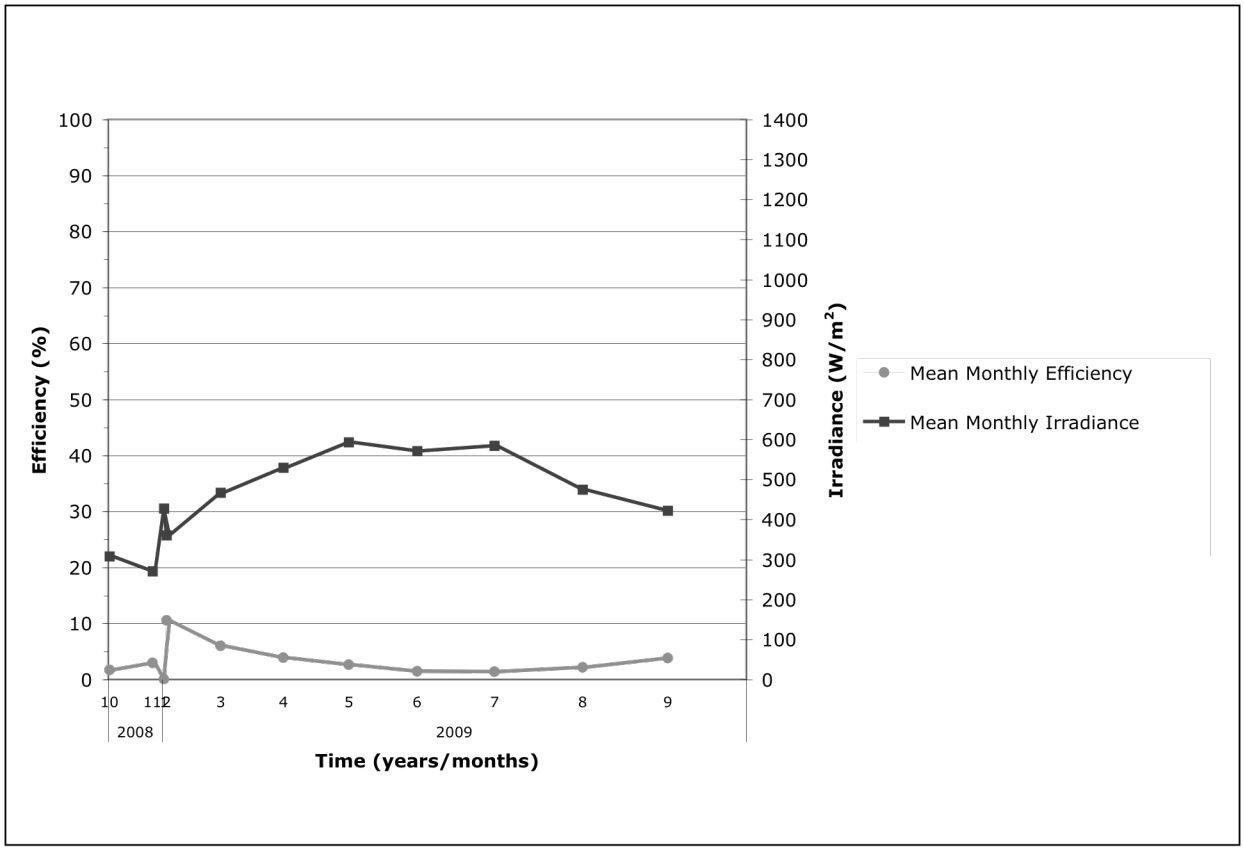

Figure 4.26. Mean monthly solar irradiance and mean monthly efficiency for collector 4 (vertical) as a function of time of year.

4.1.6 Collector 3 at 50º to Horizontal, Intermediate Flow Rate, 16 Tubes Removed

Collector 3 was eventually set up at 50º to horizontal and the intermediate flow rate on the Astro 3-Speed pump of 1.3 gpm.

A scatterplot of efficiency of collector 3 (16 tubes removed), calculated via Equation 2, as a function of solar irradiance was produced (Figure 4.27). Perhaps for this scenario more than others due to the much lower number of data points, there is no obvious simple geometric correlation, such as linear or exponential, between the two variables. The distribution indicates a density or clustering of points on the low end of the efficiency scale across a narrow range of solar irradiance values. There seem to be more data points for efficiencies below approximately 10% and for solar irradiance less than 400 W/m^2. It is difficult to distinguish any significant pattern in these data points.

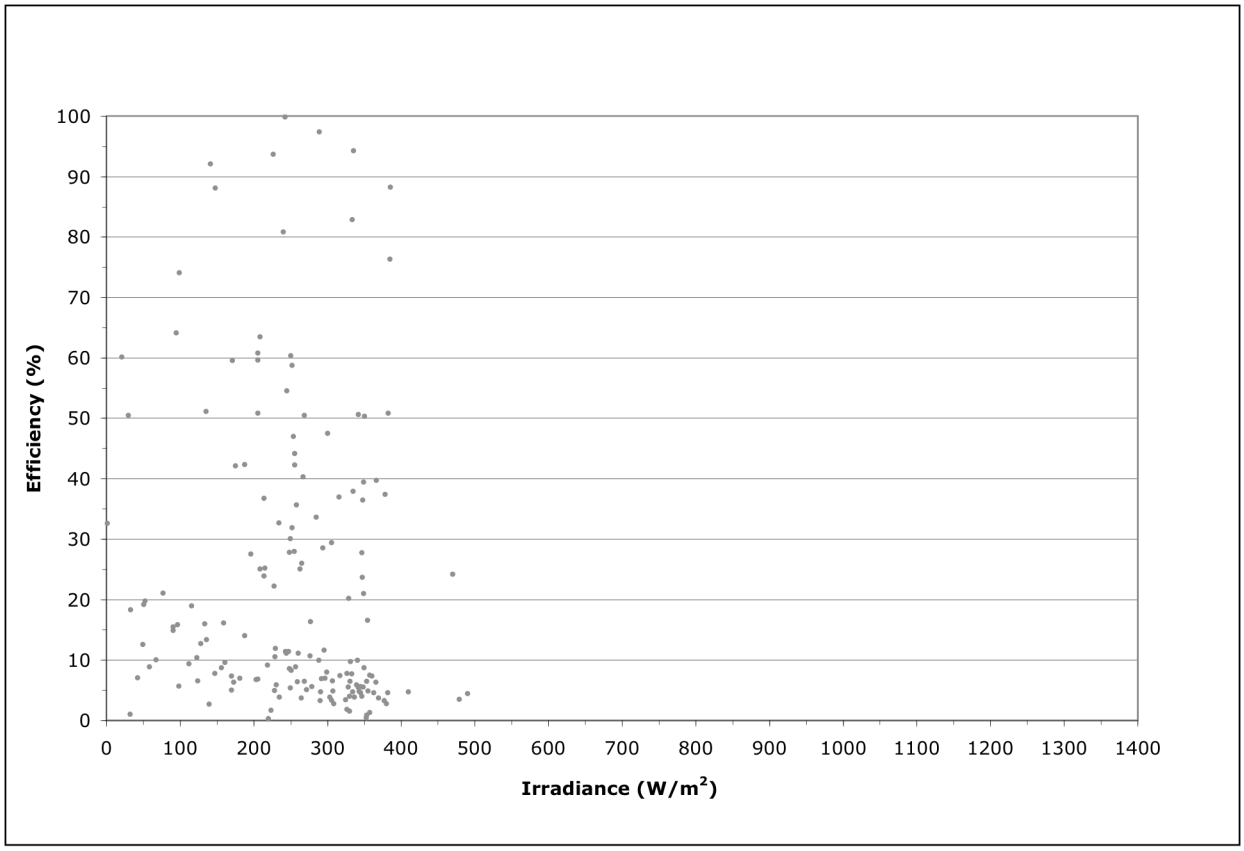

Figure 4.27. Efficiency of collector 3 (16 tubes removed) as a function of solar irradiance.

The mean daily efficiencies and mean monthly efficiencies of collector 3 (16 tubes removed) were plotted as a function of time in Figure 4.28. Due to lack of data for this collector configuration, it is not possible to determine efficiency trends as a function of time of year, since data were collected for only about one month. The graph has been included to show how the collector performed for the month of January 2010, given that it was missing 16 tubes. The average monthly efficiency for January 2010 was approximately 27%. The greatest efficiency reached during this time was 70%, and the lowest was about 2%.

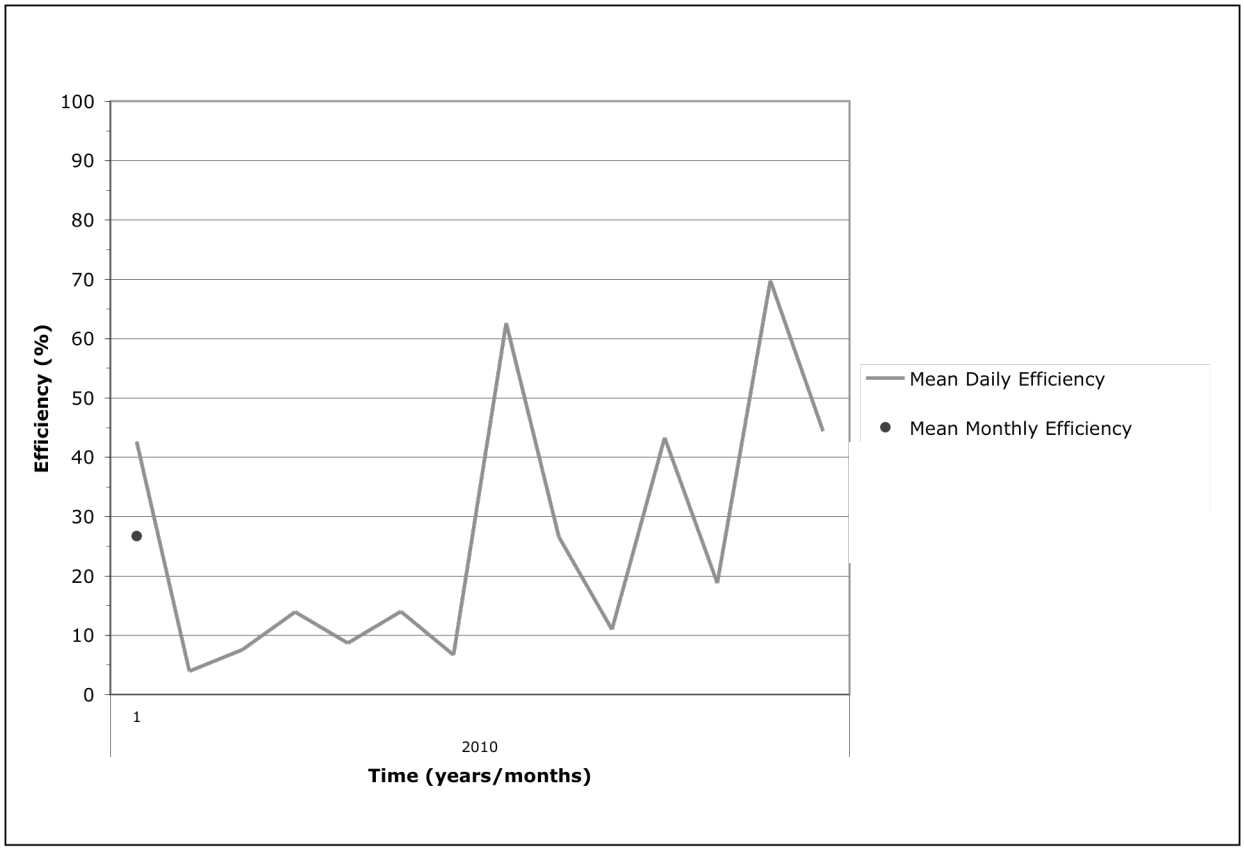

Figure 4.28. Mean daily efficiency and mean monthly efficiency for collector 3 (16 tubes removed) as a function of time of year.

The mean daily solar irradiance and mean monthly solar irradiance for collector 3 (16 tubes removed) were plotted as a function of time for the same points and duration used for the mean daily and mean monthly efficiency plot described above (Figure 4.29). As mentioned above, the lack of data for this collector configuration made it difficult to determine long-term solar irradiance trends as a function of time of year, since data were collected for only about one month. In January 2010, the greatest mean monthly solar irradiance was measured to be approximately 400 W/m^2. The average monthly solar irradiance was measured to be approximately 275 W/m^2 for the same time period.

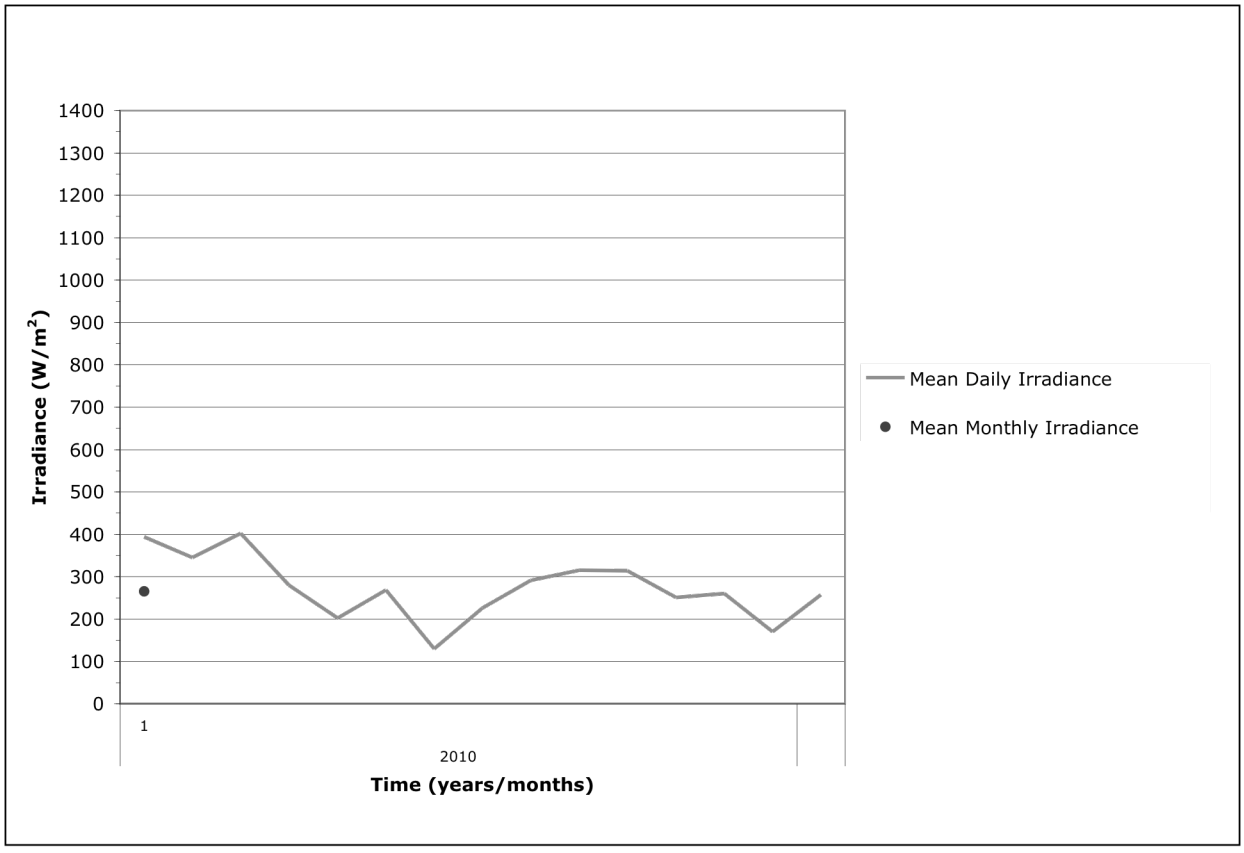

Figure 4.29. Mean daily solar irradiance and mean monthly solar irradiance for collector 3 (16 tubes removed) as a function of time of year.

Figure 4.30 presents mean monthly irradiance and mean monthly efficiency for collector 3 (16 tubes removed) plotted as a function of time. Since data were only collector for January 2010, there is only one mean monthly irradiance point and one mean monthly efficiency point for this time period. This graph has simply been included for completeness, and is not particularly useful in observing the relationship between solar irradiance and panel efficiency for this collector configuration.

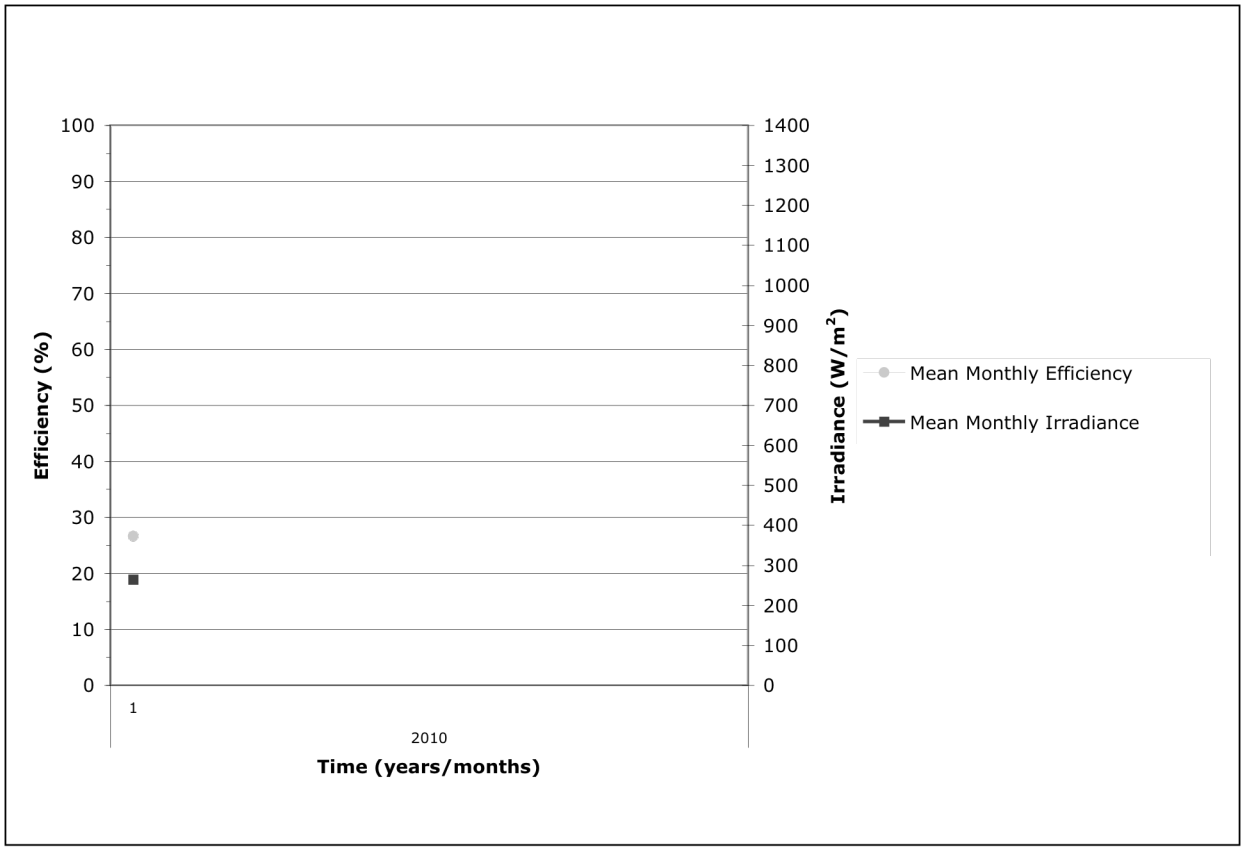

Figure 4.30. Mean monthly solar irradiance and mean monthly efficiency for collector 3 (16 tube removed) as a function of time of year.

It was difficult to make a comparison of the efficiency of collector 3 installed at 50º to horizontal, intermediate flow rate with 16 tubes removed to the control due to the lack of data. It is recommended that data collection continue on this collector.

4.1.7 Comparison of Mean Monthly Collector Efficiencies to the Control Collector

Figure 4.31 overlays the efficiency results from each collector onto one graph for efficiency as a function of time. Important dates are noted on the graph, particularly the date that Collector 1 was covered with the Suntuf panel (June 21, 2009), and the date that the flow rate was returned to intermediate speed and 16 tubes were removed from Collector 3 (January 2, 2010). The purpose of overlaying these results is to determine which collectors outperform the others and rank them accordingly. Aside from a few outliers, the efficiencies tend to be within less than 5% of each other, suggesting that the different collector configurations have minimal effect on efficiency. However, in general, it appears that the covered collector (Collector 1) performed worse than the others more often than not. The vertical collector (Collector 4) tended to outperform others during the winter months, but fell in line with the covered collector (Collector 1) in the summer. Collector 3, with increased flow rate and the control (Collector 2), fell somewhere in the middle.

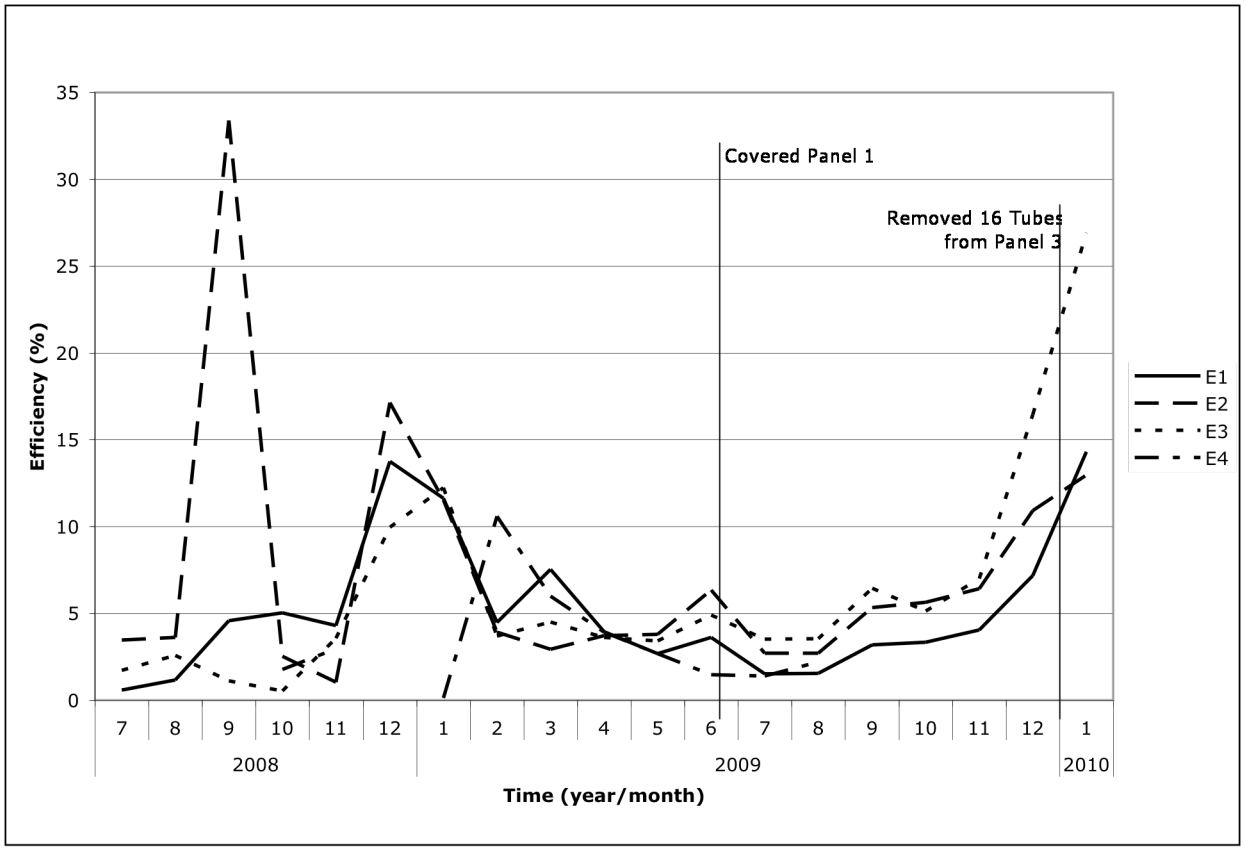

Figure 4.31. Comparison of collector efficiencies as function of time of year.

Figure 4.32 compares the mean monthly efficiency of Collector 1, installed at 50º to horizontal, intermediate flow rate, uncovered and covered to Collector 2, the control. The date that the Suntuf Panel was installed over the collector, June 21, 2009, is indicated with a labeled vertical line. Up until the point of installation of the cover, the two collectors performed in a fairly similar manner. Initially, in July through August of 2008 the control performed slightly better; October and November of 2008 saw the reverse. In general, the outperforming collector oscillated between the control and the uncovered collector, within a margin of less than 5% efficiency (except for the one outlier for the control in August of 2008, when its mean monthly efficiency bolted up to approximately

34%), until the time of cover installation. At this point the control consistently outperformed the covered collector, until January 2010.

These results were expected. The Suntuf cover will restrict the transmittance of solar radiation to the evacuated tubes, and thus cause a decline in performance, as less energy is available to the collector to convert to heat.

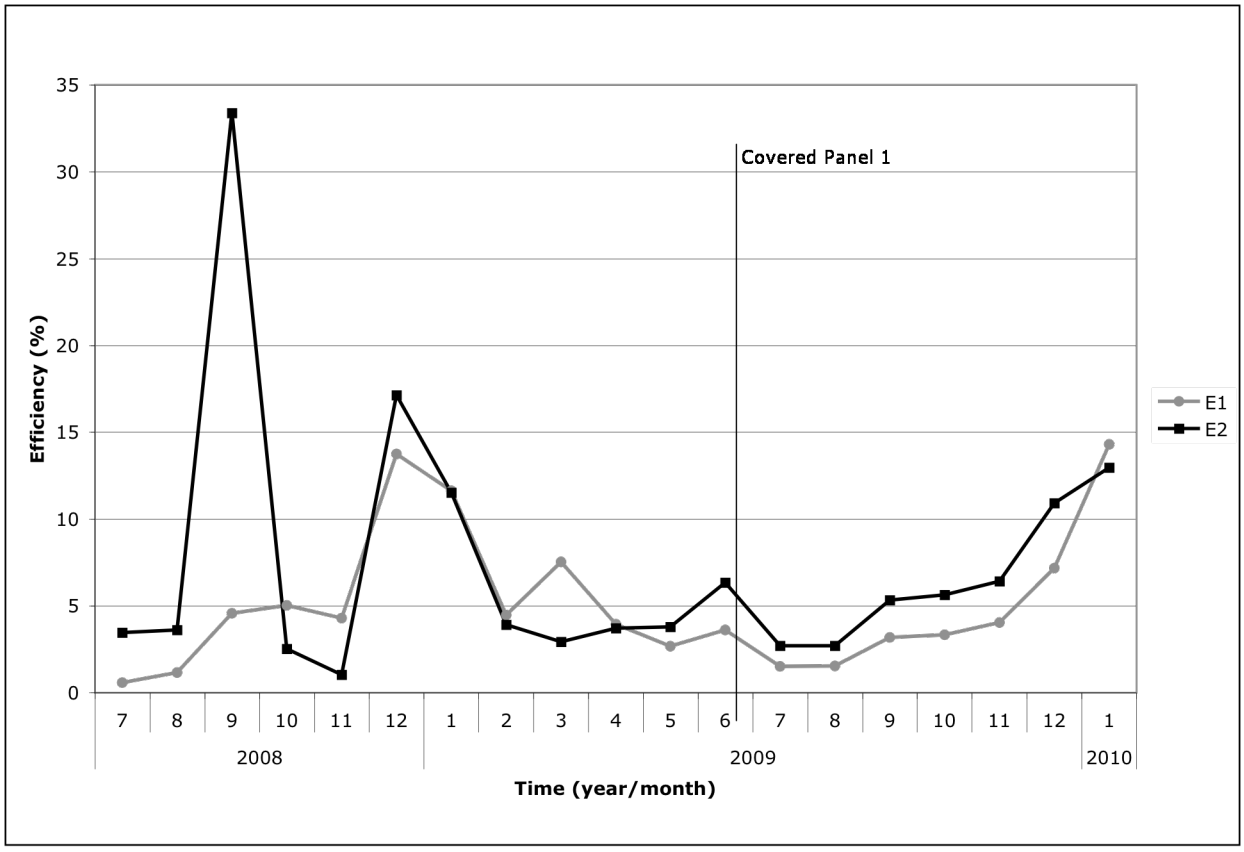

Figure 4.32. Comparison of mean monthly efficiencies of collector 1 (uncovered then covered) to the mean monthly efficiencies of collector 2 (control).

According to the mathematical expression used to calculate panel efficiency (Equation 3.2), as mass flow rate, and therefore volume flow rate, increases, the collector efficiency should also increase, all else being equal. Figure 4.33 compares the mean monthly efficiency of Collector 3, installed at 50º to horizontal, increased flow rate with to Collector 2, the control. In general, the outperforming collector oscillated between the control and collector 3, within a margin of less than 10% efficiency (except for the one outlier for the control in August of 2008, when its mean monthly efficiency bolted up to approximately 34%). In November of 2009 the efficiency of collector 3 began to rise steeply.

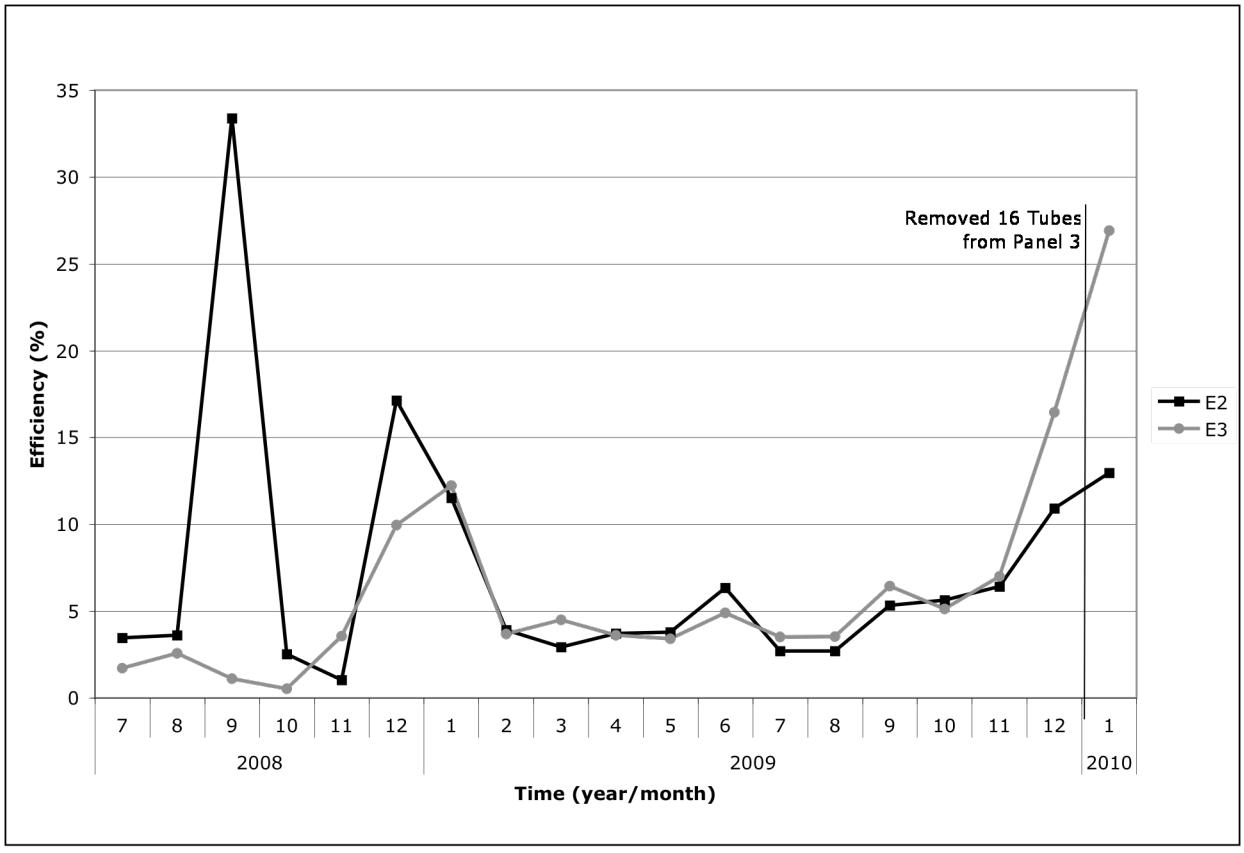

Figure 4.33. Comparison of mean monthly efficiencies for collector 3 (increased flow rate then 16 tubes removed) to the mean monthly efficiencies of collector 2 (control).

It was expected that collector 4, installed at 90º to horizontal, standard flow rate would outperform the control in the winter months since the 90-degree installation angle would be better suited to the winter sun angle. The data collection for this collector was somewhat sporadic due control malfunctions and the eventual inability to repair the system (September 2009). The best data for comparison is between the months of January to September of 2009. During this time collector 4 did perform as expected, with greater efficiencies than the control during the winter months and the opposite in the summer (Figure 4.34).

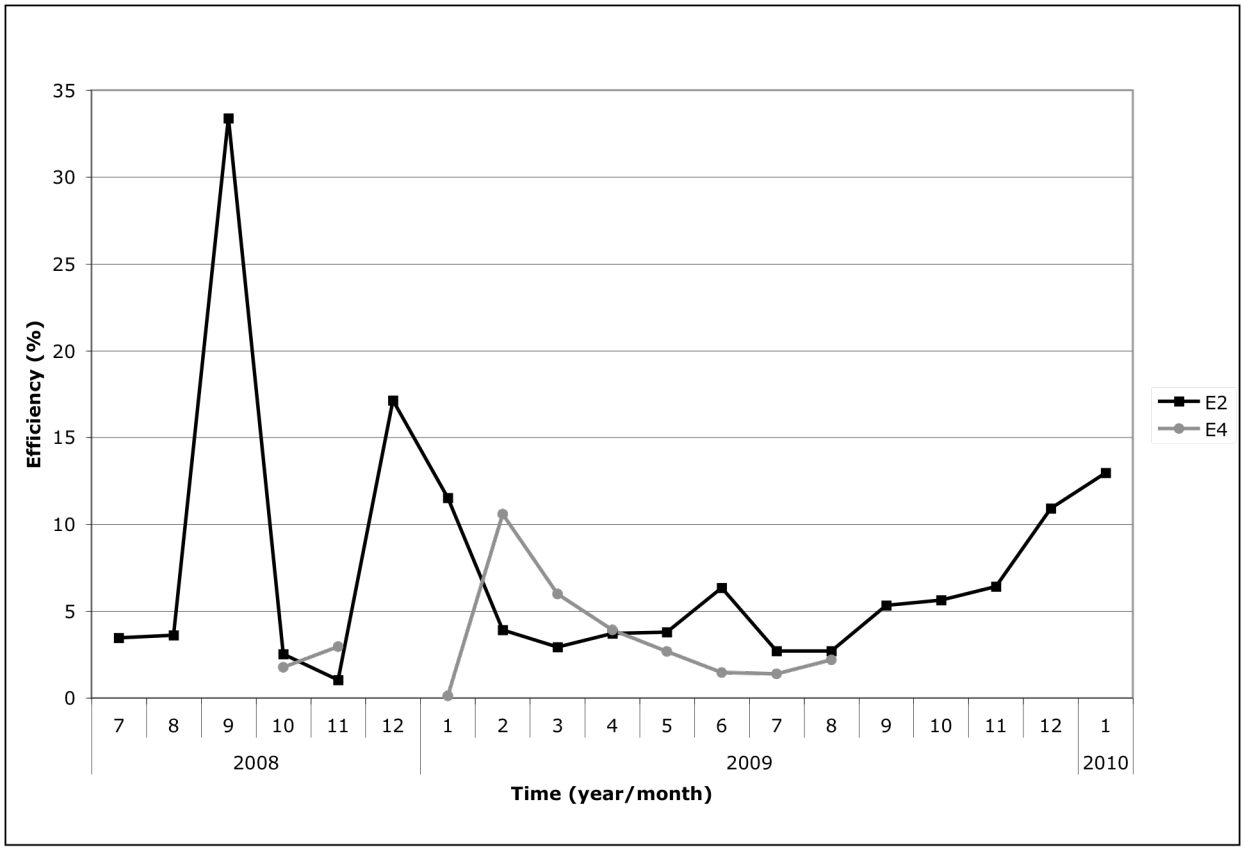

Figure 4.34. Comparison of mean monthly efficiencies for collector 4 (vertical) to the mean monthly efficiencies of collector 2 (control).

4.1.8 Overall Collector Performance Analysis

Though observation of each of the collector configurations above, a few consistent trends were noted.

Each plot of efficiency as a function of irradiance showed a similar distribution: the overall form of points indicates a density or clustering of points on the low end of the efficiency scale across a wide range of irradiance values. In general, the plotted points take on a somewhat negative association with each other; high efficiency values appearing to be more prominent at low- to mid-range irradiance values, and with high irradiance values resulting in lower efficiencies. There is no obvious simple geometric correlation between the two values.

The mean daily and monthly efficiency of each collector was plotted as a function of time and again displayed similar trends. Although the mean daily efficiencies varied, the line of mean monthly efficiency indicated that, in general, efficiencies tended to decrease as spring progresses to summer, with summer having the lowest overall efficiencies, then increase through fall, with winter having the highest overall efficiencies.

It should be noted here that for the purposes of this research project, the term "effectiveness" could be substituted for "efficiency" since the evaluation was based on collector system performance. Equation 3.2 represents a theoretical relationship between solar radiation, flow rate, inlet and outlet temperatures, collector area, etc., under optimal, controlled laboratory conditions. The efficiencies measured here were subject to

uncontrollable variables and environmental conditions. Thus, the term "effectiveness" may be more appropriate in describing collector system performance. Where "system" refers to the evacuated tube, manifold, and heat dissipation assembly.

The mean daily and monthly irradiance for each collector was plotted as a function of time, for the same points and duration used for the mean daily and monthly efficiency plots. Although the mean daily irradiances varied, the line of mean monthly irradiance indicated that, in general, solar irradiance tended to increase as spring progresses to summer, with summer having the highest overall irradiance, then decreasing through fall, with winter having the lowest overall irradiances.

Finally, the plots of mean monthly irradiance and efficiencies for each collector configuration showed that the highest efficiencies and lowest irradiances occurred in the winter months, while the lowest efficiencies and highest irradiances occurred in the summer months.

The graphs also displayed outliers during the same dates. In particular, outliers were common in August and December of 2008, as can be seen in Figures 4.5. 4.7, 4.14, 4.21, 4.22, 4.24, 4.25, 4.26, 4.32, 4.33, and 4.34. December had the most obvious and consistent outliers. Specifically, there was a dip in mean monthly irradiance and an increase in efficiency. This could be due to the lack of data points available in the month of December, where a few lower than usual measurements have skewed the entire mean.

The findings above suggest that evacuated tube collector efficiency could be inversely related to solar irradiance, although the reverse may be expected. Since solar irradiance is strongest in the summer, it may be expected that collector output would also be strongest during this time. After re-examination of the mathematical expression used to calculate panel efficiency (Equation 3.2), an alternate explanation is found. Note that as the ΔT in the numerator decreases so does collector efficiency. The measured ΔT for each collector was smallest in the summer months due to warmer and more equal ambient indoor and outdoor temperatures. During the winter months the strawbale building is heated, and maintains a temperature well above freezing, while outside the ambient temperature could dip from 0 to -40°C (approximately). To obtain the greatest difference in temperature, ΔT is measured between the inlet of the manifold, the coldest possible location on the source, and the outlet of the fin-tube, the coldest possible location on the load. Thus, due to environmental conditions, the largest ΔT occurs during the colder seasons. This also indicates that collector efficiency is related to storage capacity of the entire system and ultimately the maintenance of a large ΔT.

In addition, the efficiency of the evacuated tube collectors could be limited by the various heat transfer mechanisms inherent in the design. Ultimately, heat can only be transferred as fast as the conductance of the material or fluid will allow. That being said, it may not matter how much solar radiation is available for the taking, if in fact only X W/m^2 is useful at any given time. If this is the case, then collector performance is less dependent upon solar radiation and perhaps more dependent upon the intermediate efficiencies of heat transfer, first between the air space and the copper heat pipe, then between the

copper condenser end and the copper manifold seat, then from the manifold to the heat transfer fluid, and so on.

This still leaves the question of how, if at all, solar irradiance and collector efficiency are related. Again, looking at the mathematical expression used to calculate panel efficiency (Equation 3.2), it is noted that, all else being equal and holding delta T constant, if solar irradiance increases in the denominator, then a lower efficiency can be expected. Unfortunately with the data collected, ΔT could not be held constant, and so this relationship could not be confirmed empirically.

5 Conclusions and Recommendations

The purpose of this research program was to measure the efficiency of evacuated tube solar collectors under various operating conditions. Operating conditions including the angle of inclination towards the incident solar radiation, heat transfer fluid flow rate, glazing installation, and number of evacuated tubes were of particular interest due to design and installation consequences encountered in practice.

From a practical and architectural point of view, there are a number of possible installation scenarios for evacuated tube collectors that may be more or less appropriate under different environmental, structural, and aesthetic restrictions. This research set out to determine under which conditions different collector configurations would be most appropriate.

The findings indicated that efficiency varied by approximately 5% in general between the different collector configurations, as observed from the overlay graph of results.

That being said, it was observed that covering the collector with a polycarbonate sheet will slightly reduce its efficiency, though hardly enough to be of concern in situations where the benefit would outweigh the slight decrease in performance.

Vertical installations were found to be slightly more efficient than others during the winter months, and slightly less during the summer. This may not be an issue in situations where the demand for heat is greatest in the winter, and heat storage capacity in

the summer is a concern. In this case, the best use of the collector would be made in the winter when the load is available, and the decreased efficiency in the summer would not be missed since there would not necessarily be a load available to displace the heat.

As Equation 3.2 suggests, increasing the mass flow rate, and thus the volume flow rate, should cause and increase in collector efficiency. This was observed to be consistent in Collector 3.

The consequences of removing half of the tubes from the collector (16 tubes in total) could not accurately be observed since the duration of data collection did not yield enough data points to generate a noticeable trend. It is recommended that data collection continue on Collector 3 with the tubes removed to further study the effects of tube removal on collector efficiency.

In addition, the temperature data collected from thermocouples inserted into the manifold seats to take measurements of the temperature of the condenser ends was found to be unreliable since consistent contact could not be made with the condenser end. Since the thermocouple wire is already in place, it is recommended that a solution be found, perhaps soldering the thermocouple wire to the condenser tip, to continue monitoring and data collection at these points.

Continuation of monitoring for all collectors, especially those that did not experience a full year of data collection, such as Collector 3 with tubes removed, and collector 4 or

another operating collector installed vertically, would also provide better insight into the effects of these conditions.

Collector 4, the vertical installation, arrived with a different pump and control system, which subsequently malfunctioned and could not be repaired. Rebuilding of the control system with different components and perhaps an entirely different design, and then collecting collector output data, could make for interesting research.

It would also be interesting, and perhaps yield more consistent results, if one could determine a way to hold indoor and outdoor temperatures constant to maintain more regular ΔT between the hot outlet end of the manifold and the cool outlet end of the fin tube heat exchanger, or another load for that matter.

As mentioned in the discussion for the single evacuated tube, it seems as if tube, and consequently collector performance, may decrease over time, perhaps due to degradation of the selective coating or another component. It is therefore recommended that long-term performance be observed.

In this research the effect of environmental conditions was only taken into consideration by active observation rather than data collection. Another research opportunity lies in the comparison of collector efficiency to environmental conditions such as cloud cover, wind speed, ambient temperature, etc.

6 References

American Society of Heating, Refrigerating and Air-Conditioning Engineers, Inc. 2003. Methods of testing to determine the thermal performance of solar collectors., ANSI/ASHRAE Standard 93-2003.

Budihardjo, I. and G.L. Morrison. 2009. Performance of water-in-glass evacuated tube solar water heaters. *Solar Energy* 83:49-56.

Carvalho, M.J. and D.J. Naron. 2001. Comparison of test methods for evaluation of thermal performance of preheat and solar-only factory made systems. *Solar Energy* 69:145-156.

Chiras, D. 2006. Solar hot water systems – satisfying domestic hot water need with renewable energy. In *The Homeowner's Guide to Renewable Energy*, 71-99. Gabriola Island, BC: New Society Publishers.

Canadian Standards Association. 1988a. Solar domestic hot water systems (liquid to liquid heat transfer), CAN/CSA-F379.1-88.

Canadian Standards Association. 1988b. Solar collectors, CAN/CSA-F378-87.

Duffie, J.A. and W.A. Beckman. 2006. *Solar Engineering of Thermal Processes,* 3rd edition. Hoboken, New Jersey: John Wiley and Sons Inc.

El-Nashar, A.M. 2003. Effect of dust deposition on the performance of a solar desalination plant operating in an arid desert area. *Solar Energy* 75:421-431.

Fox, R.F. and A.T. McDonald. 1998. *Introduction to Fluid Dynamics,* 5th edition. New York, New York: John Wiley and Sons Inc.

Kalogirou, S.A. 2004. Solar thermal collectors and applications. *Progress in Energy and Combustion Science* 30:231-295.

Kemp, W.H. 2005. Space heating and cooling with renewable energy. In *The Renewable Energy Handbook*, 159-233. Tamworth, Ontario: Aztext Press.

Marshall, R. 1999. A generalized steady state collector model including pipe losses, heat exchangers, and pump powers. *Solar Energy* 66:469-477.

Mathioulakis, E. and V. Belessiotis. 2001. A new heat-pipe type solar domestic hot water system. *Solar Energy* 72:13-20.

Morrison, G.L., I. Budihardjo and M. Behnia. 2004. Water-in-glass evacuated tube solar water heaters. *Solar Energy* 76:135-140.

Nagaraju, J., S.S. Garud, K. Ashok Kumar and M. Ramakrishna Rao. 1999. 1 MW_{th} Industrial solar hot water system and its performance. *Solar Energy* 66:491-497.

Ramlow, B. 2006. *Solar Water Heating, A Comprehensive Guide to Solar Water and Space Heating Systems.* Gabriola Island, British Columbia: New Society Publishers.

Sibbitt, B., T. Onno, D. McClenahan, J. Thornton, A. Brunger, J. Kokko and B. Wong. The Drake Landing solar community project – early results. 2007. Ottawa, Canada: CANMET Energy Technology Centre, Natural Resources Canada; Almonte, Canada: Gagest Inc.; Madision, USA: Tess; Mississauga, Canada: Bodycote Testing Group; Kitchener, Canada: Enermodal Engineering; Ottawa Canada: SAIC Canada.

Sharma, S.D., T. Iwata, H. Kitano and K. Sagara. 2004. Thermal performance of a solar cooker based on an evacuated tube solar collector with a PCM storage unit. *Solar Energy* 78:416-426.

Tsilingiris, P.T. 1996. Solar water-heating design – a new simplified dynamic approach. *Solar Energy* 57:19-28.

UPONOR WIRSBO. 2004. Complete design assistance manual. Regina, Saskatchewan: UPONOR WIRSBO.

Yohanis, Y.G., O. Popel, S.E. Frid and B. Norton. 2005. The annual number of days that solar heated water satisfies a specified demand temperature. *Solar Energy* 80:1021-1030.

Appendix A – Pump Curves

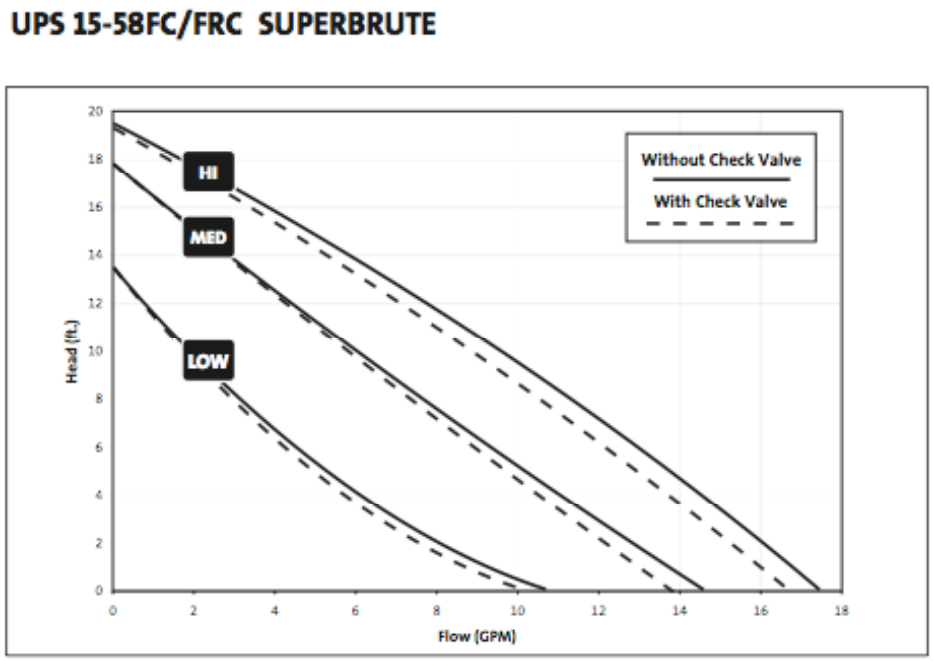

Figure A.1. Pump curve for Grundfos UPS 15-FC/FRC Superbrute circulation pump.

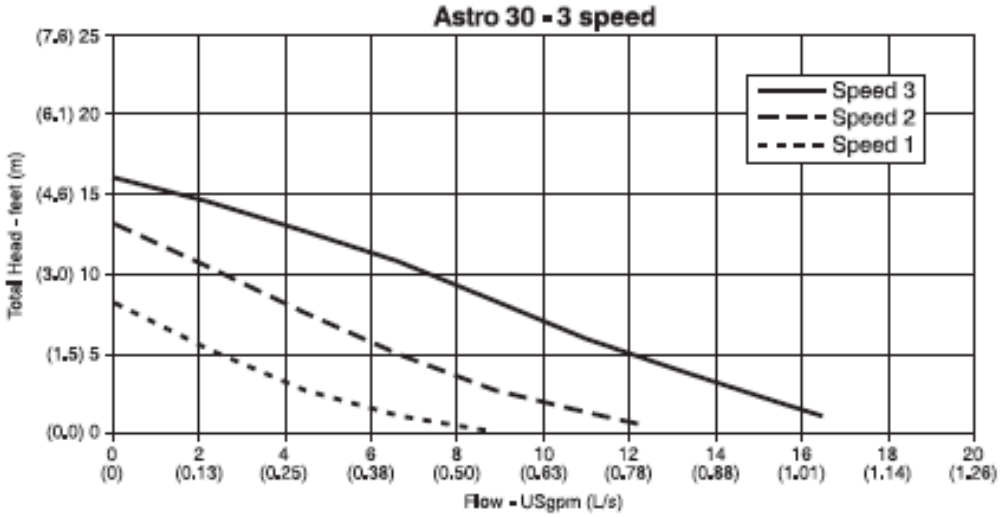

Figure A.2. Pump curve for Armstrong Astro 30 – 3 Speed circulation pump.

Appendix B – Data Acquisition Channel Labels, Measurement Locations, and Variable Names

Channel	Description	Variable Name
101	Irradiance	
102	Ambient Outdoor Air Temperature	
103	Mini Manifold Temperature	
104	Control Tube	
108	Manifold 1 IN	M1IN
109	Tube 1	M1T1
110	Tube 4	M1T4
111	Tube 8	M1T8
112	Tube 12	M1T12
113	Tube 16	M1T16
114	Tube 20	M1T20
115	Tube 24	M1T24
116	Tube 28	M1T28
117	Tube 32	M1T32
118	Manifold 1 OUT	M1OUT
119	Fin Tube 1 IN	F1IN
120	Fin Tube 1 OUT	F1OUT
201	Manifold 2 IN	M2IN
202	Tube 1	M2T1
203	Tube 4	M2T4
204	Tube 8	M2T8
205	Tube 12	M2T12
206	Tube 16	M2T16
207	Tube 20	M2T20
208	Tube 24	M2T24
209	Tube 28	M2T28
210	Tube 32	M2T32
211	Manifold 2 OUT	M2OUT
212	Fin Tube 2 IN	F2IN
213	Fin Tube 2 OUT	F2OUT
214	Manifold 3 IN	M3IN
215	Tube 1	M3T1
216	Tube 4	M3T4
217	Tube 8	M3T8
218	Tube 12	M3T12
219	Tube 16	M3T16
220	Tube 20	M3T20
301	Tube 24	M3T24
302	Tube 28	M3T28
303	Tube 32	M3T32
304	Manifold 3 OUT	M3OUT
305	Fin Tube 3 IN	F3IN
306	Fin Tube 3 OUT	F3OUT
307	Manifold 4 IN	M4IN
308	Tube 1	M4T1
309	Tube 4	M4T4
310	Tube 8	M4T8
311	Tube 12	M4T12
312	Tube 16	M4T16
313	Tube 20	M4T20
314	Tube 24	M4T24
315	Tube 28	M4T28
316	Tube 32	M4T32
317	Manifold 4 OUT	M4OUT
318	Fin Tube 4 IN	F4IN
319	Fin Tube 4 OUT	F4OUT
320	Ambient Indoor Air Temperature	

Appendix C – Stata "Do" Files and Code Used for Data Reduction and Calculations

A number of "Do" files and code lines were written in Stata language to prepare the data for the efficiency calculations. The following is a list of "Do" files and code lines used, along with explanations of their purpose. The actual code language for each step is available in Appendix C.

1_Analysis_Setup

This "Do" file was used to set up Stata to manage the size of the data set being imported by setting the working memory to 500m.

2_Analysis_Data_Prep

Prior to using Stata, the data files, previously saved by date and time of download, were combined into monthly totals, to reduce the number of working files. In addition, prior to using the code lines in this "Do" file, the data required formatting to be consistent across all data files. Each monthly data file was converted to an .xml file format. In the .xml spreadsheets, missing dates were replaced with "na" and the cells formatted as "date". Similarly, missing numbers were replaced with "0" and the cells formatted cell as "number". Columns containing dates were formatted as "date" and columns containing number were formatted as "number". It should be noted here that the date and time stamps were not consistent throughout the duration of data collection. At some point, approximately around December 28th of 2009, the data acquisition system began randomly reversing the day and month within the day/month/year date format.

Thus, the dates were broken down in Excel, into one column for each DAY, MONTH and YEAR (8, 9, or 10), and YEAR_200X (2008, 2009, 2010) and then recombined properly via the "DATE" formula. Similarly, the time stamp was also broken down into one column for each the HOUR, MINUTE, SECOND, AM_PM. The time stamp posed an additional challenge, as it needed to be converted into 24-hour time, as Excel could not recombine the time stamp properly otherwise. Code was written in Excel to convert the time from AM/PM format to 24-hour clock. In retrospect, these procedures could also have been carried out in Stata. There were 196 columns in total.

Data preparation consisted of copying the following line into the command window in Stata: xmluse data1.xml, doctype(excel) datestring missing

The "datestring" missing tells Stata that certain cells formatted as "date" will contain missing values. The resulting Stata data file was saved as:

data = year_month_month_Stata.xml.

For example, the above code might use Excel file "2008_07_July_Stata.xml" and be converted to the Stata data file "2008_07_July_Stata.dta". Stata memory was then cleared to prepare for the next data file, by typing "clear".

The above process was repeated for all .xml data files. To combine all .dta files into one complete data set the following code lines were executed in Stata, one at a time":

```
use data1
append using data2
append using data3
append using data…
```

The above append command and code was continued for all dataX.dta files. The resulting file was saved as: "combined_data.dta". This is the Stata data file used as the starting point for all further data manipulation and analysis.

3_Analysis_Rename_Variables

The "combined_data.dta" consisted of 196 columns, each corresponding to a different measured variable or a time stamp associated with a measured variable. In total, there were 60 variables of interest. Each of the 196 columns was assigned a variable number when imported into Stata. These numbers were renamed to meaningful titles via the "Analysis_Rename_Variables.do" program. For example, "variable 40" was renamed to "M1IN_TEMP", which refers to the inlet temperature of manifold 1, by the Stata coding "rename var40 M1IN_TEMP". Refer to Appendix C for the code used to rename all the variables in this program.

4_Analysis_Drop_TS

5_Analysis_Drop_S

The suffixes "TS" and "S" refer to the date/time stamp, and the corresponding time in seconds, respectively. A time stamp and seconds value was assigned to each measured variable. For ease of analysis, all "time stamps" (TS) were dropped except for the time stamp corresponding to the measured solar irradiance. This time stamp was used in all subsequent calculations. It should also be noted that this is the only time stamp that was deconstructed and then reconstructed into separate date and time values in Excel. (As previously noted, the date and time had to be broken down into its constituent parts (day, month, year, hour, minute, etc.) since date and time were recorded together as one combined value and could not be properly dealt with in Excel otherwise). In addition, the "seconds" (S) were of little use in this particular analysis, and were therefore dropped.

6_Analysis_Drop_Negative_Insolation_Values

Negative insolation values correspond to night-time or otherwise dark conditions when the sun was not shining (note that insolation is a misnomer in this case and actually represents solar irradiance over time, and thus subsequent discussions refer to irradiance (W/m^2)). These negative values were of no use in the efficiency calculations for each collector and were therefore dropped from the data set.

7_Analysis_Generate_n

8_Analysis_Generate_d

9_Analysis_Generate_B1_B2_B3_B4

10_Analysis_Generate_AI1_AI2_AI3_AI4

11_Analysis_Generate_ZA

12_Analysis_Generate_Rb

13_Analysis_Generate_G

15_Analysis_Generate_Ag

16_Analysis_Generate_D1_D2_D3_D4

17_Analysis_Generate_Q1_Q2_Q3_Q4

18_Analysis_Generate_m1_m2_m3_m4

19_Analysis_Generate_E1_E2_E3_E4

"Do" files 7 through 19 were created to generate the necessary terms for the efficiency calculation for each collector. These terms are described in detail in Section 3.7 and will not be repeated here.

20_Analysis_Generate_DeltaT

It was observed from the output of "19_Analysis_Generate_E1_E2_E3_E4" that E4, the efficiency of collector 4, was mostly negative. This implied that the "M4OUT_TEMP" and "M4IN_TEMP" thermocouples had been accidentally switched in the data acquisition system (refer to Appendix B for definitions of variable names). The "DeltaT" variable was generated as a check; if "DeltaT" was positive, then the resulting efficiency would also be positive, and vice versa (as per Equation 2). In this case, "DeltaT" for collector 4 was mostly negative. By testing the output of the thermocouples when ice was held to the end, it was confirmed that indeed they had been switched. Corrections were made in all subsequent programming to account for this mix-up; X4_2 refers to collector 4, with the proper temperature readings.

21_Analysis_Generate_deltaT

22_Analysis_Drop_deltaT_C1

22_Analysis_Drop_deltaT_C2

22_Analysis_Drop_deltaT_C3

22_Analysis_Drop_deltaT_C4

22_Analysis_Drop_deltaT_C4_2

The temperature difference between the hot side of the manifold (MXOUT_TEMP) and the cold side of the fin tube heat exchanger (FXOUT_TEMP), "deltaT" represents the greatest possible temperature difference. The collectors are programmed to start the pumps once this temperature difference is equal to 2 degrees Celsius. If "deltaT" is less than 2, the collector is not actually operating, even if solar irradiance is available. Thus, for all collectors, observations where "deltaT" was less than 2 were dropped from the data set. The resulting data sets contained observations for which the circulation pumps were actually operating. Note also that step 22 is when "Do" files for each collector were run separately on the combined data set to produce a unique data set for each collector. This was done for ease programming and as a method of tracking mistakes.

23_Analysis_Drop_Greaterthan100_E_Values_C1

23_Analysis_Drop_Greaterthan100_E_Values_C2

23_Analysis_Drop_Greaterthan100_E_Values_C3

23_Analysis_Drop_Greaterthan100_E_Values_C4

23_Analysis_Drop_Greaterthan100_E_Values_C4_2

Through initial plotting of the efficiency data, efficiencies greater than 100% were observed. These data points were outliers and were skewing the graphical analysis. Thus, all observations resulting in greater than 100% efficiency were dropped from the data set via "Do" file 23 for each collector.

24_Analysis_Drop_Negative_E_Values_C1

24_Analysis_Drop_Negative_E_Values_C2

24_Analysis_Drop_Negative_E_Values_C3

24_Analysis_Drop_Negative_E_Values_C4.

24_Analysis_Drop_Negative_E_Values_C4_2

Through initial plotting of the efficiency data, efficiencies less than 0% were observed. These data points were outliers and were skewing the graphical analysis. Thus, all observations resulting in less than 0% efficiency were dropped from the data set via "Do" file 24 for each collector.

25_Analysis_DAYandMONTH_fixed_all_data

25_Analysis_DAYandMONTH_fixed_C1

25_Analysis_DAYandMONTH_fixed_C2

25_Analysis_DAYandMONTH_fixed_C3

25_Analysis_DAYandMONTH_fixed_C4

25_Analysis_DAYandMONTH_fixed_C4_2

As previously noted, the date and time had to be broken down into its constituent parts (day, month, year, hour, minute, etc.) since date and time were recorded together as one combined value and could not be properly dealt with in Excel otherwise. Also as previously noted, at some point, approximately around December 28th of 2009, the data acquisition system began randomly reversing the day and month within the day/month/year date format. Even after correcting most of this issue directly in Excel, a few incorrect dates persisted. Thus, code was written in Stats to correct this swapping of day and month once and for all. "Do" file 25 was run on the data set for each collector, and on the entire combined data set.

26_Analysis_Mean_Daily

26_Analysis_Mean_Daily_C1

26_Analysis_Mean_Daily_C2

26_Analysis_Mean_Daily_C3

26_Analysis_Mean_Daily_C4_2

26_Analysis_Mean_Daily_CT

A program was written to calculate the mean daily solar irradiance and efficiency values for each collector. The output of this program generated a table of data, with a column for mean daily solar irradiance and another for mean daily efficiency for each day of the month. A .log file was generated and converted to a text file so that output could be directly copied into Microsoft Excel 2004 for Mac. Prior to copying over the data, some manipulation was required in TextEdit 1.3 (v202) to ensure that each data value copied into its own cell. Essentially, tabs were added between entries to create a tab delimited file. This output was used to generate some of the graphs in the Results and Discussion section.

27_Analysis_Drop_Negative_CT_Temp

The temperature of the condenser end of the single evacuated tube was measured over the same duration as the collectors. Negative temperature measurements correspond to night-time or otherwise dark conditions. Thus they were dropped from the data set via “Do” file 27.

Analysis_Setup
clear
set memory 500m

Analysis_Data_Prep
*in xml spreadsheets, replace missing dates with "na" and format cell as date, and replace missing numbers with "0" and format cell as number
*format date columns as "date" and format number columns as "number"
*there are 196 columns

*copy the following line into the Command window in Stata
xmluse *data1.xml*, doctype(excel) datestring missing
*SaveAs "*data1.dta*"
clear

*copy the following line into the Command window in Stata
xmluse *data2.xml*, doctype(excel) datestring missing
*SaveAs "*data2.dta*"
clear

*repeat the above for all .xml data files

*copy the following lines into the Command window in Stata (execute one at a time)
use *data1*
append using *data2*
append using *data3*
*Continue above append command for all *dataX.dta* files
*SaveAs "combined_data.dta"

**data* = year_month_month_Stata.xml

Analysis_Rename_Variables.do

```
rename var1 BL_TS

rename var2 DAY
rename var3 MONTH
rename var4 YEAR
rename var5 YEAR_200X
rename var6 DATE
rename var7 HOUR
rename var8 MINUTE
rename var9 SECOND
rename var10 AM_PM
rename var11 HOUR1
rename var12 HOUR2
rename var13 HOUR_24H
rename var14 TIME
rename var15 TIME_DIFF_HRS
rename var16 TIME_DIFF_INT
rename var17 w_HOUR_ANGLE

rename var18 INS_S
rename var19 INS

rename var20 AOAT_TS
rename var21 AOAT_S
rename var22 AOAT_TEMP

rename var23 MM_TS
rename var24 MM_S
rename var25 MM_TEMP

rename var26 CT_TS
rename var27 CT_S
rename var28 CT_TEMP

rename var29 MMT1_TS
rename var30 MMT1_S
rename var31 MMT1_TEMP

rename var32 MMT2_TS
rename var33 MMT2_S
rename var34 MMT2_TEMP

rename var35 MMT3_TS
rename var36 MMT3_S
rename var37 MMT3_TEMP
```

```
rename var38 M1IN_TS
rename var39 M1IN_S
rename var40 M1IN_TEMP

rename var41 M1T1_TS
rename var42 M1T1_S
rename var43 M1T1_TEMP

rename var44 M1T4_TS
rename var45 M1T4_S
rename var46 M1T4_TEMP

rename var47 M1T8_TS
rename var48 M1T8_S
rename var49 M1T8_TEMP

rename var50 M1T12_TS
rename var51 M1T12_S
rename var52 M1T12_TEMP

rename var53 M1T16_TS
rename var54 M1T16_S
rename var55 M1T16_TEMP

rename var56 M1T20_TS
rename var57 M1T20_S
rename var58 M1T20_TEMP

rename var59 M1T24_TS
rename var60 M1T24_S
rename var61 M1T24_TEMP

rename var62 M1T28_TS
rename var63 M1T28_S
rename var64 M1T28_TEMP

rename var65 M1T32_TS
rename var66 M1T32_S
rename var67 M1T32_TEMP

rename var68 M1OUT_TS
rename var69 M1OUT_S
rename var70 M1OUT_TEMP
```

```
rename var71 F1IN_TS
rename var72 F1IN_S
rename var73 F1IN_TEMP

rename var74 F1OUT_TS
rename var75 F1OUT_S
rename var76 F1OUT_TEMP

rename var77 M2IN_TS
rename var78 M2IN_S
rename var79 M2IN_TEMP

rename var80 M2T1_TS
rename var81 M2T1_S
rename var82 M2T1_TEMP

rename var83 M2T4_TS
rename var84 M2T4_S
rename var85 M2T4_TEMP

rename var86 M2T8_TS
rename var87 M2T8_S
rename var88 M2T8_TEMP

rename var89 M2T12_TS
rename var90 M2T12_S
rename var91 M2T12_TEMP

rename var92 M2T16_TS
rename var93 M2T16_S
rename var94 M2T16_TEMP

rename var95 M2T20_TS
rename var96 M2T20_S
rename var97 M2T20_TEMP

rename var98 M2T24_TS
rename var99 M2T24_S
rename var100 M2T24_TEMP

rename var101 M2T28_TS
rename var102 M2T28_S
rename var103 M2T28_TEMP
```

```
rename var104 M2T32_TS
rename var105 M2T32_S
rename var106 M2T32_TEMP

rename var107 M2OUT_TS
rename var108 M2OUT_S
rename var109 M2OUT_TEMP

rename var110 F2IN_TS
rename var111 F2IN_S
rename var112 F2IN_TEMP

rename var113 F2OUT_TS
rename var114 F2OUT_S
rename var115 F2OUT_TEMP

rename var116 M3IN_TS
rename var117 M3IN_S
rename var118 M3IN_TEMP

rename var119 M3T1_TS
rename var120 M3T1_S
rename var121 M3T1_TEMP

rename var122 M3T4_TS
rename var123 M3T4_S
rename var124 M3T4_TEMP

rename var125 M3T8_TS
rename var126 M3T8_S
rename var127 M3T8_TEMP

rename var128 M3T12_TS
rename var129 M3T12_S
rename var130 M3T12_TEMP

rename var131 M3T16_TS
rename var132 M3T16_S
rename var133 M3T16_TEMP

rename var134 M3T20_TS
rename var135 M3T20_S
rename var136 M3T20_TEMP
```

```
rename var137 M3T24_TS
rename var138 M3T24_S
rename var139 M3T24_TEMP

rename var140 M3T28_TS
rename var141 M3T28_S
rename var142 M3T28_TEMP

rename var143 M3T32_TS
rename var144 M3T32_S
rename var145 M3T32_TEMP

rename var146 M3OUT_TS
rename var147 M3OUT_S
rename var148 M3OUT_TEMP

rename var149 F3IN_TS
rename var150 F3IN_S
rename var151 F3IN_TEMP

rename var152 F3OUT_TS
rename var153 F3OUT_S
rename var154 F3OUT_TEMP

rename var155 M4IN_TS
rename var156 M4IN_S
rename var157 M4IN_TEMP

rename var158 M4T1_TS
rename var159 M4T1_S
rename var160 M4T1_TEMP

rename var161 M4T4_TS
rename var162 M4T4_S
rename var163 M4T4_TEMP

rename var164 M4T8_TS
rename var165 M4T8_S
rename var166 M4T8_TEMP

rename var167 M4T12_TS
rename var168 M4T12_S
rename var169 M4T12_TEMP
```

```
rename var170 M4T16_TS
rename var171 M4T16_S
rename var172 M4T16_TEMP

rename var173 M4T20_TS
rename var174 M4T20_S
rename var175 M4T20_TEMP

rename var176 M4T24_TS
rename var177 M4T24_S
rename var178 M4T24_TEMP

rename var179 M4T28_TS
rename var180 M4T28_S
rename var181 M4T28_TEMP

rename var182 M4T32_TS
rename var183 M4T32_S
rename var184 M4T32_TEMP

rename var185 M4OUT_TS
rename var186 M4OUT_S
rename var187 M4OUT_TEMP

rename var188 F4IN_TS
rename var189 F4IN_S
rename var190 F4IN_TEMP

rename var191 F4OUT_TS
rename var192 F4OUT_S
rename var193 F4OUT_TEMP

rename var194 AIAT_TS
rename var195 AIAT_S
rename var196 AIAT_TEMP
```

Analysis_Data_Drop_TS.do

```
drop AOAT_TS MM_TS CT_TS MMT1_TS MMT2_TS MMT3_TS M1IN_TS M1T1_TS M1T4_TS M1T8_TS M1T12_TS M1T16_TS M1T20_TS M1T24_TS M1T28_TS M1T32_TS M1OUT_TS F1IN_TS F1OUT_TS M2IN_TS M2T1_TS M2T4_TS M2T8_TS M2T12_TS M2T16_TS M2T20_TS M2T24_TS M2T28_TS M2T32_TS M2OUT_TS F2IN_TS F2OUT_TS M3IN_TS M3T1_TS M3T4_TS M3T8_TS M3T12_TS M3T16_TS M3T20_TS M3T24_TS M3T28_TS M3T32_TS M3OUT_TS F3IN_TS F3OUT_TS M4IN_TS M4T1_TS M4T4_TS M4T8_TS M4T12_TS M4T16_TS M4T20_TS M4T24_TS M4T28_TS M4T32_TS M4OUT_TS F4IN_TS F4OUT_TS AIAT_TS
```

Analysis_Data_Drop_S.do

```
drop INS_S AOAT_S MM_S CT_S MMT1_S MMT2_S MMT3_S M1IN_S M1T1_S M1T4_S M1T8_S M1T12_S M1T16_S M1T20_S M1T24_S M1T28_S M1T32_S M1OUT_S F1IN_S F1OUT_S M2IN_S M2T1_S M2T4_S M2T8_S M2T12_S M2T16_S M2T20_S M2T24_S M2T28_S M2T32_S M2OUT_S F2IN_S F2OUT_S M3IN_S M3T1_S M3T4_S M3T8_S M3T12_S M3T16_S M3T20_S M3T24_S M3T28_S M3T32_S M3OUT_S F3IN_S F3OUT_S M4IN_S M4T1_S M4T4_S M4T8_S M4T12_S M4T16_S M4T20_S M4T24_S M4T28_S M4T32_S M4OUT_S F4IN_S F4OUT_S AIAT_S
```

Analysis_Drop_Negative_Insolation_Values.do

```
drop if INS<=0
```

Analysis_Generate_n.do

```
generate n=DAY
replace n=DAY+0 if MONTH==1
replace n=DAY+31 if MONTH==2
replace n=DAY+59 if MONTH==3
replace n=DAY+90 if MONTH==4
replace n=DAY+120 if MONTH==5
replace n=DAY+151 if MONTH==6
replace n=DAY+181 if MONTH==7
replace n=DAY+212 if MONTH==8
replace n=DAY+243 if MONTH==9
replace n=DAY+273 if MONTH==10
replace n=DAY+304 if MONTH==11
replace n=DAY+334 if MONTH==12
```

Analysis_Generate_d.do
```
generate d=23.45*(sin(360*((284+n)/365)))
```

Analysis_Generate_B1_B2_B3_B4.do
```
generate B1=0.86
generate B2=0.86
generate B3=0.86
generate B4=1.57
```

Analysis_Generate_AI.do
```
generate COS_AI1 = sin(d)*sin(0.86)*cos(B1) - sin(d)*cos(0.86)*sin(B1)*cos(0) +
cos(d)*cos(0.86)*cos(B1)*cos(w_HOUR_ANGLE) +
cos(d)*sin(0.86)*sin(B1)*cos(0)*cos(w_HOUR_ANGLE) +
cos(d)*sin(B1)*sin(0)*sin(w_HOUR_ANGLE)

generate COS_AI2 = sin(d)*sin(0.86)*cos(B2) - sin(d)*cos(0.86)*sin(B2)*cos(0) +
cos(d)*cos(0.86)*cos(B2)*cos(w_HOUR_ANGLE) +
cos(d)*sin(0.86)*sin(B2)*cos(0)*cos(w_HOUR_ANGLE) +
cos(d)*sin(B2)*sin(0)*sin(w_HOUR_ANGLE)

generate COS_AI3 = sin(d)*sin(0.86)*cos(B3) - sin(d)*cos(0.86)*sin(B3)*cos(0) +
cos(d)*cos(0.86)*cos(B3)*cos(w_HOUR_ANGLE) +
cos(d)*sin(0.86)*sin(B3)*cos(0)*cos(w_HOUR_ANGLE) +
cos(d)*sin(B3)*sin(0)*sin(w_HOUR_ANGLE)

generate COS_AI4 = sin(d)*sin(0.86)*cos(B4) - sin(d)*cos(0.86)*sin(B4)*cos(0) +
cos(d)*cos(0.86)*cos(B4)*cos(w_HOUR_ANGLE) +
cos(d)*sin(0.86)*sin(B4)*cos(0)*cos(w_HOUR_ANGLE) +
cos(d)*sin(B4)*sin(0)*sin(w_HOUR_ANGLE)
```

Analysis_Generate_Rb.do
```
generate COS_ZA = sin(d)*sin(0.86) + cos(d)*cos(0.86)*cos(w_HOUR_ANGLE)
```

Analysis_Generate_Rb.do
```
generate Rb1 = abs(COS_AI1/COS_ZA)
generate Rb2 = abs(COS_AI2/COS_ZA)
generate Rb3 = abs(COS_AI3/COS_ZA)
generate Rb4 = abs(COS_AI4/COS_ZA)
```

Analysis_Generate_G.do
generate G1 = Rb1*INS
generate G2 = Rb2*INS
generate G3 = Rb3*INS
generate G4 = Rb4*INS

Analysis_Generate_Cp.do
generate Cp=3558.78

Analysis_Generate_Ag.do
generate Ag=3.429

Analysis_Generate_D1_D2_D3_D4.do
generate D1=1.060
generate D2=1.060
generate D3=1.055
generate D4=1.055

Analysis_Generate_Q1_Q2_Q3_Q4.do
generate Q1=1.3*0.0630901964
generate Q2=1.3*0.0630901964
generate Q3=1.475*0.0630901964
generate Q4=1.675*0.0630901964

Analysis_Generate_m1_m2_m3_m4.do
generate m1=D1*Q1
generate m2=D2*Q2
generate m3=D3*Q3
generate m4=D4*Q4

Analysis_Generate_E1_E2_E3_E4.do
generate E1=(m1*Cp*(M1OUT_TEMP - M1IN_TEMP))/(Ag*G1)
generate E2=(m2*Cp*(M2OUT_TEMP - M2IN_TEMP))/(Ag*G2)
generate E3=(m3*Cp*(M3OUT_TEMP - M3IN_TEMP))/(Ag*G3)
generate E4=(m4*Cp*(M4OUT_TEMP - M4IN_TEMP))/(Ag*G4)
generate E4_2=(m4*Cp*(M4IIN_TEMP - M4OUT_TEMP))/(Ag*G4)

Analysis_Generate_DeltaT.do
generate DT1 = M1OUT_TEMP-M1IN_TEMP
generate DT2 = M2OUT_TEMP-M2IN_TEMP
generate DT3 = M3OUT_TEMP-M3IN_TEMP
generate DT4 = M4OUT_TEMP-M4IN_TEMP
generate DT4_2 = M4IN_TEMP-M4OUT_TEMP

Analysis_Generate_deltaT.do
generate dT1 = M1OUT_TEMP-F1OUT_TEMP
generate dT2 = M2OUT_TEMP-F2OUT_TEMP
generate dT3 = M3OUT_TEMP-F3OUT_TEMP
generate dT4 = M4OUT_TEMP-F4OUT_TEMP

Analysis_Drop_deltaT_C1.do
drop if dT1<2

Analysis_Drop_deltaT_C2.do
drop if dT2<2

Analysis_Drop_deltaT_C3.do
drop if dT3<2

Analysis_Drop_deltaT_C4.do
drop if dT4<2

Analysis_Drop_deltaT_C4_2.do
drop if dT4_2<2

Analysis_Drop_Greaterthan100_E_Values_C1.do
drop if E1>100

Analysis_Drop_Greaterthan100_E_Values_C2.do
drop if E2>100

Analysis_Drop_Greaterthan100_E_Values_C3.do
drop if E3>100

Analysis_Drop_Greaterthan100_E_Values_C4.do
drop if E4>100

Analysis_Drop_Greaterthan100_E_Values_C4_2.do
drop if E4_2>100

Analysis_Drop_Negative_E_Values_C1.do
drop if E1<0

Analysis_Drop_Negative_E_Values_C2.do
drop if E2<0

Analysis_Drop_Negative_E_Values_C3.do
drop if E3<0

Analysis_Drop_Negative_E_Values_C4.do
drop if E4<0

Analysis_Drop_Negative_E_Values_C4_2.do
drop if E4_2<0

Analysis_DAYandMONTH_fixed_C1.do
generate DAY_fixed = MONTH in 22117/22254
replace DAY_fixed = DAY in 1/22116
generate MONTH_fixed = DAY in 22117/22254
replace MONTH_fixed = MONTH in 1/22116

Analysis_DAYandMONTH_fixed_C2.do
generate DAY_fixed = MONTH in 11481/11494
replace DAY_fixed = DAY in 1/11480
generate MONTH_fixed = DAY in 11481/11494
replace MONTH_fixed = MONTH in 1/11480

Analysis_DAYandMONTH_fixed_C3.do
generate DAY_fixed = MONTH in 22412/22593
replace DAY_fixed = DAY in 1/22411
generate MONTH_fixed = DAY in 22412/22593
replace MONTH_fixed = MONTH in 1/22411

Analysis_DAYandMONTH_fixed_C4_2.do
```
generate DAY_fixed = MONTH in 18969/19404
replace DAY_fixed = DAY in 1/18968
generate MONTH_fixed = DAY in 18969/19404
replace MONTH_fixed = MONTH in 1/18968
```

Analysis_DAYandMONTH_fixed_all_data.do
```
generate DAY_fixed = MONTH in 52999/54300
replace DAY_fixed = DAY in 1/52998
generate MONTH_fixed = DAY in 52999/54300
replace MONTH_fixed = MONTH in 1/52998
```

Analysis_Mean_Daily.do
```
bysort YEAR MONTH_fixed: tabstat INS E1, by(DAY_fixed) stats(mean)
bysort YEAR MONTH_fixed: tabstat INS E2, by(DAY_fixed) stats(mean)
bysort YEAR MONTH_fixed: tabstat INS E3, by(DAY_fixed) stats(mean)
bysort YEAR MONTH_fixed: tabstat INS E4_2, by(DAY_fixed) stats(mean)
bysort YEAR MONTH_fixed: tabstat INS CT_TEMP, by(DAY_fixed) stats(mean)

* do for each panel configuration and create .log file while running
```

Analysis_Drop_Negative_Values_CT.do
```
drop if CT<0
```

Appendix D – Energy Flow Diagram for Domestic Hot Water System

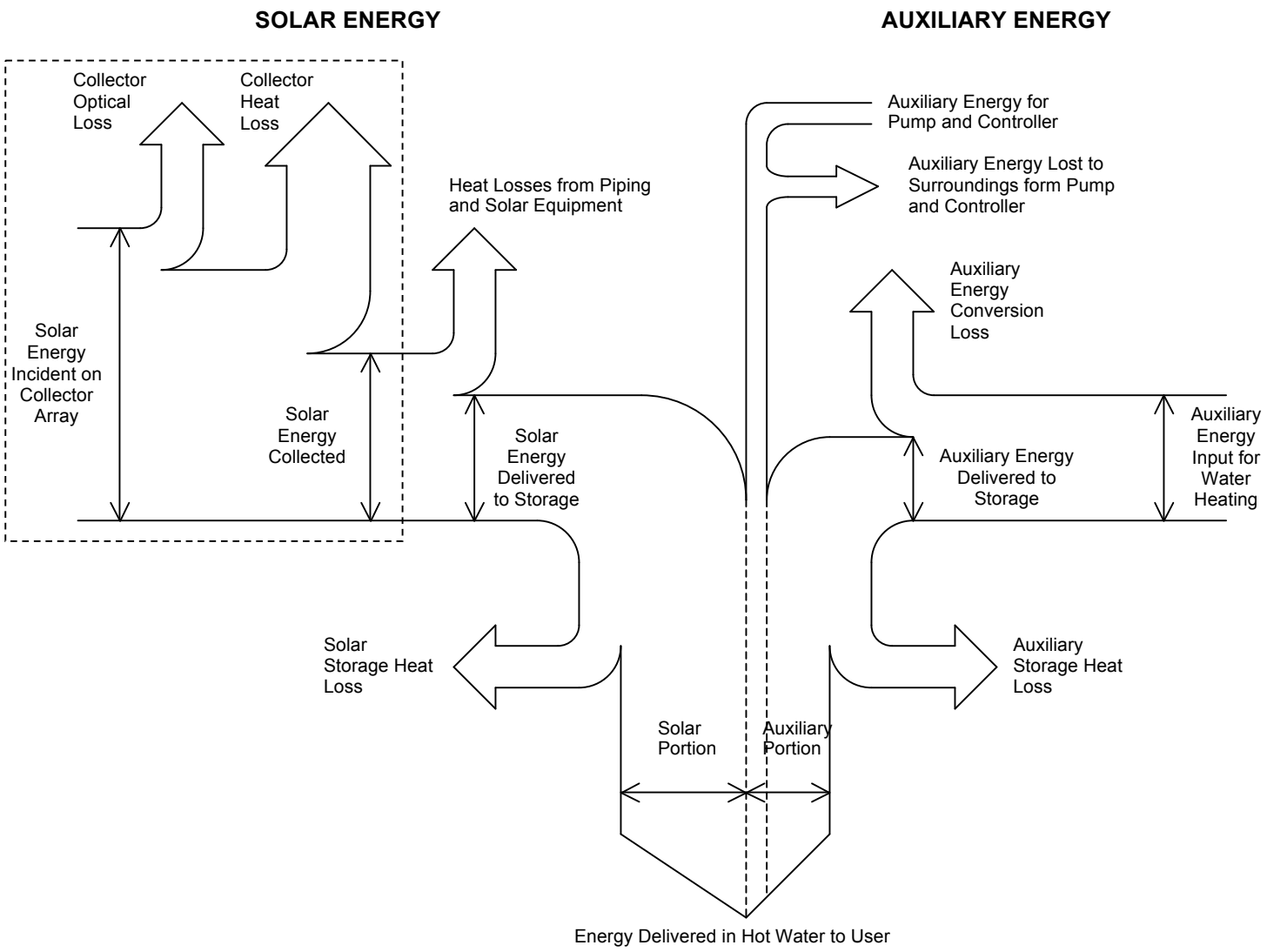

Figure D.1. Adapted from CAN/CSA-F379.1-88 (1988), indicates schematically the energy flow in a solar domestic hot water system. To the left is the energy obtained through solar radiation, indicating potential energy losses. To the right is the auxiliary energy required to heat the water to the desired temperature, if required, and to operate the pumps and controls. The area within the dashed box represents the efficiency of the evacuated tube panel alone, and is the focus of the current research.